ABİTTER GÜNAY DEPARTMENT OF GEOLOGICAL ENGINEERING MASTER OF SCIENCE MUĞLA

REPUBLIC OF TURKEY
MUĞLA SITKI KOÇMAN UNIVERSITY
GRADUATE SCHOOL OF
NATURAL AND APPLIED SCIENCES

DEPARTMENT OF GEOLOGICAL ENGINEERING

ORIGIN OF GOLD MINERALIZATION, SOURCE OF ORE FLUID AND STRUCTURAL CONTROLS OF KEŞKEK HILL GOLD MINERALIZATION (GÖRDES, MANİSA)

MASTER OF SCIENCE

ABİTTER GÜNAY

JULY 2020
MUĞLA

REPUBLIC OF TURKEY
MUĞLA SITKI KOÇMAN UNIVERSITY
GRADUATE SCHOOL OF
NATURAL AND APPLIED SCIENCES

DEPARTMENT OF GEOLOGICAL ENGINEERING

ORIGIN OF GOLD MINERALIZATION, SOURCE OF ORE FLUID AND STRUCTURAL CONTROLS OF KEŞKEK HILL GOLD MINERALIZATION (GÖRDES, MANİSA)

MASTER OF SCIENCE

ABİTTER GÜNAY

JULY 2020
MUĞLA

MUĞLA SITKI KOÇMAN UNIVERSITY

Graduate School of Natural and Applied Sciences

Approval of the thesis submitted by **ABİTTER GÜNAY** with the title of **"ORIGIN OF GOLD MINERALIZATION, SOURCE OF ORE FLUID AND STRUCTURAL CONTROLS OF KEŞKEK HILL GOLD MINERALIZATION (GÖRDES, MANİSA)"** has been unanimously accepted by the jury members on the 16th of July, 2020 to fulfill the requirements for the degree of Master of Science in the Department of Geological Engineering.

THESIS JURY MEMBERS

Prof. Dr. Tolga OYMAN (**Head of the Jury)** Signature

Department of Geological Engineering,

Dokuz Eylül University, İzmir

Prof. Dr. Gonca Kuşcu (**Member**) Signature

Department of Geological Engineering,

Muğla Sıtkı Koçman University, Muğla

Prof. Dr. İlkay KUŞCU (**Supervisor**) Signature

Department of Geological Engineering,

Muğla Sıtkı Koçman University, Muğla

APPROVAL OF HEAD OF THE DEPARTMENT

Prof. Dr. Murat GÜL Signature

Head of Department of Geological Engineering,

Muğla Sıtkı Koçman University, Muğla

Prof. Dr. İlkay KUŞCU Signature

Supervisor, Department of Geological Engineering,

Muğla Sıtkı Koçman University, Muğla

Defense Date: 16/07/2020

I hereby declare that all information in this document has been obtained and presented in accordance with academic rules and ethical conduct. I also declare that, as required by these rules and conduct, I have fully cited and referenced all material and results that are not original to this work.

Abitter GÜNAY

16/07/2020

ABSTRACT

ORIGIN OF GOLD MINERALIZATION, SOURCE OF ORE FLUID AND STRUCTURAL CONTROLS OF KEŞKEK HILL GOLD MINERALIZATION (GÖRDES, MANİSA)

Abitter GÜNAY
Master of Science (M.Sc.)
Graduate School of Natural and Applied Sciences
Department of Geological Engineering
Supervisor: Prof. Dr. İlkay KUŞCU
July 2020, 112 pages

This thesis aims to identify the origin of alteration - mineralization, source of ore fluid, and the relationship between mineralization and host rock characteristics along with constraints on structural controls in Keşkek Hill prospect in Gördes, Manisa.

The mineralization is hosted by jasperoids hosted by gray recrystallized limestones as blocks within ophiolitic mélange. Ophiolitic mélange consists of serpentinized peridotites, epi-ophiolitic sequences including mudstone, radiolarite, light gray laminated limestones, beige-colored laminated limestones (wall rock of mineralization) and dark gray recrystallized limestones. Basement rocks of the study area belong to metamorphic rocks of Menderes Massif.

Jasperoid is the main host rock which is mapped and identified by petrographic studies. It is formed by pervasive silicification and decarbonatization of the carbonate rocks. Silicification and decarbonatization are the first stage of the alteration in the study area. Jasperoid consists of very fine grained-massive quartz. It is cut by or infilled by comb textured quartz, and locally exhibit boxwork texture in decarbonized limestones. Calcification and oxidization are also characteristic alterations formed at the late stages of alteration. Calcification is typically observed in oxidized jasperoids and occur either as veins or as filling the empty spaces between the comb and boxwork textured quartz crystals. Oxidization of jasperoids is very common at surface outcrops, and

intersections at drill holes showed that the degree of oxidation decreases with depth. The most significant texture observed on oxidized jasperoids is the liesegang texture. Mineralization in the area only observed in jasperoidal rocks associated with disseminated fine-grained pyrite, arsenopyrite, and stibnite. Gold is the only precious metal in the study area. Base metal abundances are very low in jasperoidal rocks.

Jasperoid occurrences observed in high angle normal faults with NW-SE direction. High angle (73° to 90°) normal faults in NW-SE direction truncating the thrust faults within the ophiolitic mélange acted like a conduit for the ore fluids and mineralization. Mineralized jasperoids are cut by post mineralized normal and strike slips faults.

The fluid inclusion studies include analyses of primary fluid inclusions on the samples from pre-syn ore stage quartz and syn-ore stage quartz crystals. The primary inclusions are of type-2 inclusions that refers to two-phase inclusions with variable amounts of liquid-vapor (L-V) inclusions. These inclusions subdivided into two as type 2a and type 2b depending on the relative abundance of liquid-vapor ratio in the inclusions. The microthermometric analyses of the inclusions showed that the mean homogenization temperature for pre-syn ore stage quartz minerals is 295.83 °C (ranging between 288.7 °C and 313 °C), and the salinity values range from 5.71 to 7.59 wt. % NaCl eq. The mean homogenization temperature for the inclusions from ore-stage quartz is calculated to be 169 °C (ranging from 136 °C to 182.7 °C) with salinity ranging from 0.70 to 15.86 wt. % NaCl eq. The salinity values for both samples are measured as relatively low salinity for inclusions.

The calculated value $\delta^{18}O_{(fluid)}$ values for syn-ore stage quartz sample ranging between –5.69‰ and -1.77‰. $\delta D_{(fluid)}$ calculated values for syn-ore stage whole rock (jasperoid) sample ranging between -105.79‰ and -101.87‰. Stable isotope data suggest that the hydrothermal fluids that formed jasperoid have been originated by mixing of meteoric water mixing and formation water. The $\delta^{34}S$ isotope value for stibnite is -0.6‰. $\delta^{34}S$, and suggests magmatic sulfur, due to the deep circulation of the meteoric water within the ultramafic rocks in ophiolitic mélange.

The decarbonatization followed by pervasive silicification along with collapse breccia is typical for many sediments hosted gold deposits such as Carlin-type gold deposits.

Additionally, the normal faults formed during a regional extension just after the main thrusting (compression), and silicification along the faults within the carbonate rocks also resemble to structural controls and mechanism of silicification for the Carlin-type deposits. Therefore, the similarities in nature and morphology of the jasperoidal rock hosting the main gold mineralization, and geologic-structural setting suggest that of the gold mineralization at the Keşkek Hill prospect is a Carlin-type gold mineralization.

Keywords: Carlin-Type, Jasperoid, Decarbonatization, Fluid Inclusions, O And H Stable Isotope

ÖZET

KEŞKEK TEPE ALTIN CEVHERLEŞMESİNİN KÖKENİ, AKIŞKANININ KAYNAĞI VE YAPISAL KONTROLLERİ (GÖRDES, MANİSA)

Abitter GÜNAY
Yüksek Lisans Tezi
Fen Bilimleri Enstitüsü
Jeoloji Mühendisliği Anabilim Dalı
Danışman: Prof. Dr. İlkay KUŞCU
Temmuz 2020, 112 sayfa

Bu çalışma, Manisa'nın Gördes ilçesinde bulunan Keşkek Tepe altın cevherleşmesinde gözlemlenen alterasyonun ve mineralizasyonun kökenini, cevher yapan akışkanın kaynağını ve mineralizasyon ile yapısal ilişkisini ortaya koymak için yapılmıştır. Çevherleşme ofiyolitik melanj içerisinde blok halinde bulunan kireçtaşlarının silisleşmesiyle oluşan jasper tarafından barındırılmaktadır. Ofiyolitik melanj genel olarak serpantinleşmiş ultramafik kayaçlar, (ofiyolit üzeri sedimenter kayaçları, açık gri renkli tabakalı kireçtaşları, bej renkli tabakalı kireçtaşları (mineralizasyonun yan kayacı) ve koyu gri renkli rekristalize kireçtaşlarından oluşmaktadır. Çalışma alanının temel kayaları ise Menderes Masifinin metamorfik kayaçlarıdır.

Petrografik çalışmalar, jasper oluşumunun kireçtaşlarındaki dekarbonizasyon ve silisleşmen ve ürünü olduğunu göstermektedir. Silisleşme ve dekarbonizasyon kireçtaşlarındaki ilk alterasyonlardır. Jasper, çok ince taneli massif kuvarsların yanında, jasper kütlelerini damarlar halinde kesen veya boşlukları doldurur şekilde bulunan tarak dokulu kuvarslar veya dekarbonatlaşmaya uğramış kireçtaşlaı içinde boksvörk yapılı oluşumları da içerir. Cevherleşmeden sonra oluşan karbonatlaşma (kalsitleşme) ve oksidasyon ise alterasyonun son aşamasıdır. Cevherleşme, saçınımlı ince taneli pirit, arsenopirit ve stibnit mineralleri ile birlikte sadece jasperler içerisinde gözlenebilmektedir. Yapılan analizler sonucunda çalışma alanı içerisinde altın dışında

herhangi bir değerli metal oluşmadığı anlaşılmıştır. Jasperler, diğer baz metaller açısından olduça düşük içeriğe sahiptirler. Kalsitleşme, oksitlenmiş jasperler içerisinde, tarak dokusundaki boşluklarda ve ağsı doku içerisindeki boşluklarda gözlenmektedir. Yüzeyde bulunan jasperlerde ise oksidasyon seviyesi kayda değer biçimde yüksektir ve sondaj çalışmalarında bu oksidasyonun derinlere gidildikçe yer yer azaldığı gözlenmektedir. Liesegang dokusu oksitlenmiş jasperlar üzerinde gözlemlenen en belirgin dokudur.

Yapılan arazi çalışmaları neticesinde, Keşkek Tepe bölgesinde yer alan jasper oluşumlarının da kuzeybatı-güneydoğu yönlü yüksek açılı normal fay zonlarında oluştuğu gözlenmektedir. Bu faylar bölgede yer alan ve ofiyolitik melanjın bölgeye bindirmesini sağlayan bindirme faylarını kesen yüksek açılı (73° to 90°) normal faylardır. Bu faylar mineralizasyonun oluşumunda kanal vazifiesi gören önemli faylardır.

Sıvı kapanımı analizleri, cevherleşme ile eş zamanlı-önce oluşan kuvars ve cevherleşme ile eş zamanlı kuvars minerallerinden alınan örneklerdeki birincil kapanımlar üzerinde yapılmıştır. Birincil kapanımlar, sıvı-gaz içeriğine sahip çift fazlı kapanımları temsilen Tip-2 olarak adlandırılan tek tip kapanımlardır. Tip-2 kapanımları içerdikleri sıvı-gaz oranalarına göre tip 2a ve tip 2b olmak üzere iki alt gruba ayrılmıştır. Cevherleşme ile eş yaşlı-öncesinde oluşan kuvars kristallerine ait kapanımlardan elde edilen homojenleşme sıcaklıklarının ortalama değeri (T_h°C) 295.83 °C (288.7 °C and 313 °C aralığında), ve tuzlulukları 5.71 ile 7.59 wt. % NaCl eq aralığında hesaplanmıştır. Cevherleşme ile eş zamanlı olan kuvarslara ait kapanımlardan elde edilen homojenleşme sıcaklıklarının ortalaması ise 169 °C (136 °C ile 182.7 °C aralığında), tuzlulukları from 0.70 ile 15.86 wt. % NaCl eq aralığında hesaplanmıştır. Her iki örnek içinde elde edilen tuzluluk oranları göreceli düşük tuzluluk olarak hesaplanmıştır.

Cevherleşme ile eş zamanlı oluşan kuvars kristallerinden akışkana göre hesaplanmış $\delta^{18}O_{(akışkan)}$ değerleri -5,69‰ ve -1,77‰ arasında değişmektedir. Cevherleşme ile eş zamanlı oluşan tüm kayaçtan (jasper) elde edilen $\delta D_{(akışkan)}$ değerleri -105,79 ve 101,87 aralığında yer alamaktadır. Sıvı kapanımı ve duraylı izotop çalışmaları jasperoidleri

ve cevherleşmeyi oluşturan akışkan yüzey suları karışmış formasyon suyu olduğunu göstermiştir. Cevherleşme ile eş zamanlı oluşmuş tarak dokulu kuvarslardan alınan stibniteait $\delta^{34}S$ değeri -0,6'dır. Cevherleşmeyi oluşturan meteorik akışkanlar ultramafik kayaçlar içinde sürekli dolaşımda olduğu için bu $\delta^{34}S$ değeri kükürtün magmatik kökenli olduğu önermektedir. Carlin-tipi altın cevherleşmeleri için dekarbonatlaşma ve çökme breşlerinin eşlik ettiği silisleşme tipik özelliklerdir. Bu tip oluşumlar Keşkek tepe cevherleşmelerinde görülmektedir. Buna ek olarak Ana sıkışma evresini takiben oluşan normal faylar ve bu faylar boyunca gerçekleşen silisleşme Carlin-tipi cevherleşmelere benzer yapısal karakteristikleri ve oluşum mekanizmalarını içermektedir. Dolayısıyla, cevherleşmeleri kontrol eden yapısal ve jeolojik kontrollerin Carlin-tipi cevherleşmelere benziyor olması; cevherleşmeleri barındıran jasperlerin oluşumu mekanizmaları ve morfolojileri, Keşkek Tepe altın cevherleşmesinin Carlin benzeri bir cevherleşme olduğunu göstermektedir.

Anahtar Kelimeler: Carlin-Tipi, Jasper, Dekarbonizasyon, Sıvı Kapanımı, O Ve H Duraylı Izotop

To My Family...

ACKNOWLEDGMENTS

I wish to extend my best thankfulness to my supervisor Prof. Dr. İlkay KUŞCU for sharing his effective advices. Without his guidance and imprescriptible feedback, this thesis would not have been completed. I would love to thank you to him for providing me with the opportunity to study with him and allowing me to pursue my interest in ore deposits, and second for his comprehensive editing, valuable prompts and support over the last four years. Working with such a capable, considerate, and helpful advisor is a big chance for me.

I thank Meta Nikel Kobalt A.Ş. (a subsidiary of Zorlu Holding) management for giving a chance me to study in their licenses, sharing data, and also logistic support for the field works of this study. I would like to thank my manager Metin AVĞAN for his full support, help, and his understanding. I am grateful to all my friends from META; Tuna ERCİVAN, Eralp ŞEN, Murat PARLAYAN, Fatmagül PEHLİVAN, Harun KURT, and Şükrü Talha GÜNALTAY for their help whenever I need.

I would love to thank Mustafa Erde BİLİR and Göksu USLULAR. Without their help, thin section studies and geochemical data calculations cannot be succeeded.

I know I could not complete this thesis without Tuna ERCİVAN. His support, pump me up for writing up the thesis and our discussions on geology help me to complete this thesis. I will always remember what you have done for me. I owe you one.

I would like to thank Emine BOZKURT for her friendship and support whenever I need it.

Finally, I extend my most sincere and loving thanks to my family. I would like to dedicate this thesis to my family for all their love and encouragement.

TABLE OF CONTENTS

LIST OF TABLES

LIST OF FIGURES

1. INTRODUCTION

1.1. Purpose and Scope

Mineral deposits of Turkey generally occur as magmatic-related deposits such as porphyry copper-gold, skarn, epithermal (high sulfidation, low sulfidation, and intermediate sulfidation) and also volcanogenic massive sulfide deposits. These deposits are related to a series of magmatism in response to a collision between Eurasian and Afro-Arabian plates ranging from Late Cretaceous to Late Miocene (Yiğit, 2009 and 2012; Kuşcu et al., 2013).

The term "Carlin" was originated from the little settlements of Carlin in Northwestern Nevada (the US). It is used to refer to the linear arrangement of gold deposits called the Carlin trend where this type of gold deposits was first identified and explored (Michaud, 2015). The 5.2 % of the earth's gold production is supplied from Carlin-type deposits (Goldfarb, 2016). Carlin-Type Au deposits can be described widely as silicified replacement rock bodies formed by decarbonatization of dirty carbonates (silty-limestone or clay including limestones), (Cline et al., 2005). The Carlin deposits discovered and mined to date have various Au content and grades that change one district to another. For example, ten deposits on Carlin Trend, Getchell, and Battle Mountain-Eureka deposits contain more than 5 million ounces (Moz) of Au, and four deposits were calculated to contain more than 10 Moz of Au. The total gold content of these deposit clans is likely to exceed 50 Moz by more exploration works (Cline et al., 2005).

Keşkek Hill Au mineralization in Gördes (Manisa, Turkey), the main focus of this thesis, share some geological features and structural controls similar to those defined in Carlin-like gold deposits. The prospect has been discovered by Meta Nickel Cobalt Inc., and the exploration work is still going on for more details. 22 diamond drill holes (total of 2366 meters) collared on Keşkek Hill, have been completed in the prospect during spring and summer 2018. The resource calculations based on 0.5 ppm Au cut off and 0.7 ppm Au average was obtained by the company. Block model has been

prepared by using 22 drill holes and average gold content calculations and this model shows that resource in the Keşkek Hill prospect as 60000 ounces of gold.

The major focus of the exploration work by the company was to identify the ore-bearing horizons and/or levels at the Keşkek Hill gold prospect, and the data on the general geological characteristics alteration of the host carbonate rocks, mineralogical assemblages have been missing. The lacking of information wall rock alteration, fluid inclusion, and mineralogical features of the mineralization resulted in poor definition and classification of the deposit. Besides, no sound data to infer to the source of hydrothermal fluid, and also poor understanding of structural controls during alteration and mineralization further complicates the better understanding of the mineralization at Keşkek hill. For these reasons, this study aims to; (1) determine the spatial characteristics and two – dimensional field distribution of alterations and ore bodies,; (2) identify the host and wall rock lithologies and their spatial associations with the mineralization, alteration, and structural elements; (3) determine the structural controls of the mineralization; (4) determine the geochemical and lithogeochemical features of the silicified rocks (jasperoid); (5) microthermometric analyses of the alteration to understand the physicochemical conditions and evolution of ore-forming fluids.

1.2. Geographic Setting

The Keşkek hill prospect is located in Gördes (Manisa-Turkey, Figure 1.1). The nearest village, Kerpiçli, and Hanpaşa. Kerpiçli Village is located approximately 1 km NE to study area and, Hanpaşa is located approximately 4-5 km SW to study area. The prospect is 4 km far away from the operational base of the Nickel plant site of META NICKEL COBALT INC at Gördes. The study area covers the whole concession of the company and is accessible by an asphalt road via META NICKEL COBALT INC. Gördes Nickel plant site (Figure 1.1).

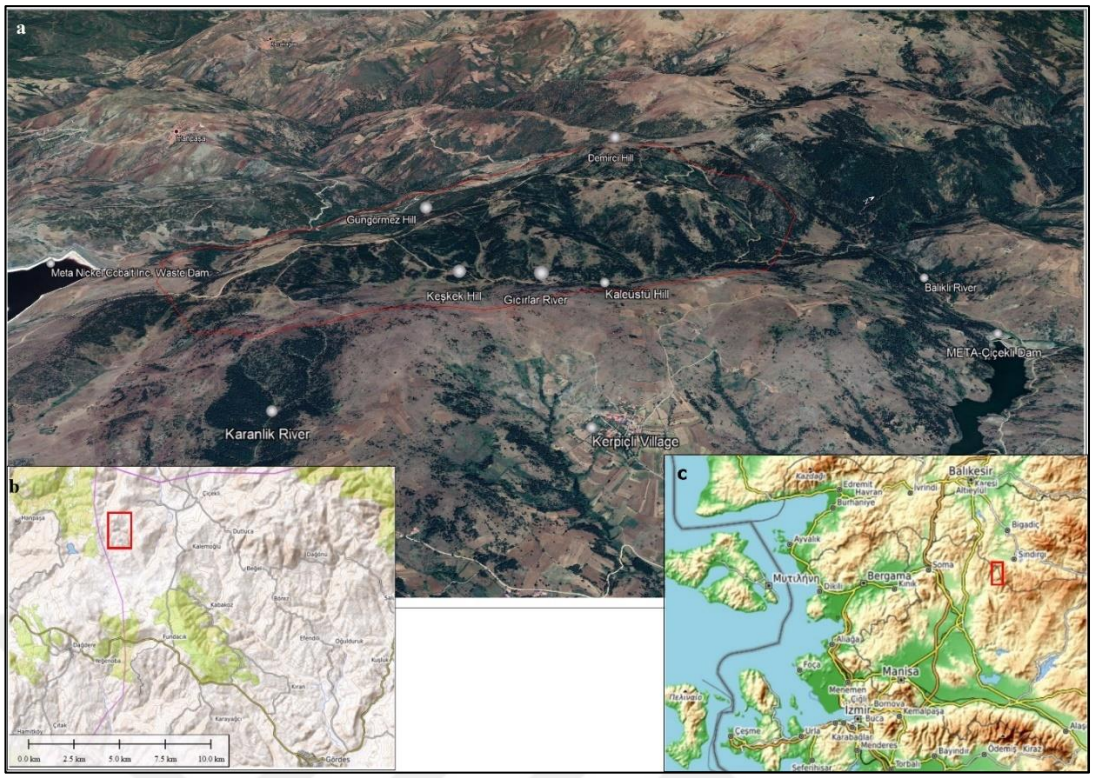

Figure 1.1. (a) Geographic setting of the study area showing the license and study area along with Nickel plant site; (b) geographic setting of the study area showing Gördes and nearest villages; (c) general view of Western Anatolia (Red square in maps is study area)

The study area has a relatively smooth topography. The highest elevation in the area is approximately 1100 m and the lowest elevation is approximately 854 m. Four important hills (Keşkek Hill, Demirci Hill, Gungormez Hill, and Kaleüstü Hill) are observed in the area. Three mainstreams traverse the area; the Gicirlar river flows from south to north and it merges with the Balikli river which flows from east to west (Figure 1.1). The third one is the Karanlık river which flows from west to east in the eastern part of the study area. A dam (Çiçekli Dam) build by the corporation between General Directorate of State Hydraulic Works-META NIKEL COBALT INC is located in the NE corner of the study area.

1.3. Previous works on Study area and surroundings

The first study in Gördes and the surrounding area belongs to Tchihatcheff (1850) who explained that Azimdag zeolites in the western part of Gördes and metamorphics around Marmara Lake.

Arpat and Norman (1961) examined the Hasköy formation in the eastern part of Akhisar covering the rock units within the study area, and termed them as schist and classified two marble levels transition to the schists. They assigned Paleozoic age for marbles and schists and classified Jura-Cretaceous limestone above them as discordant. Serpentinized gabbros and diabase, sandstone, grey sandstone, marl, and radiolarite group in the upper levels as intrusive (Apart and Norman, 1961).

Nebert (1961a and 1961b) worked on the age and general characteristics of the volcanic rocks between Akhisar and Gördes. According to him volcanic rocks in the area are granitic to granodioritic in composition, and the ages range from lower to middle Miocene.

Canik (1962) classified two types of limestone in Gördes basin, one on the other with discordance, and assigned Upper Jurassic-Lower Cretaceous age for the lower one using fossils; and the upper one was said to be Upper Cretaceous. Upper Cretaceous Mixed Series ophiolites sit on limestones as discordance from Upper Cretaceous to Paleocene. The researcher identified three discordances.

According to Dubertret and Kalafatçıoğlu (1973), in Gördes River, conglomerate and Permian-Mesozoic limestones were deposited on Precambrian Paleozoic metamorphic rocks. Ultramafic rocks are located on Maastrichtian limestones.

Yağmurlu (1984) stated that the Gördes basin begins with early Miocene alluvial fans (Göcek Formation) and take place unconformably upward to middle Miocene Yeniköy formation and Küçükderbent formation. Miocene acidic volcanic rocks cut the Küçükderbent formation.

Helvacı (2015) stated that Menderes Massif to the east and ophiolitic mélange components of the Bornova flysch zone to the west are bordering the Gördes Basin.

He divided the Gördes basin-fill into two sections; lower part starting with sedimentary units which a boulder conglomerate and coarse to medium sandstones passing upwards to marls of early-middle Miocene, and an unconformably overlying upper sedimentary unit including basal conglomerate, alteration of tuff (Zeolite), marl and silicified limestone of Pliocene.

The Bornova Flysch Zone (BFZ) is located between İzmir-Ankara-Erzincan suture northwest and the Menderes Massive in the southeast. BFZ is a regional olistostrome-melange belt in western Anatolia (Okay et al., 2012). Bornova zone units are thrusted over the Karakaya Complex and related Triassic clastic sediments of the Sakarya zone in the north (Robertson et al., 2009). Robertson et al., (2009) divided the Bornova zone units two different, but related mélanges. The first divided part explained by them sedimentary – volcanic units of BFZ. BFZ ophiolitic mélange named as the second type by Robertson et al., (2009). This type includes ophiolitic and pelagic sedimentary blocks (Robertson et al., 2009). BFZ ophiolitic blocks include generally serpentinized peridotite, gabbro, diabase, and basalt (Okay et al., 2012). The percentage of the ophiolitic blocks increases with expanding of limestone blocks in the southeast direction, in Sındırgı the BFZ determined as ophiolitic mélange (Okay et al., 2012).

1.4. Methodology

Studies pertaining to this project were carried out in six stages: (I) desk/office studies; (II) field works performed during the summer-spring period of 2018-2019 on the study area; (III) petrographic studies; (IV) geochemical studies; (v) fluid inclusion works, and (vi) office works to evaluate the results and writing up.

1.4.1. Desk studies

Desk studies involve the planning for field works and digitizing the geological maps after field works. Besides, a literature survey for the compilation of the previous works for regional and local geology along with data related to Nickel mineralization at the prospect has been completed during desk studies. Besides, drill hole data has been compiled where available and were georeferenced.

1.4.2. Fieldworks

The field works began in mid-spring 2018 and were completed by the end of September 2019. During the filed works, the geological units and alterations have been mapped at a scale of 1/10000. Google Earth images used as a base map for geological mapping purposes.

During the field works and mapping, samples representative of alterations and lithologies have been collected. The sampling involves grab, channel sampling, and core sampling. The grab samples refer to 2-3 kg of samples taken randomly from the silicified outcrops at the ore bodies. The channel sampling refers to channels along with V-shape cuttings of 2-3 cm deep and at least 1.5 m long (Figure 1.2). The samples have been used for geochemical analysis, fluid inclusion, isotope characteristics, and petrographic studies. 52 grab rock samples were collected from different locations in the study area. 47 channel samples have been collected from jasperoidal outcrops in the field to have the gold grade and gold mineralization at the prospect (Figure 1.2).

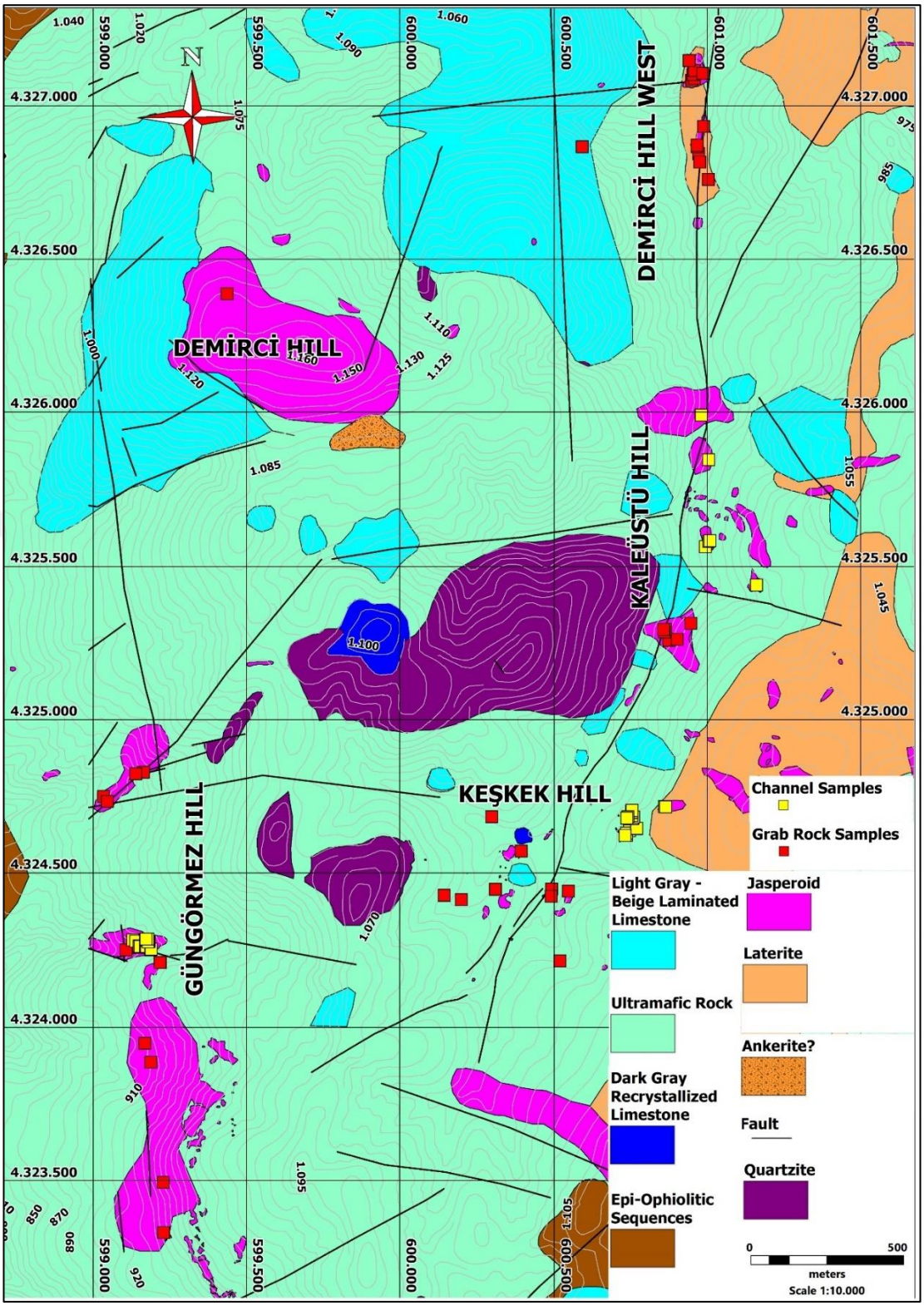

Figure 1.2. Surface grab and channel samples locations on alteration map of the Keşkek Hill study area

Seventeen drill holes totaling 1874.30 m were selected and re-logged to better understand the vertical extension of the alterations and mineralization (Figure 1.3). During logging, a total of 48 core collected. 1530 core sample has been taken. The locations of these drill holes are shown on the map (Figure 1.4) and also depth and directions of the drill holes given in Table 1.1.

Table 1.1. Keşkek Hill Project drill holes information table.

Project	Hole ID	Easting	Northing	Elevation	Azimuth	Dip	Depth (m)
Keskek	KT-1	600313.16	4324406.75	1017.02	110	45	67.20
Keskek	KT-2	600311.48	4324407.13	1016.61	0	90	120.00
Keskek	KT-3	600334.48	4324401.68	1014.77	270	45	109.00
Keskek	KT-4	600336.45	4324401.26	1014.68	0	90	83.00
Keskek	KT-5	600278.52	4324380.90	1017.50	110	45	113.40
Keskek	KTS-6	600484.52	4324434.02	987.33	60	45	121.50
Keskek	KTS-7	600482.80	4324433.42	987.39	60	75	101.20
Keskek	KTS-7A	600482.07	4324433.17	987.28	60	75	43.50
Keskek	KTS-8	600345.18	4324484.93	1010.41	60	45	122.50
Keskek	KTS-9	600343.21	4324484.24	1010.55	60	75	91.50
Keskek	KTS-10	600345.09	4324449.27	1014.14	60	45	131.00
Keskek	KTS-11	600343.41	4324448.61	1014.24	60	75	131.00
Keskek	KTS-12	600362.26	4324311.37	999.37	60	45	171.00
Keskek	KTS-13	600360.35	4324310.24	999.53	60	75	153.10
Keskek	KTS-14	600361.93	4324310.57	999.45	180	45	163.10
Keskek	KTS-17	600342.25	4324509.95	1007.21	60	45	73.60
Keskek	KTS-18	600339.88	4324509.21	1007.29	0	90	112.50
Keskek	KTS-19	600321.63	4324375.43	1015.32	60	45	138.00
Keskek	KTS-20	600318.80	4324374.38	1015.84	0	90	128.50

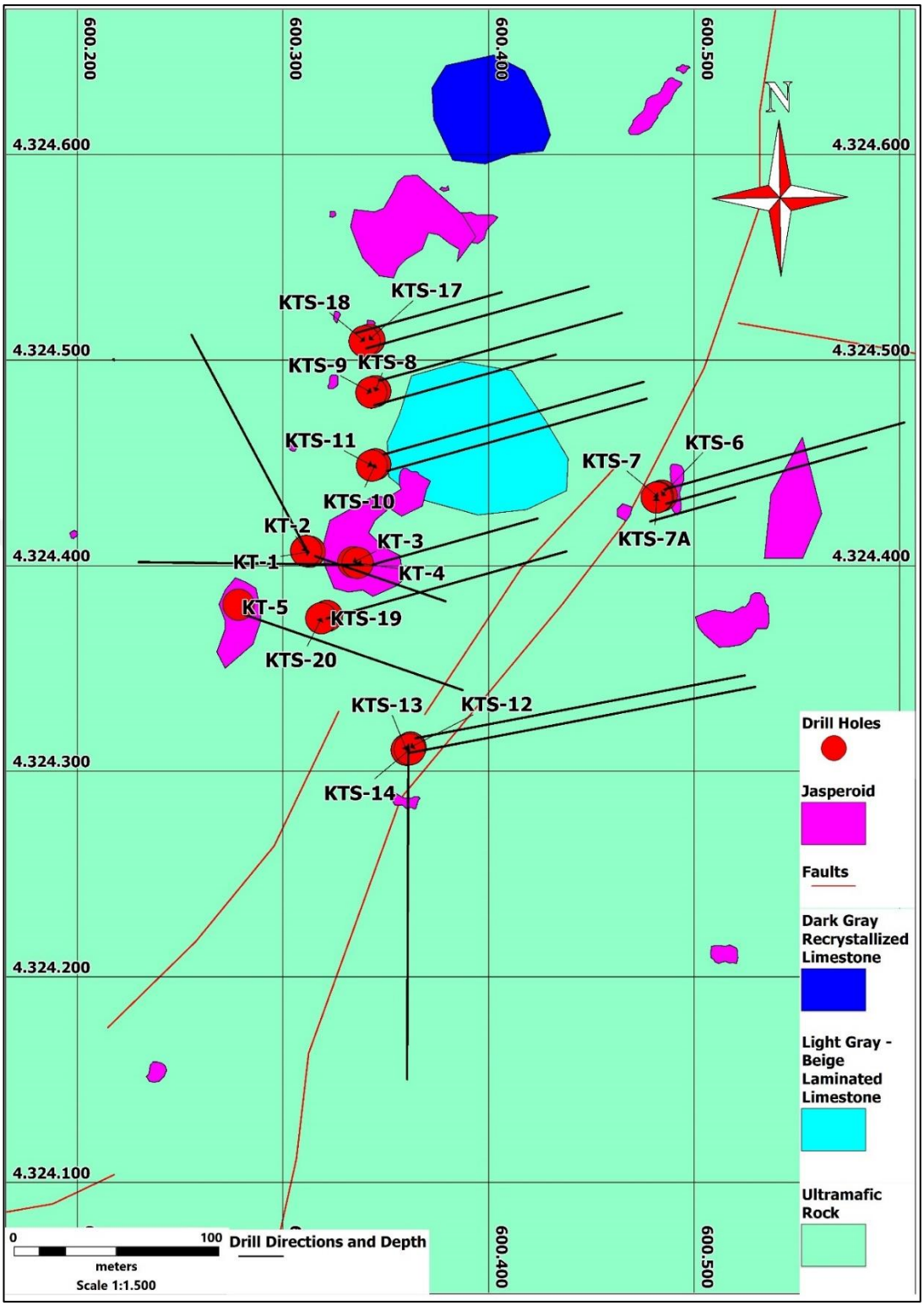

Figure 1.3 Detailed map showing drill locations in Keşkek Hill Orebody

1.4.3. Laboratory studies

The laboratory studies include (1) petrographic studies, (2) sample selection for geochemical analyses including isotopes and whole-rock, sample selection for fluid inclusions, (3) geochemical analyses, and (4) fluid inclusion analyses. Petrographic studies were conducted on a total of 19 rock samples that were thin-sectioned for microscopic examination, and a total of 3 samples were polished for ore microscopy studies at Geological Engineering Department of Middle East Technical University (METU). All of the thin and polished sections were examined using Leica DM EP refracted and reflected light microscope at Geological Engineering Department of Muğla Sıtkı Koçman University (MSKU). Petrographic studies helped to select samples for fluid inclusion, isotope analyses, and whole-rock analyses. For the whole rock analyses, the least altered samples identified during petrographical studies have been determined. The altered rock samples with abundant silicification and quartz-calcite veins have been selected for fluid inclusion works and isotope analyses.

1.4.3.1. Stable isotope analyses

Based on petrographic works, 3 samples from the alteration zones within the Keşkek hill ore body have been selected for oxygen, hydrogen, and sulfur (O-H-S) stable isotope analyses. The sample preparation for O, H, and S stable isotope analyses was done at the Geological Engineering Department of Muğla Sıtkı Koçman University (MSKU). The stable isotope analyses were done at Queen's Facility for Isotope Research (QFIR) of Queen's University Canada. The sample preparation including cutting into slices and mineral separation for stibnite were held at Muğla Sıtkı Koçman University (MSKU, Muğla, Turkey). Oxygen isotope analyses have been conducted on syn-ore stage quartz. Hydrogen isotope analyses performed on the same rock (whole rock sample) that contains syn-ore stage quartz (Q-1) veinlet Sulfur stable isotope analyses have been carried out on stibnite formed during second phase quartz veinlets and silicified jasperoidal rocks (jasperoids and quartz veins; QSB-1 syn-to-post ore stage) (Figures 1.4 and 1.5).

Figure 1.4. Q-1 sample syn-ore stage quartz veinlets included jasperoid

4.5 gr of quartz for oxygen isotope analyses, 0.65 gr of stibnite for sulfur isotope analyses (Figure 1.5), and 52 gr of whole-rock sample for hydrogen isotope analyses have been used for the analyses. Oxygen, hydrogen, and sulfur isotope analyses were done in Queens University Facility for Isotope Research Laboratory. Stibnite crystals were separated from approximately 1.5 kg of the sample containing quartz-stibnite and jasperoid-stibnite was selected from jasperoid core samples (Figure 1.5).

Sulfur isotope samples were weighed into tin capsules and the sulfur isotopic composition measured using a MAT 253 Stable Isotope Ratio Mass Spectrometer coupled to a Costech ECS 4010 Elemental Analyzer. δ34S values were calculated by normalizing the 34S/32S ratios in the sample to that in the Vienna Canyon Diablo

Troilite (VCDT) international standard, values are reported using the delta (δ) notation in units of permil (‰) and are reproducible to 0.2 permil.

Oxygen was extracted from 5mg sample at 550-600°C according to the conventional BrF5 procedure of Clayton and Mayeda (1963) and analyzed via a dual inlet on a Thermo-Finnigan DeltaPlus XP Isotope-Ratio Mass Spectrometer (IRMS). $\delta^{18}O$ values are reported using the delta (δ) notation in units of permil (‰) relative to Vienna Standard Mean Ocean Water (VSMOW) international standard, with a precision of 0.4‰.

The whole-rock sample for hydrogen isotope was weighed into silver capsules, degassed for 1 hour at 100°C then crushed and loaded into a zero-blank autosampler. The hydrogen isotopic composition was measured using a Thermo-Finnigan thermo-combustion elemental analyzer (TC/EA) coupled to a Thermo-Finnigan DeltaPlus XP Continuous-Flow Isotope-Ratio Mass Spectrometer (CF-IRMS). $\delta^{2}H$ values are reported using delta (δ) notation in permil (‰), relative to Vienna Standard Mean Ocean Water (VSMOW), with a precision of 3‰.

Figure 1.5. Stibnite crystals separated for sulfur isotope analyses collected from QSB-1.

1.4.3.2. Fluid inclusion analyses

During petrographic analysis, two samples with silicified outcrops and quartz veins were selected for fluid inclusion works. Fluid inclusion sections were prepared at the General Directorate of Mineral Research and Exploration (MTA). Microthermometric works on fluid inclusions were done at Fluid Inclusion Laboratory of Ankara

University by using Leica DM LP (Leica THMSG 600) microscope. The fluid inclusion studies involve the analyses of 22 fluid inclusion from a total of two doubly polished sections collected from jasperoidal rocks and quartz veinlets in jasperoids. Fluid inclusion samples were prepared on the basis of a method defined by Roedder (1963). A total of two doubled polished section ~150μm thick sections were prepared at Petrographical laboratories of the General Directorate of Mineral Exploration (MTA). The polished sections then were attached to Leica DM LP microscope LINKAM THMSG 600 TS 1500 with the heating-freezing stage in Earth Science Applications and Research Center of Ankara University (Figure 1.6), and the samples were then incrementally heated and frozen.

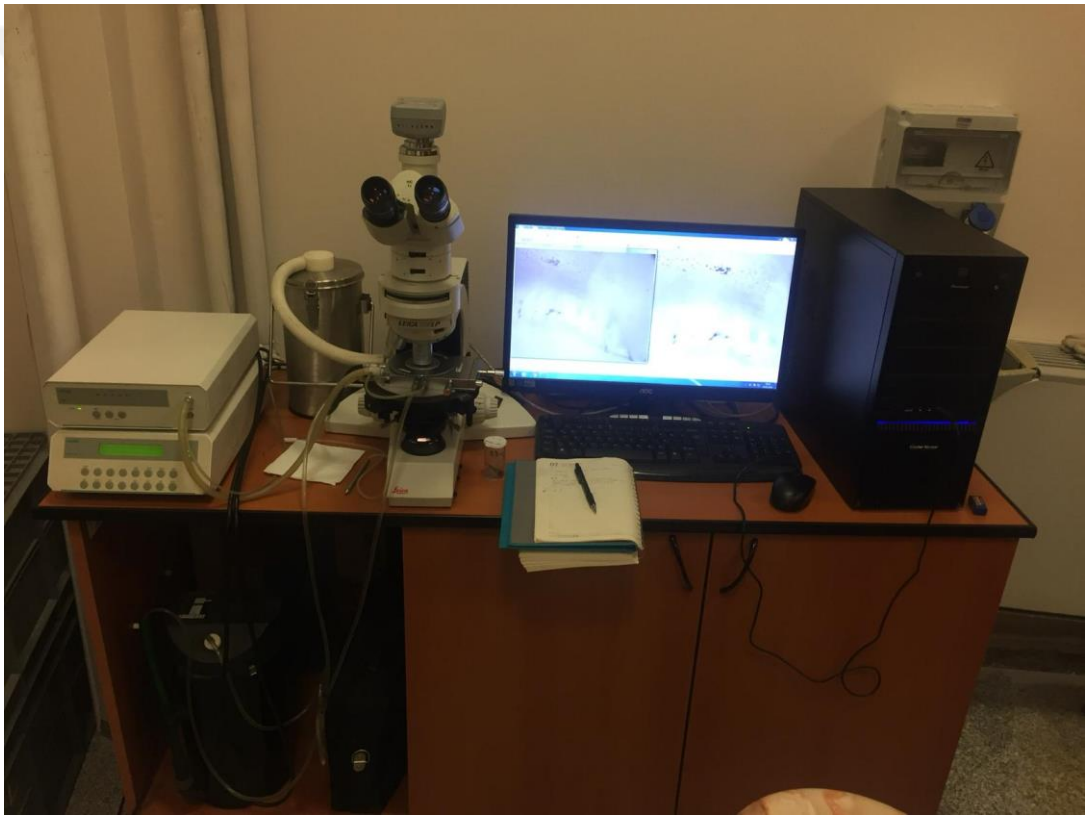

Figure 1.6. Leica DM LP microscope LINKAM THMSG 600 TS 1500 used for fluid inclusions from double polished sections.

The geochemical analyses for precious metals have been carried out using inhouse analytical facilities. The grab and channel samples collected from the ore bodies have been analyzed in Meta Nikel Kobalt Inc. laboratory by using the fire assay analysis method. Fire assay is considered the best reliable method for accurately determining the content of gold. This method includes melting a gold-bearing sample in a clay crucible with a mixture of fluxes (in this laboratory fluxes includes 20 gr of borax, 60 gr of lead oxide, 35 gr of sodium carbonate, and as a reducing agent 3 gr of flour). The fluxes decreasing the melting point of the oxidic materials, allowing them to fuse, and molten litharge is reduced by the flour to extremely fine drops of lead dispersed throughout the charge. The drops of lead dissolve the gold then coalesce and gradually descend through the sample to form a metallic layer at the bottom of the cruible. After cooling, the lead “pearl” is separated from the slag layer and heated under oxidizing conditions to oxidized and eliminate the lead. The bead is boiled in nitric acid to dissolve the silver, and the gold residue is weighed.

2. REGIONAL GEOLOGY

Different geological units starting with Paleozoic which are observed in the area (Figure 2.1). These units are summarized below according to their geological times. The study area is part of the rock units from the Bornova Flysch zone (BFZ) that consists of sedimentary rocks and ophiolitic mélange from the Izmir-Ankara-Erzincan Suture zone (IAESZ). These form the basement rocks. The basement rocks are overlain by Neogene cover rocks consisting of sedimentary and volcanic rocks collectively deposited within the Gördes basin.

2.1. Basement Rocks

The Bornova Flysch zone and ophiolitic mélange form the oldest rock in the region covering the study area. It represents a sedimentary mélange with blocks of ultramafic rocks derived from IAESZ. The BFZ is juxtaposed to Menderes core complex (MCC) along a regional İzmir-Balıkesir Transfer Zone (IBTZ) (Figure 2.2a), and are known to be part of regional ophiolitic mélange (Figure 2.3). The ophiolitic mélange represents the larger Izmir-Ankara-Erzincan suture zone (IAESZ) (Figure 2.1) The IAESZ represents a suite of high-pressure low-temperature (HP-LT) and greenschist facies rocks of the former Eurasian continental margin accreted to Anatolides and metamorphosed from Late Cretaceous to Eocene times. It refers to the former subduction zone of Neotethys beneath Eurasia overlain by the Late Cretaceous-Paleocene ophiolitic Bornova flysch (Okay and Siyako, 1993). It consists of several types of ultramafic rocks including peridotites (dunite and harzburgite) and serpentinites are observed in the lower levels of the Bornova flysch zone, and upper parts consist of deep-sea sediments (e.g., radiolarite, claystone, sandstone), limestone and igneous rocks (e.g., gabbro, diabase, spilite, and basalt). Depending upon the fossil ages found in the sedimentary rocks, age of the ophiolitic mélange an Upper-Cretaceous age is assigned (Konak et al., 1980).

2.2. Cover Rocks

The ophiolitic mélange units of the Bornova flysch zone to the west are delimited by the Gördes basin (Helvacı, 2015) (Figure 2.1), and has previously been investigated by Nebert (1961a and 1961b), Yağmurlu (1984), Seyitoğlu and Scott (1994a, b), Purvis and Robertson (2004). The basement units together with granitic plutons were unconformably overlain by volcano-sedimentary succession that comprises intercalations of thick fluvial and volcaniclastic deposits within the Gördes basin. Gördes Basin is characterized by lacustrine sedimentary rocks at the base and volcanic and volcano-sedimentary rocks on top (Figure 2.3).

The lacustrine basal part of the basin starts with sedimentary units which a boulder conglomerate and coarse to medium sandstones passing upwards to marls of early-middle Miocene, and an unconformably overlying upper sedimentary unit including basal conglomerate, alteration of tuff (zeolite), marl and silicified limestone of Pliocene. (Figure 2.3). Yağmurlu (1984) states that the basin fill begins with early Miocene alluvial fans (Göcek Formation) and grades upward into middle Miocene Yeniköy formation and Küçükderbent formation. Miocene acidic volcanic rocks cut the Küçükderbent formation. Küçükderbent formation overlain by tuffs (Karaboldere formation). These Formations are covered by late Miocene Ahmetler formation which is composed of alluvial fans (Figure 2.3, and 2.4). The basal part of the basin is represented by the conglomerates and sandstones of the Dağdere formation in the north and Tepeköy formation in the south. Sandstone-mudstone alternation of Kuşlukköyü formation, which is intercalated with acidic tuff, overlay the Dağdere and Tepeköy formations (Helvacı, 2015). The Kuşlukköy Formation covers a large area throughout the Gördes basin (Figure 2.5). The Formation includes conglomerate-sandstone and sandstone-claystone alternations of fluvio-lacustrine origin. The upper part of the formation is represented by marl and limestone. In the western part of the formation contains coal deposits (Çıtak and Dağdere villages) (Seyitoğlu and Scott, 1994a, b).

The volcanic and volcano-sedimentary rocks at the upper part of the basin consist of more than 400-meters-thick ignimbrites and ash fall deposits, which are dominant in the upper parts of the succession in the north-western part of the Eğrigöz and Koyunoba plutons (Figure 2.3).

The volcanic rocks, termed as Kayacık (18.4 ± 0.8 Ma – 16.3 ± 0.5 Ma) cut all the basin and also leucogranite dike (24.2 ± 0.8 Ma – 21.1 ± 1.1 Ma) observable in the eastern margin of the Gördes basin (Seyitoğlu and Işık, 2015) (Figures 2.3 and 2.5).

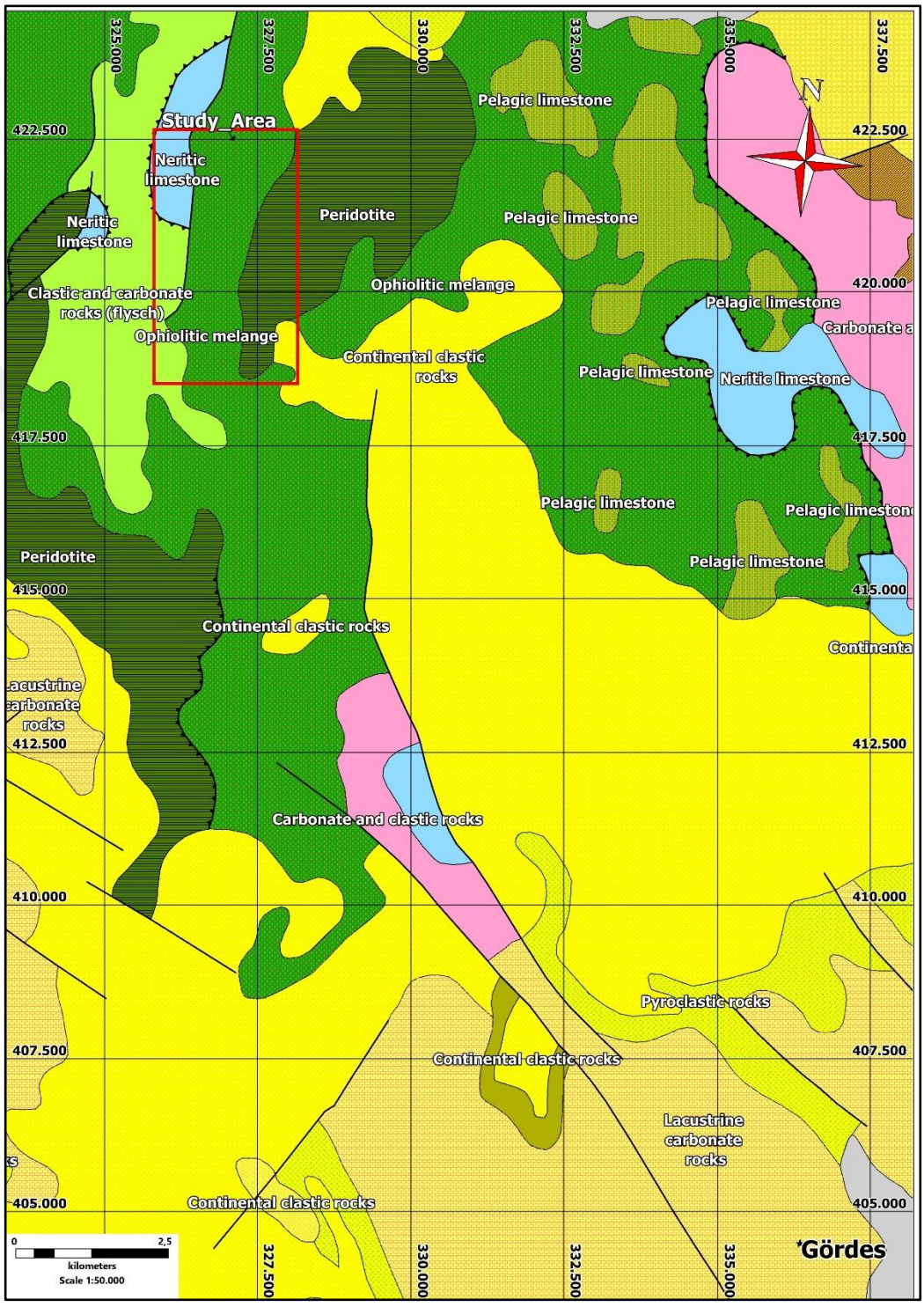

Figure 2.1. 1/500000 geological map of Turkey around Gördes (MTA, 2002) with red square encircling the study area.

.

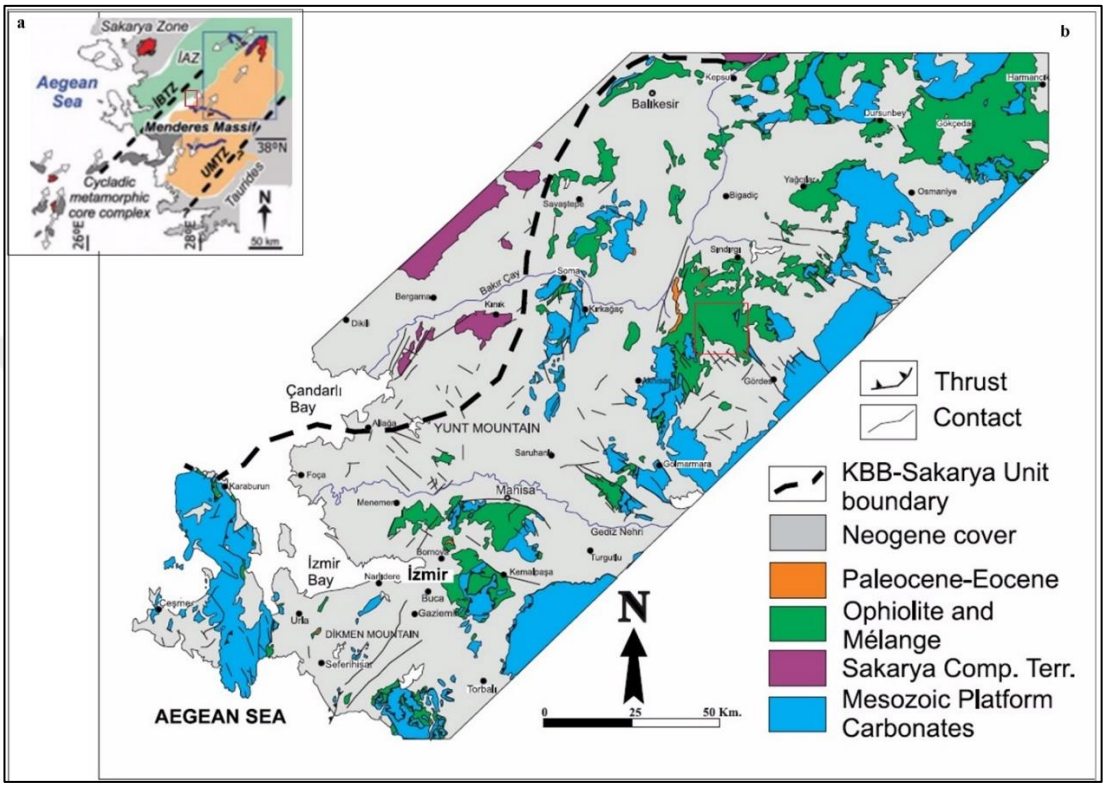

Figure 2.2. (a) İzmir-Balıkesir and Uşak-Muğla Transfer Zones (İBTZ & UMTZ) (b) Simplified geological map of Bornova Flysch Zone (simplified after MTA, 2002) (Erkül et al. 2017); (Red square showing study area).

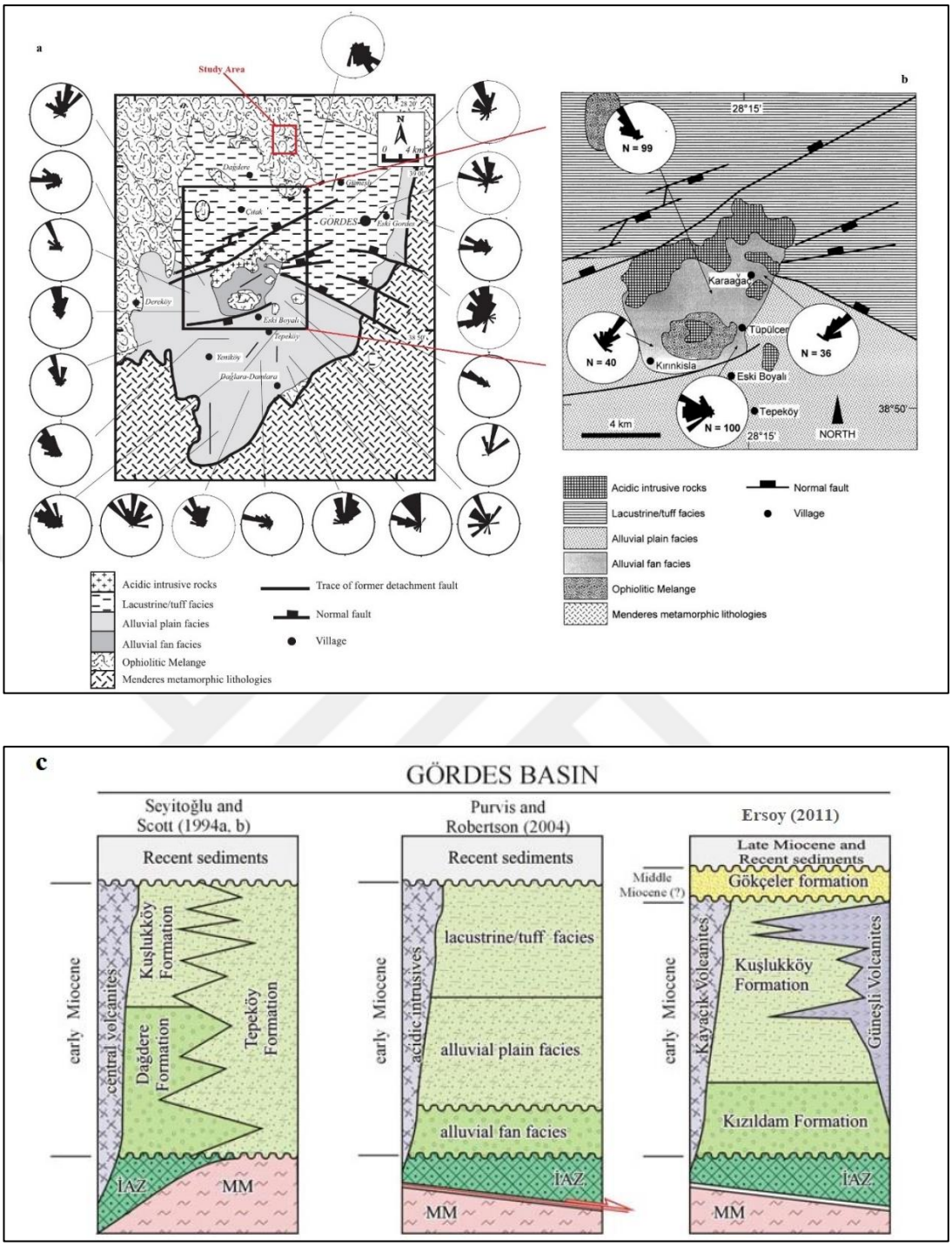

Figure 2.3. (a) Geological map of the Gördes basin also showing measured paleocurrent, the central area is enlarged in b (Purvis and Robertson, 2005); (c)The stratigraphic sections proposed for the NE–SW-trending Gördes basin. MM-Menderes Massif, İAZ-İzmir-Ankara Zone rocks, EG-Eğrigöz granitoid (Ersoy 2011).

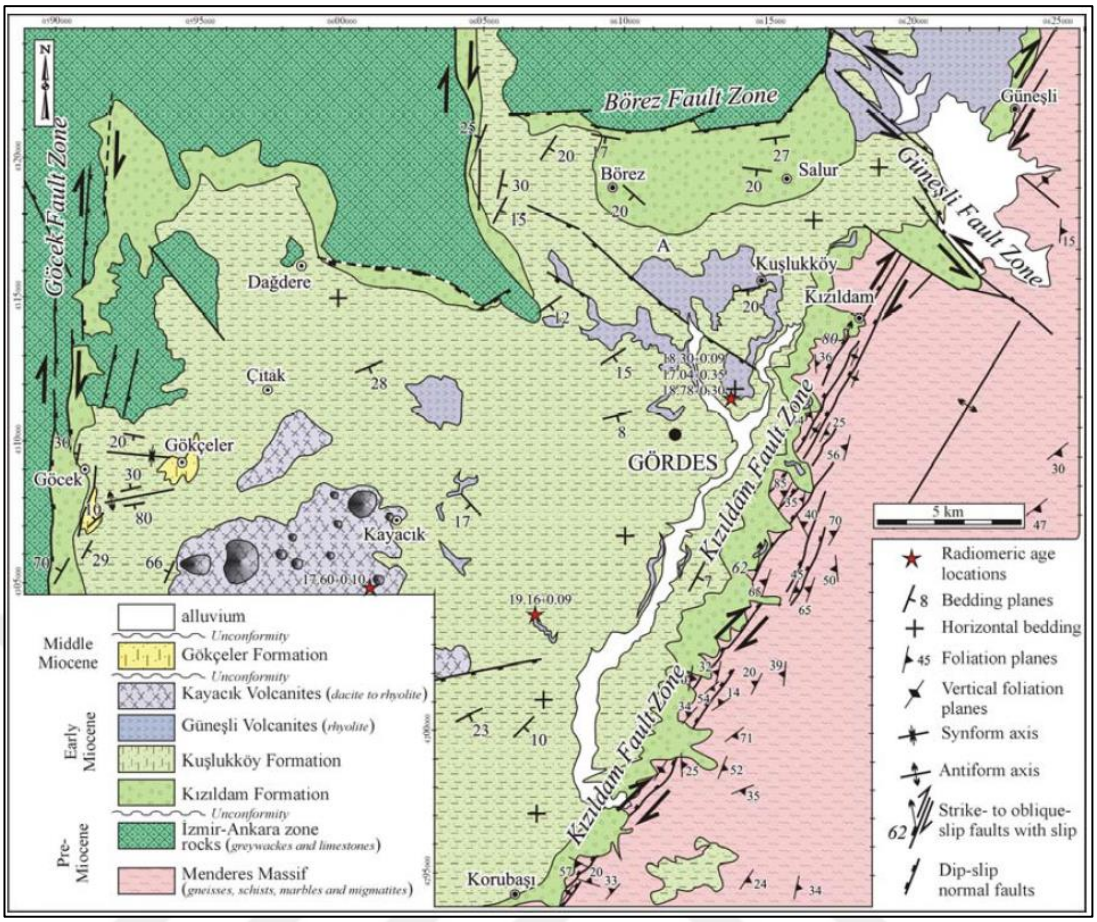

Figure 2.4. Geological map of Gördes basin (Seyitoğlu and Scott, 1994a, b; Ersoy, 2011)

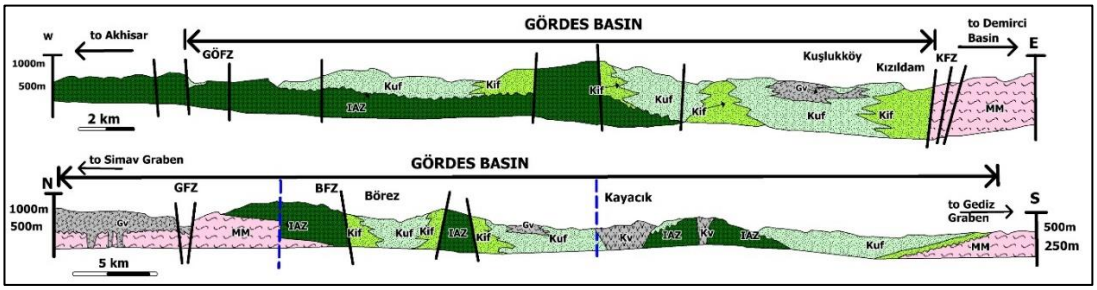

Figure 2.5. Geological cross-sections across the Gördes basin (modified from Ersoy, 2011). MM-Menderes Massif, İAZ-İzmir-Ankara Zone rocks, Kıf-Kızıldam Formation, Kuf-Kuşlukköy Formation, Gv-Güneşli Volcanites, Kv- Kayacık Volcanites, GFZ-Göcek fault zone, Gfz-Güneşli fault zone, KFZ-Kızıldam fault zone.

3. LOCAL GEOLOGY

The study area is mainly covered by ophiolitic mélange with large blocks of limestones (Figures 3.1; 3.2 and 3.3), and epi-ophiolitic sedimentary rocks. Larger masses of circular to ellipsoidal exposure of quartzites are also present in the study area. The ultramafic rocks in the ophiolitic mélange are overlain by thick lateritic layers that could have traced for long distances (Figure 3.1). A quartzitic rock as an isolated block is also exposed to the central parts of the study area (Figure 3.1).

3.1. The Ophiolitic Mélange and Ultramafic Rocks

Ophiolitic mélange in the study area consists mainly of brecciated and intensively sheared, cataclastically deformed serpentinites, dunite, harzburgite (Engin and Özkan, 2008) and Jura-Cretaceous limestone blocks, radiolarites, and pelagic red mudstone-sandstone. The ultramafic rocks occupy more than %50 of the mapped rocks in the study area (Figure 3.1). Serpentinization and alterations of ultramafic rocks into the talk (Figure 3.4) predominate mainly along the shear zones. Serpentine is mostly developed on harzburgite and dunite. Unserpentinized equivalents of ultramafic rocks are exposed out of the study area in the north. The age of the ultramafic rocks is said to be Upper-Cretaceous (Engin and Özkan, 2008). They are rocks thrusted over the recrystallized and dark gray Jurassic limestones (Figure 3.3). The thrust planes and imbricated structure of the ophiolitic mélange have been offset by normal faults formed mainly during the western Anatolian extensional regime (Rojay, 2014).

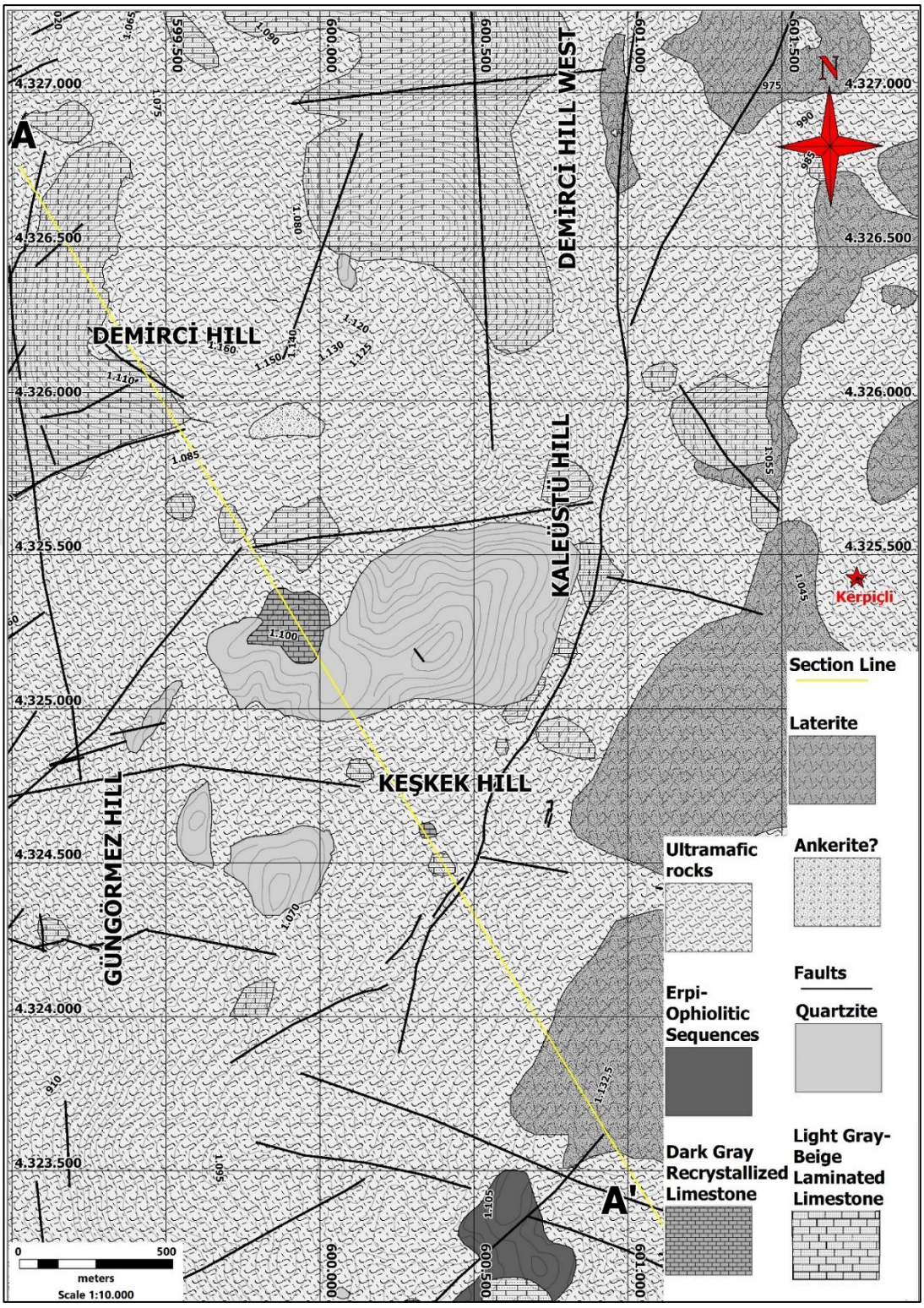

Figure 3.1. Geological map of the study area showing main rock units

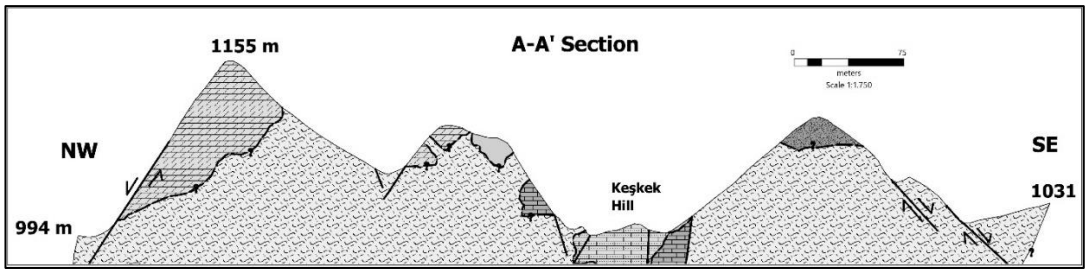

Figure 3.2. A-A' cross-section of the study area (symbols and explanation as in Figure 3.1).

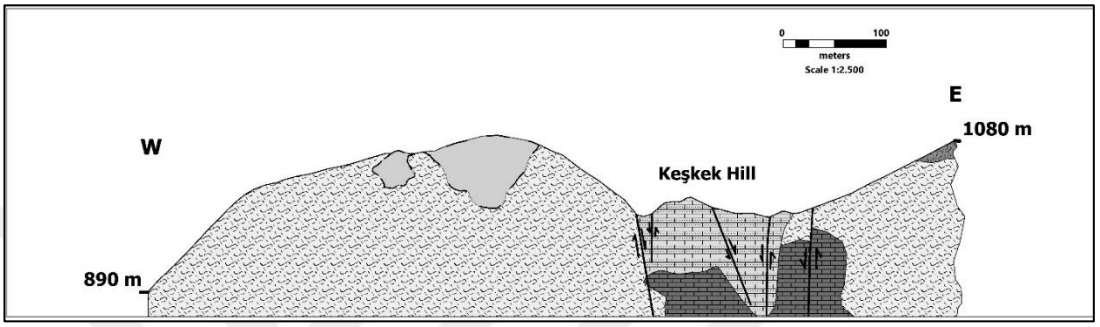

Figure 3.3. East to the west directed cross-section of the area, section line is the 4324500-grid line (symbols and explanation as in Figure 3.1).

Figure 3.4. (a) Talk formed mainly along with fractures, and (b) Serpentinized ultramafic rocks around the Demirci Hill.

3.2. Limestones

The limestones occur as isolated blocks within the sheared and serpentinized ultramafic rocks (Figure 3.5). The field studies and the examination of drill cores enabled the recognition of three types of limestones and matrix-supported breccia -in the study area. The limestones include (1) dark gray massive recrystallized limestone,

the oldest one Jurassic in age and forms the basement; (2) laminated and beige limestone Jurassic to Cretaceous in age; and (3) light-gray limestone Jurassic to Cretaceous in age (Konak et al., 1980).

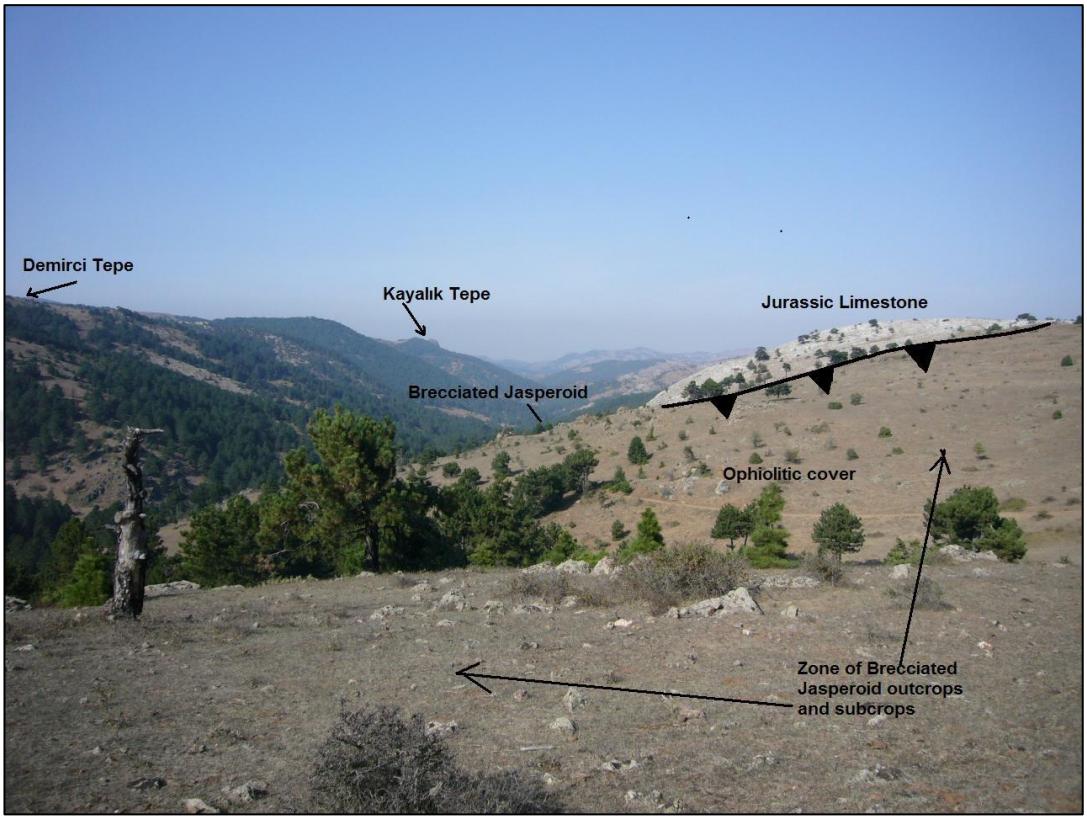

Figure 3.5. General view of ultramafic rocks at Kaleüstü Hill from south to north

3.2.1. Dark gray massive recrystallized limestone

Dark gray recrystallized limestones (RXL) exposed as blocks within the ophiolitic mélange are termed as Dark gray massive limestones in this study. They do not show bedding and exhibit massive nature (Figure 3.7). They are locally thrusted over by ultramafic rocks with blocks of beige limestone (Figure 3.6). The thrust plane between the limestone and ultramafic rocks were recognized at the deeply incensed valleys (Figure 3.6). Recrystallization is locally observed, this is mostly observed at the drill cores in particular. The petrographic studies, field observations, and alizarin red tests show that the RXL does not only contain recrystallized calcite but also dolomite as the main carbonate mineral (Figure 3.9). The dolomitization tends to increase at locations where the dissolution of calcite is identified. The petrographic observations also

showed that dolomite is replaced by calcite (Figure 3.9) along the microfracture zones, and this is referred to be dedolomitization. The rock effected by faulting exhibits cataclastic texture whereas the rest exhibits massive texture. The dark gray recrystallized limestones are traversed by sub-vertical quartz veins exhibiting comb textures (Figure 3.10). In places where the dissolution and massive silicification is recognized, the RXL is directly overlain by jasperoids (Figure 3.8a). The quartz veins exhibit irregular patterns and are likely to form a network of quartz veins.

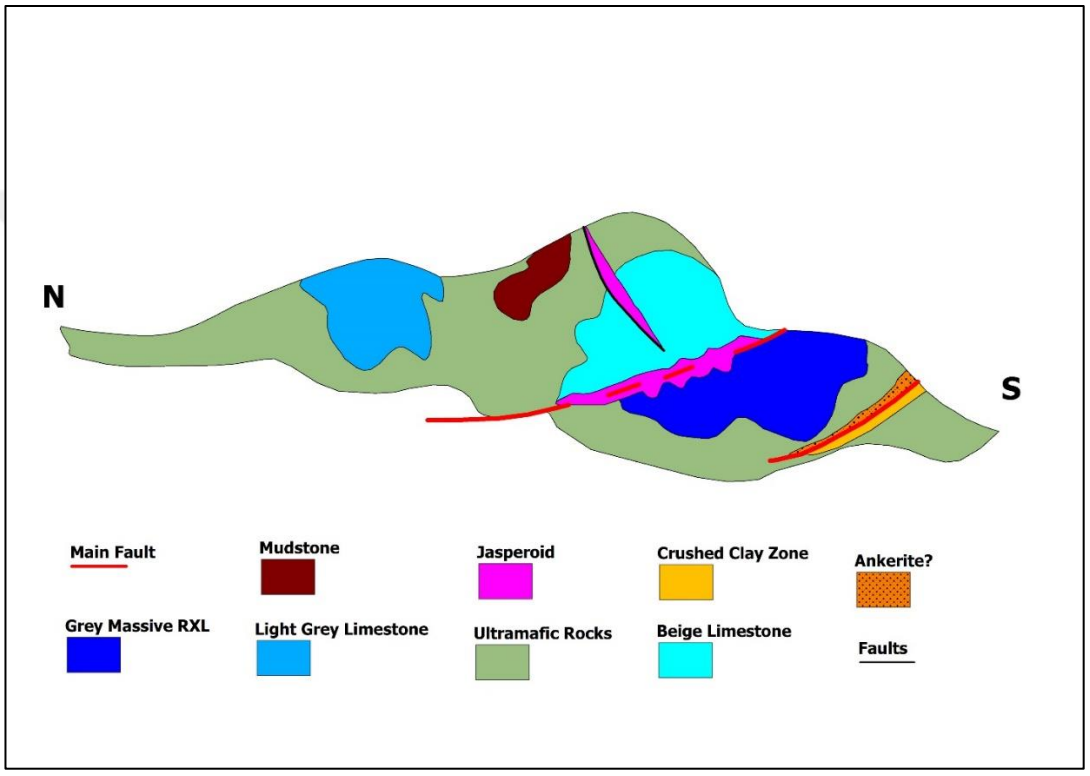

Figure 3.6. N-S cross-section showing the spatial and structural relations between the rock units in the study area (not to scale, modified from Kuşcu, 2018)

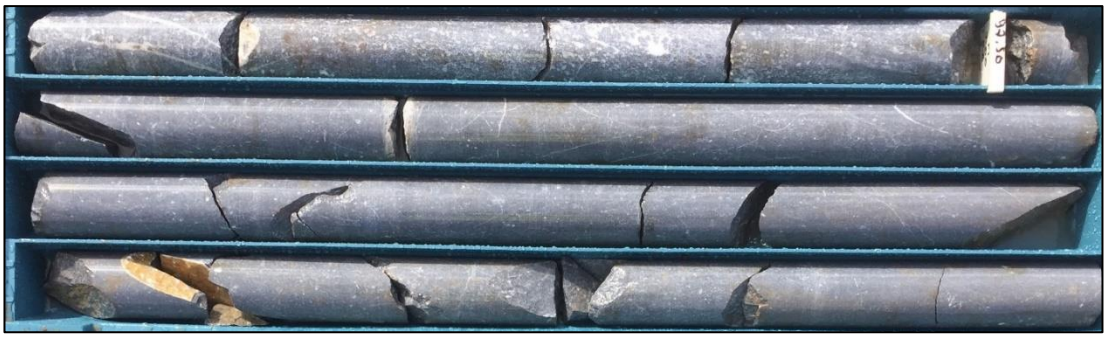

Figure 3.7. The core photograph for the gray massive recrystallized limestone intersected at one of the drill holes.

Figure 3.8. Field photograph showing (a) contact relations between jasperoidal rock and RXL (RXL at the bottom, mineralized zone, and low angle fault plane in red line), and (b) the overthrust fault and strongly sheared zone

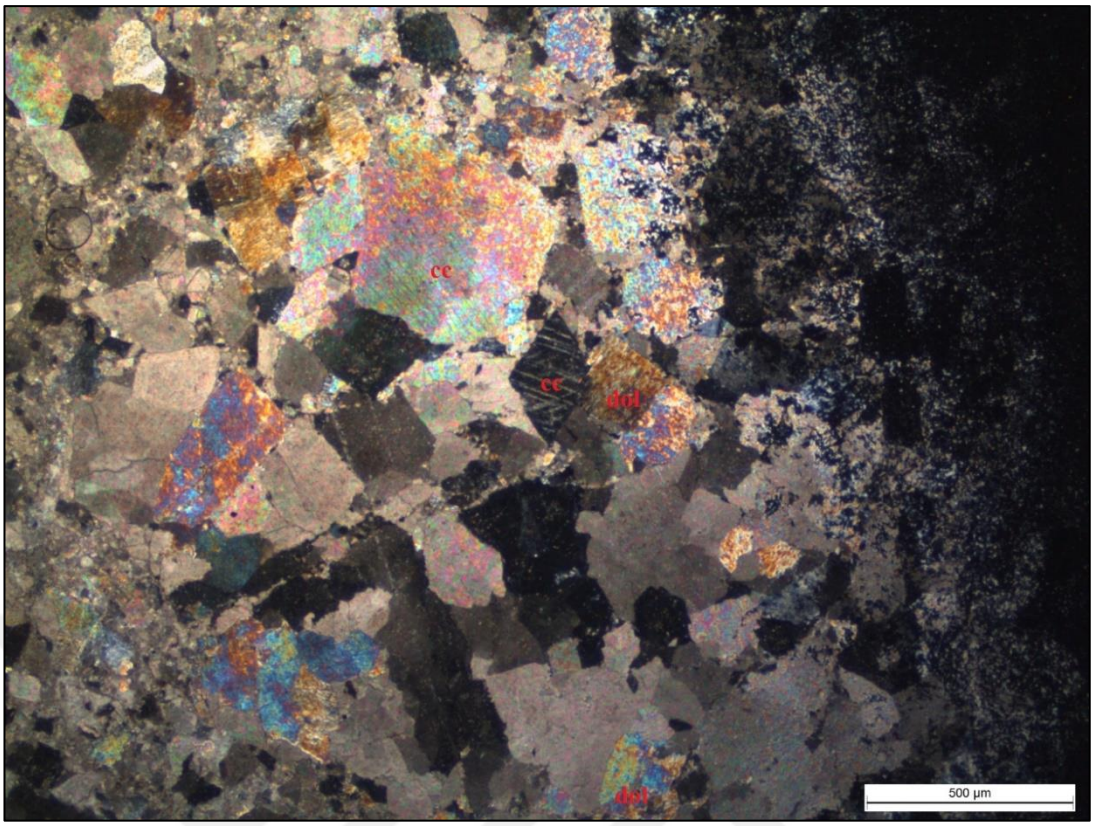

Figure 3.9. The photomicrograph showing dolomite (dol) and recrystallized calcite (cc) in gray recrystallized dolomitic limestone

Figure 3.10. Comb textured quartz vein traversing dark-gray recrystallized limestone

Konak et al. (1980) reported that it is fossiliferous, and a Jurassic age was assigned based on the fossil content (Okay and Güncüoğlu, 2004). The structural relations and overthrusting contact are also recognized at the drill cores in that that all the ophiolitic rocks tectonically overlie the gray massive recrystallized limestone (RXL).

3.2.2. Beige laminated limestone

The beige to whitish-gray limestones with laminated to thinly bedded nature (Figure 3.11) are termed as beige colored laminated limestone (BLL) in this study. The BLL locally contain silty laminations and micritic limestone layers as well and is cut by stockworking calcite (Figure 3.12) and bladed calcite textured veins. The alizarin red test on the samples from these rocks showed that the carbonate minerals are mainly of calcite (Figure 3.13). The petrographic studies showed that the rock consists mostly of a very fine-grained silty matrix cut by fine-grained stylolites of calcite veinlets (Figure 3.14).

Figure 3.11. The field photographs showing the BLL outcrop

The jasperoidal silicified rocks with gold mineralization in the area are hosted by BLL. It exhibits highly deformed nature as the ophiolitic rocks. The BLL is offset/displaced by E-W and N-S striking normal faults, and this appears to have formed stylolites in several directions (Figure 3.14).

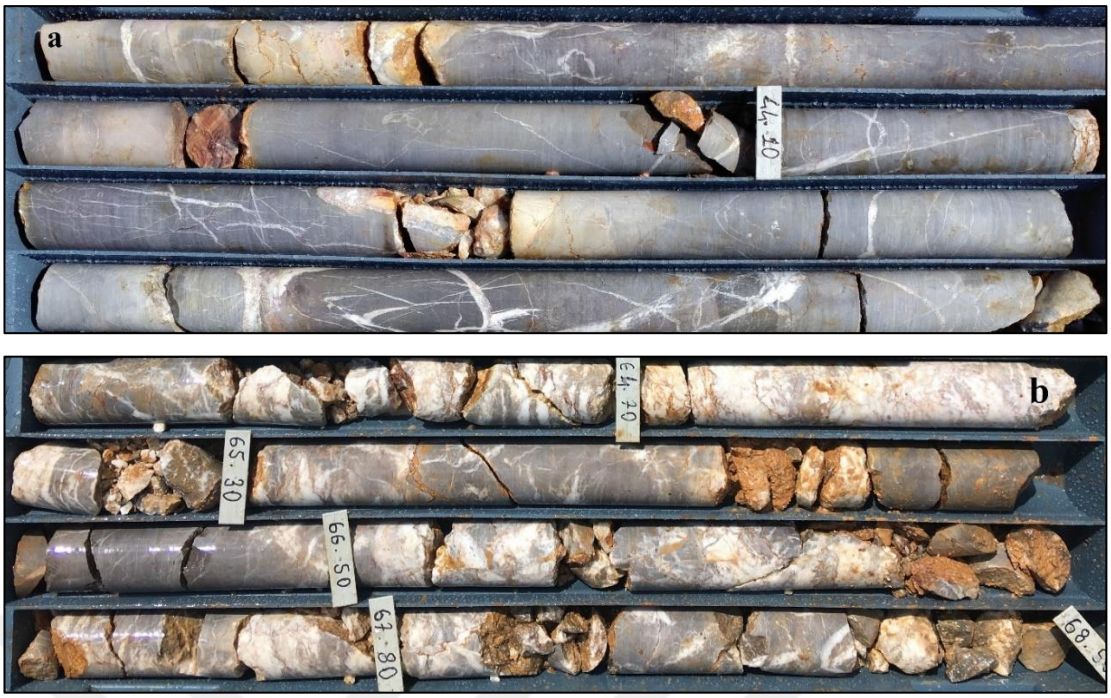

Figure 3.12. (a) Beige colored, laminated limestones and (b) stockworking calcite veins traversing the BLL, intersected at drill hole KTS-8

Figure 3.13. Alizarin red to test the composition of carbonate minerals at a sample from BLL.

Deformation by the normal faults is evidenced by stylolite occurrences. The petrographic observations revealed that some of the calcite veins contain recrystallized limestone suggesting that weak metamorphism (Figure 3.14).

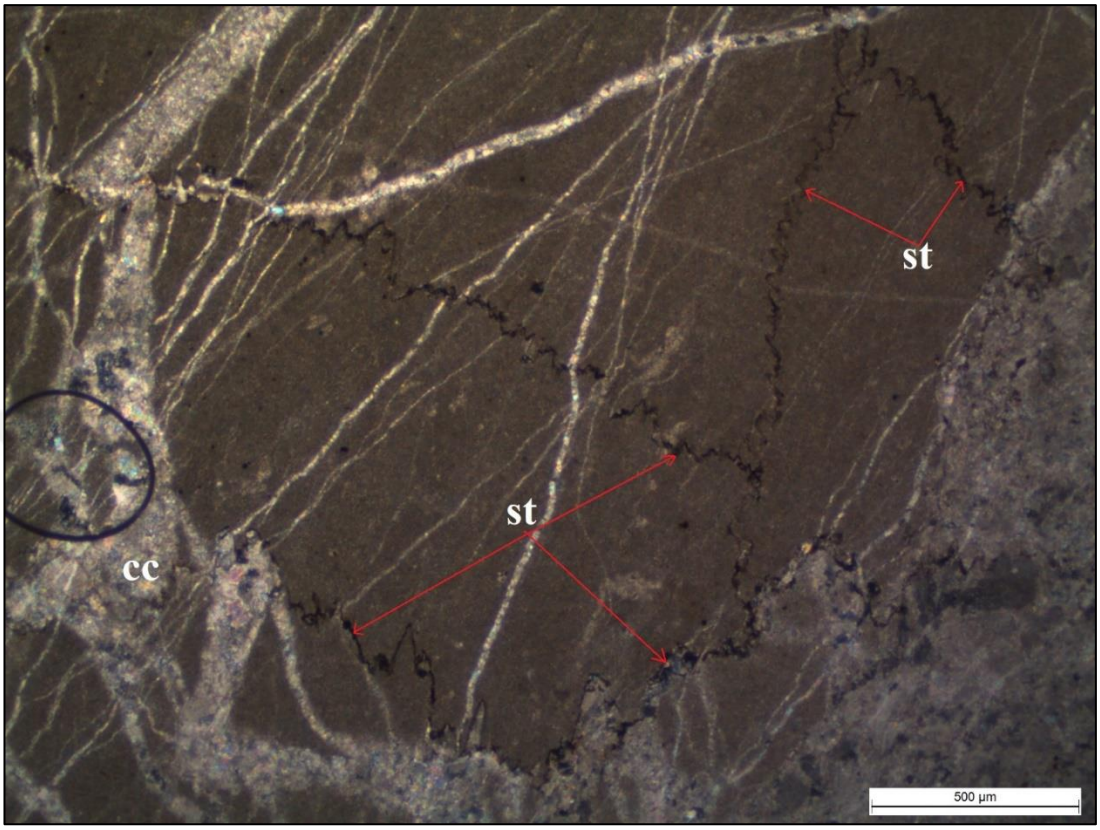

Figure 3.14. The photomicrograph showing stylolite (st), calcite (cc) minerals, and stockworks of calcite veinlets (XPL).

The host rock for gold mineralization is jasperoidal rocks formed by the infilling of dissolution cavities due to the decarbonatization of BLL (Table 3.1). The jasperoids in the BLL have mutual contacts with planar to irregularly shaped matrix-supported breccia bodies mostly within the dissolution cavities along the fault planes.

Table 3.1. Gold assay for jasperoids formed in dissolution cavities at drill hole KTS-6 (BLL returns very low gold grades)

Hole ID	From	To	Interval	Lithology/Alteration	Au(ppm)
KTS-6	0.00	0.70	0.70	Overburden	0.084
KTS-6	0.70	1.25	0.55	Overburden	0.102
KTS-6	1.25	2.00	0.75	Jasperoid	0.499
KTS-6	2.00	2.75	0.75	Jasperoid	0.558
KTS-6	2.75	3.20	0.45	Jasperoid	0.657
KTS-6	3.20	3.65	0.45	Jasperoid	0.091
KTS-6	3.65	4.30	0.65	Jasperoid	0.534
KTS-6	4.30	5.80	1.50	Jasperoid	0.430
KTS-6	5.80	7.00	1.20	Jasperoid	0.403
KTS-6	7.00	8.00	1.00	Jasperoid	0.331
KTS-6	8.00	8.80	0.80	Jasperoid	1.930
KTS-6	8.80	9.80	1.00	Jasperoid	0.371
KTS-6	9.80	10.80	1.00	BLL	0.047
KTS-6	10.80	11.80	1.00	BLL	0.034
KTS-6	11.80	12.40	0.60	Jasperoid	0.303
KTS-6	12.40	13.20	0.80	Jasperoid	0.368
KTS-6	13.20	14.45	1.25	Jasperoid	0.366
KTS-6	14.45	15.90	1.45	Jasperoid	0.315
KTS-6	15.90	17.00	1.10	Jasperoid	0.286
KTS-6	17.00	18.00	1.00	Jasperoid	0.064
KTS-6	18.00	19.40	1.40	BLL	0.035
KTS-6	19.40	20.40	1.00	BLL	0.043
KTS-6	20.40	21.70	1.30	BLL	0.032
KTS-6	21.70	22.50	0.80	BLL	0.077
KTS-6	22.50	23.30	0.80	BLL	0.066
KTS-6	23.30	24.60	1.30	BLL	0.040

3.2.2.1. Matrix-supported collapse breccia

The breccia bodies are mostly embedded in the dissolution cavities that are partly or pervasively silicified to form jasperoids. As these breccias have irregular morphologies, they are more like those formed by the collapse of the undissolved carbonates, mostly dolomitic ones into the cavities formed by dissolution. The clasts in the breccia are set in a pervasively silicified carbonate matrix. The fact that they are set in a matrix, and are deposited in dissolution cavities, they are referred to be matrix-supported collapse breccia. The carbonate matrix is kept as small to irregular islands or unreplaced masses within pervasively silicified breccia. The matrix-supported breccia consists of angular-subangular clasts of mineralized rocks (Table 3.2). They

exhibit color anomalies by reddish to brown oxidation zones at the surface outcrops. However, they also exhibit oxidation at deeper intersections by the drill holes (e.g. KTS_13; 38.40 meters to 42.00 meters) (Figure 3.15).

Figure 3.15. Matrix-supported breccia from 38.40 meters to 42.00 meters.

The angular clasts are also derived from pervasively silicified rocks. They are generally as silicified limestone, but may also contain fragments derived from ultramafic rocks and jasperoids. as well. The geochemical analyses on the surface samples and core samples by the company showed that the breccia is also one of the main host rock gold mineralization (Table 3.2)

Table 3.2. Gold assay from the matrix-supported breccia

Hole ID	From	To	Interval	Lithology	Au (ppm)	Cu (ppm)	Ag (ppm)	As (ppm)	Sb (ppm)
KTS-13	38.40	39.30	0.90	Matrix Supported Breccia	1.591	31	5	320	347
KTS-13	39.30	40.00	0.70	Matrix Supported Breccia	0.820	24	5	104	43
KTS-13	40.00	40.90	0.90	Matrix Supported Breccia	0.618	30	5	178	87
KTS-13	40.90	42.00	1.10	Matrix Supported Breccia	0.481	23	5	98	38

Considering that the breccia contains both BLL and jasperoidal fragments, and silicified nature of the matrix, multiple formation phase could be suggested; (1) earlier, formed by dissolution of BLL, and (ii) later, after silicification of dissolution cavities. Besides, a formation by faulting is not completely ruled out. It seems that the

brecciation has also been contributed by faulting, and silica-rich fluid percolated along the fault planes, and as a result of this the matrix and angular clasts have been silicified. The petrographical works on the breccia showed that both silicified matrix and clasts contain fine-grained disseminations of pyrite.

3.2.3. Light gray limestone

The limestones light gray in color that occurs as large and chaotic blocks within the ultramafic rocks are termed as the light gray limestone (LGL) in this study. The LGL is said to be Jurassic-Cretaceous in age (Konak et al., 1980). No clear contact relations with the other limestone types are recognized in the field. The blocks have no regular bedding due to the chaotic nature of the blocks. The ultramafic rocks exhibit shearing and deformation around the blocks. The most characteristic feature of the LGL is joint sets commonly infilled by calcite veinlets (Figure 3.16). The LGL is displaced by the youngest normal faults.

Figure 3.16. The field exposure of the light gray limestones traversed by calcite veins infilling the joint planes at the study area

3.2.4. Epi-ophiolitic sedimentary sequences

The epi-ophiolitic sequences are characterized by red to dark brown colored, radiolarite-bearing, and laminated layers of radiolarites, pelagic red mudstones that occur as blocks within the ophiolitic mélange. The radiolarite is occasional but does occur as fine layers within the dark-colored mudstones. The mudstone outcrops are generally observed at the top of all units in the field. It covers large areas around the study area. Folding and faulting are common on the mudstone. The mudstone is locally intercalated with limestones and radiolarian cherts. It is fractured and highly weathered to form reddish oxidized outcrops with eolith-like nature with some siliceous/chert particles (Figure 3.17). As these are in red color, they are easily confused with laterite.

Figure 3.17. Field photograph showing highly weathered mudstone with reddish color anomaly along a fracture zone (red solid line showing the faults).

3.3. Quartzites

The silicified and metamorphosed clastic rocks at the center of the study area are termed as the quartzite. They occur as larger blocks and are cut by milky quartz

veinlets or locally by comb textured quartz veins (Figure 3.18). This unit is observed on the summit of the hills. Whole-rock geochemical data shows that the silica (SiO_2) content of the rock is 93.7%. The petrographic studies showed that the quartzite consists mostly of metamorphosed quartz (Figure 3.19). The quartz is fine-grained exhibit undoluse extinction suggesting that the rock has been metamorphosed (Figure 3.19).

Figure 3.18. Field photographs showing (a) the outcrops of quartzite (b) milky quartz veins, euhedral quartz crystals, and comp textured empty space filling milky quartz veinlets.

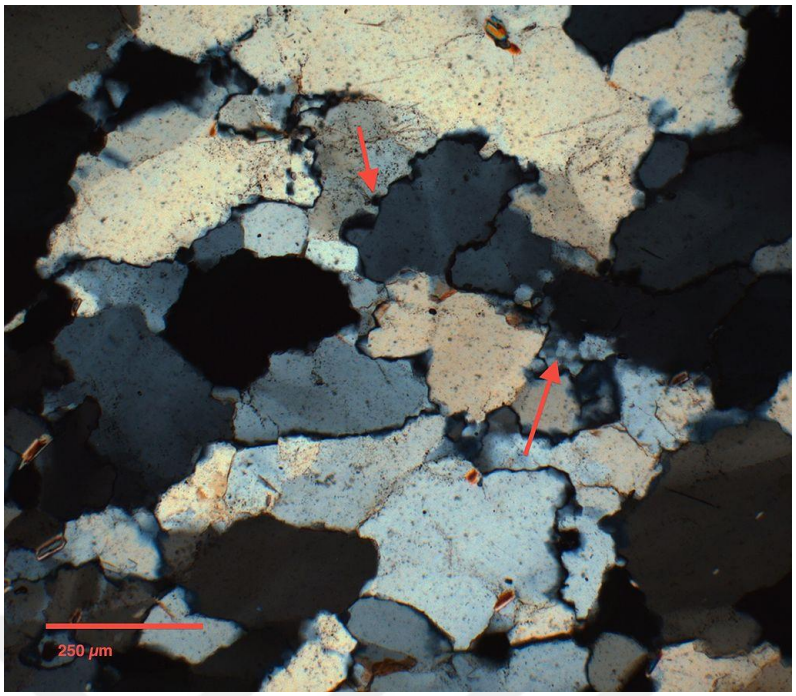

Figure 3.19. Metamorphosed quartz crystals in thin section (XPL)

3.4. Laterite

Dark red to brown oxidized rocks developed by weathering of ultramafic rocks at the study area are called laterite. The laterites are essentially composed of clay minerals (mainly kaolinite, smectite), iron minerals (mainly limonite, hematite, goethite), and siliceous minerals. These rocks were formed through alteration and leaching of ultramafic rocks, and have a loose, soil-like, earthy nature and because of enrichment in iron-oxide and iron-hydroxide minerals, their color is generally yellow reddish yellow, and reddish-brown. Laterites in the study area are observed on topographic highs or hills. Near or inside the lateritic zone silicified serpentinite rocks also observable especially fault zones in laterite.

The lateritic zones are the main Ni-bearing rocks for the main nickel processing plant to the south of the study area. Production and mining activities by Meta Nickel Cobalt Inc. currently focus on lateritic zones. Laterite also covers outcrops containing limonite and nontronite (Figures 3.21; 3.22). Lateritic rocks observed only on the serpentinized ultramafic rocks (harzburgite and dunite).

Figure 3.20. Laterite profile from the open pit area

Figure 3.21. Limonite and hematite-bearing lateritic zone within the ultramafic rocks

4. WALL ROCK ALTERATION AND MINERALIZATION

The wall rock alteration exposed in the study area is limited mainly to silicification largely in the form of irregular outcrops, and carbonate alteration following the silicification. The silicification in this study refers to the development of amorphous to microcrystalline quartz infilling or replacing the clays within the fractures of decarbonized and dissolved limestones and carbonate cement within the matrix-supported collapse breccias. The amorphous to microcrystalline to very fine-grained to microcrystalline siliceous rocks developed mostly within deformed and brecciated BLL are simply termed as the jasperoids (Figures 4.1; 1.2).

4.1. Silicification

The silicification in this study are is characterized by the dissolution of almost 80 to 90% of the original calcite and replacement by fine-grained quartz. The petrographical works partly supplemented by field observations enabled the recognition of three main phases of silicification. The first phase is responsible for silicification and decarbonatization of the BLL, and this phase named as the pre-syn ore stage. This phase resulted in the pervasive silicification of BLL and matrix-supported collapse breccia is just after the dissolution of BLL during or after faulting. This phase includes a small amount of pyrite, arsenopyrite, and gold mineralization. This phase could be the phase that prepares the wall rock and area by increasing the temperature and permeability of the limestones for mineralization. The second phase is also associated with fine-grained pyrite generation that could be termed as syn-ore pyrite (Figures 4.5; 4.12 and 4.13). This phase is the main ore-bearing phase during which stibnite, arsenopyrite, and gold mineralizations occurred. The second phase can be also characterized by the medium to coarse-grained druzy quartz generation with boxwork texture traversing both the jasperoidal rocks and BLL (Figure 4.8). In this respect, this phase is considered to be syn-ore stage silicification. The main texture of this type is the comb texture (Figure 4.9). The third phase refers to amorphous quartz infilling open spaces between the comb-textured drusy quartz (Figure 4.9). This phase post-

dates the first two silicifications and is also termed as post-ore stage silicification (Figure 4.20). The degree of silicification decreases getting away from the feeder fault zones (Figure 4.10)

4.1.1. Jasperoids

The jasperoids are the main host for gold mineralization, and geochemical analyses on the drill core and channel samples from these rocks return high-grade gold. The field works supported by petrographical studies enabled the recognition of several jasperoid types in the area; (1) massively silicified type hosted by BLL consisting of fine-grained quartz crystals with fine-grained pyrite disseminations (Figures 4.2; 4.5); (2) red to brown colored, massive jasperoid formed by pervasive silicification of the matrix-supported to collapse breccia with pyrite. The clasts in this type are also silicified and strongly oxidized (Figures 4.1; 4.15); (3) pervasively oxidized jasperoid traversed by drusy, coarse-grained and comb-textured quartz and rocks (Figure 4-8); (4) weakly oxidized jasperoid containing fine to coarse-grained quartz; and (5) pervasively oxidized jasperoid characterized by liesegang-texture (Figures 4.3; 4.6 and 4.7). Apart from the first two types, the others are formed by the oxidation of the sulfides within the first two types of jasperoids. Among these, the liesegang-textured jasperoid (Figures 4.3; 4.6) is very diagnostic in that they are easily identified at the drill holes, surface exposures, and under the microscope (Figure 4.7). The liesegang texture on jasperoids tends to localize at the silicified breccias. The oxidation process that resulted in the liesegang texture also gave rise to the generation of oxidation in the massive jasperoids formed by silicification of BLL with pyrite, and have created pervasively oxidized jasperoids. Gold grades tend to increase with oxidation. Therefore, the oxidized jasperoids including the liesegang textured one both on the drill holes and at the surface help to pinpoint the higher gold-bearing rocks.

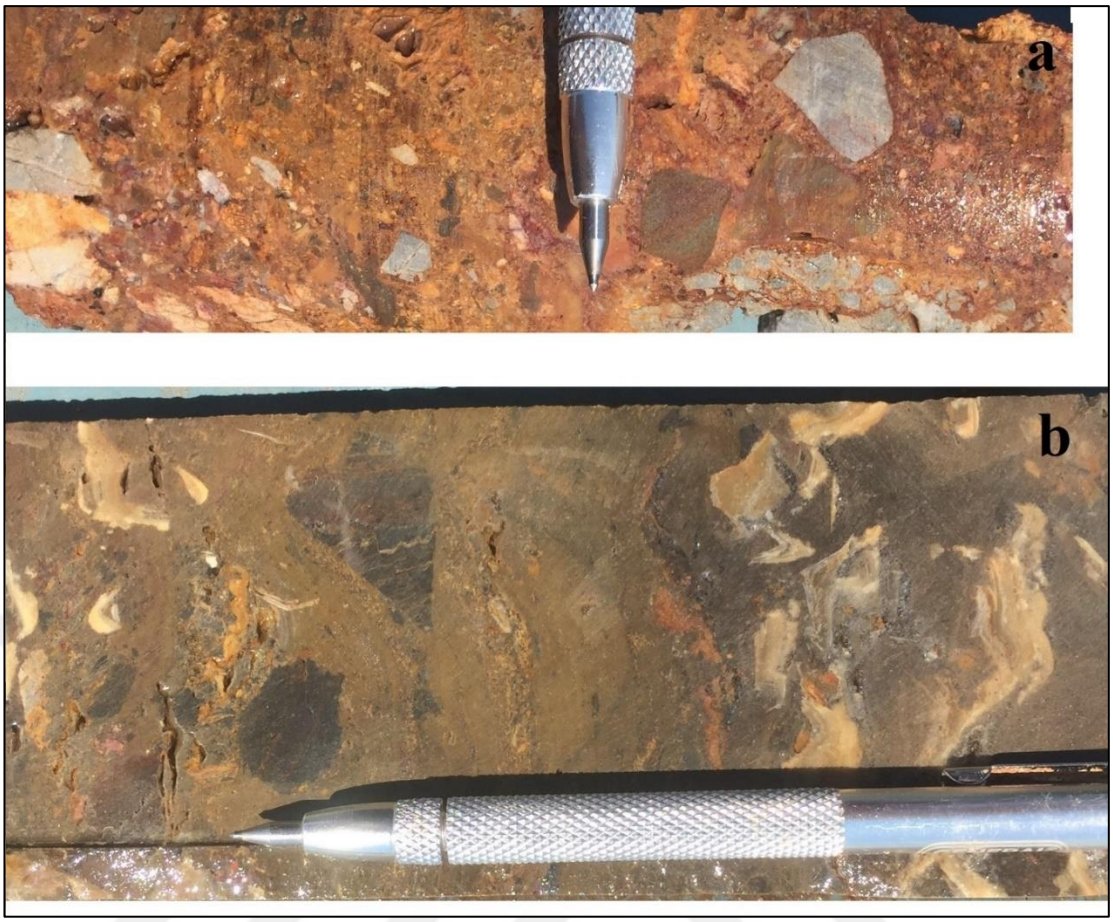

Figure 4.1. (a) Oxidized, matrix-supported breccia (collapse breccia), the clasts and matrix are strongly silicified and includes moderately oxidized pyrite; (b) deeper part of the same rock unit above fine-grained pyrites are not oxidized.

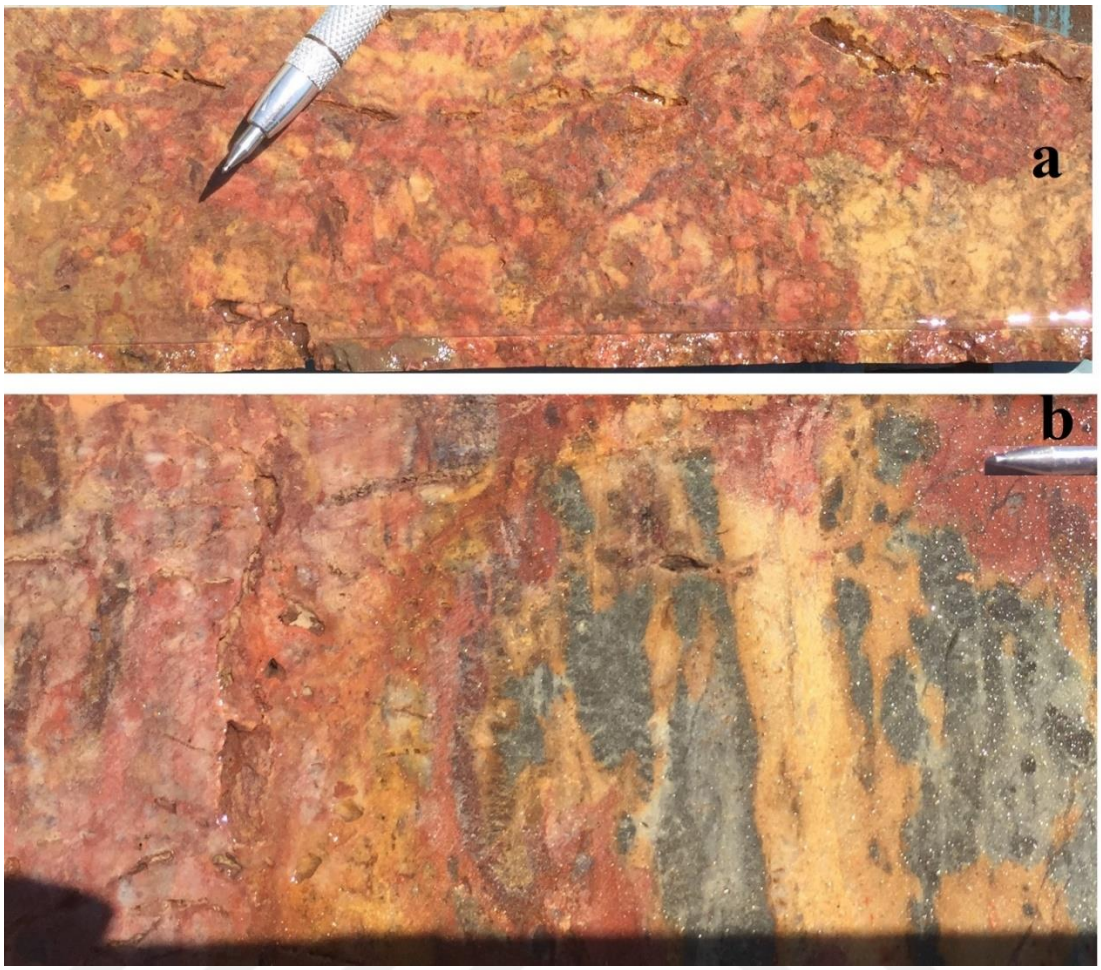

Figure 4.2 (a) Pervasively silicified and strongly oxidized jasperoid; (b) deeper part of the same rock unit, fine-grained pyrites observable in grayish areas

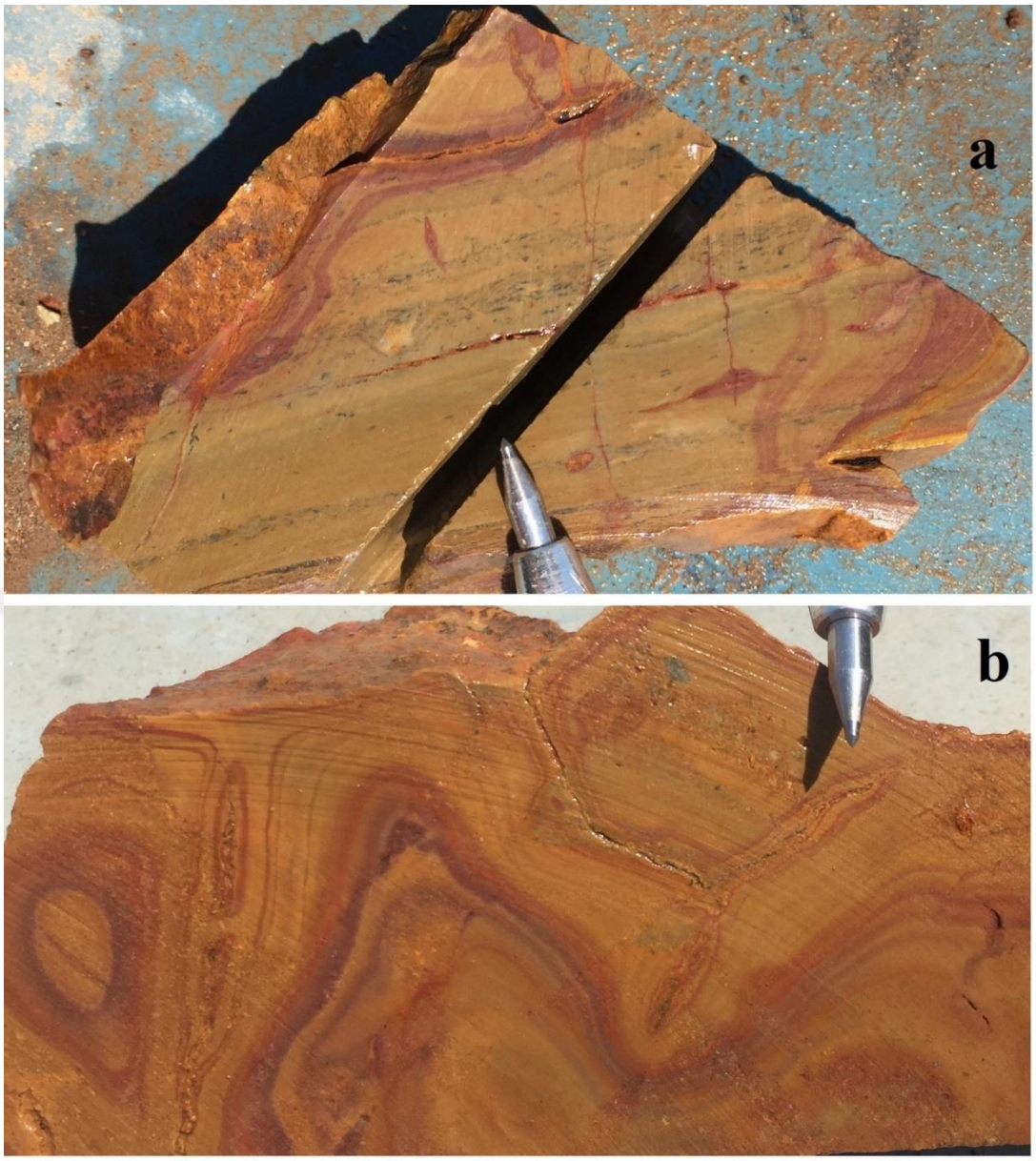

Figure 4.3. (a) Pervasively silicified and oxidized jasperoid within limestone; (b) liesegang textured jasperoid.

Boxwork and comb textures are the most common textures observed on the cavities within the jasperoids. The boxwork texture observed at cavities confined to contacts between BLL and jasperoid (Figure 4.11). Comb texture is restricted to druzy quartz traversing the jasperoids, and also to dissolution cavities between the clasts in the breccias at the surface. This texture is also identified under the microscope (Figure 4.12).

Figure 4.4. Jasperoid outcrops in the study area; a) siliceous rocks at Keşkek Hill and b) jasperoid outcrops at Güngörmez Hill

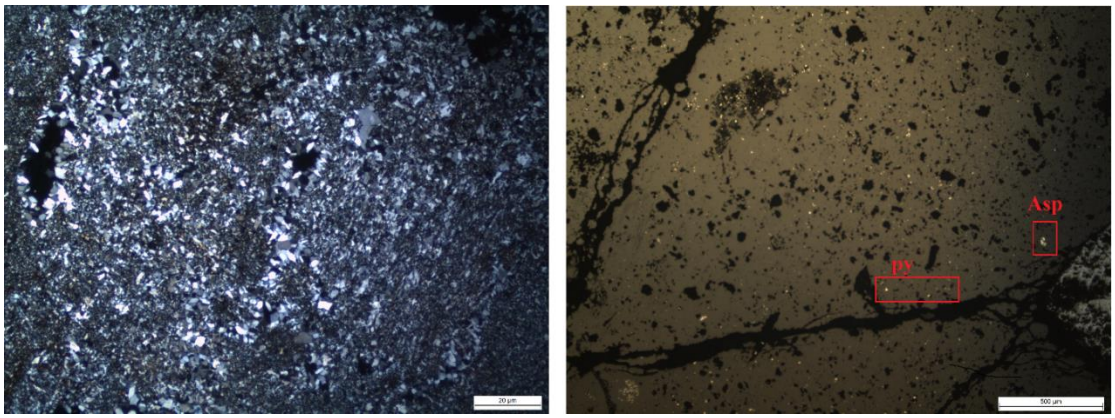

Figure 4.5. Fine-grained quartz crystals on the left and fine-grained pyrite (py) mineralization and arsenopyrite (Asp) on fine-grained quartz on the right

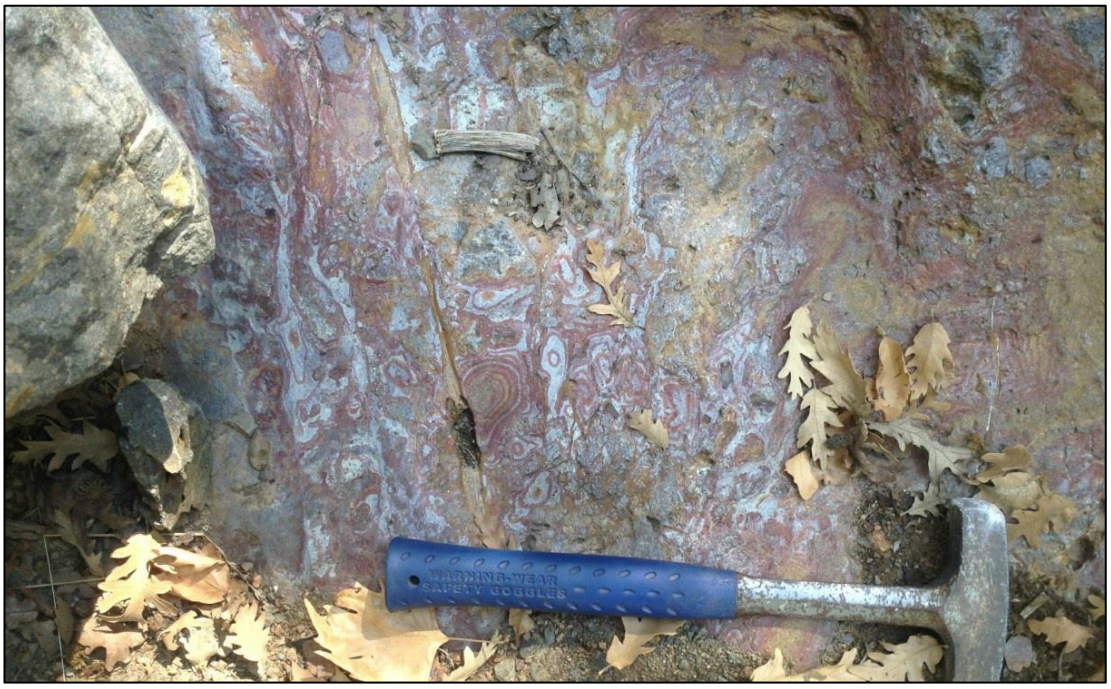

Figure 4.6. An outcrop with liesegang textured jasperoidal rocks

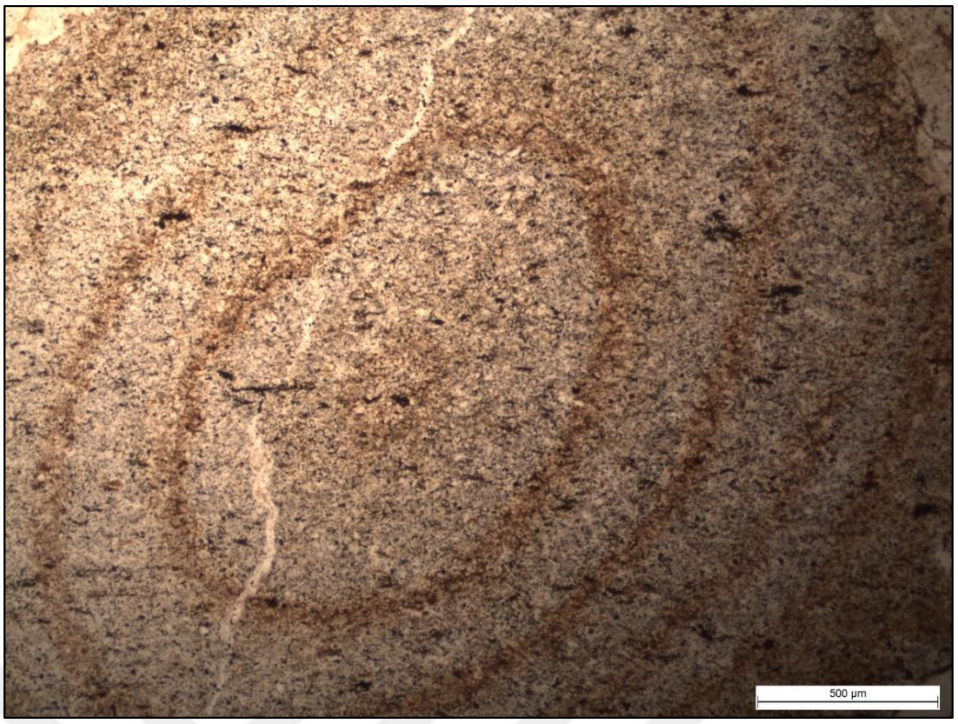

Figure 4.7. Photomicrograph showing liesegang gang texture on fine-grained quartz matrix

Figure 4.8. Outcrops of silicified rocks with boxwork texture

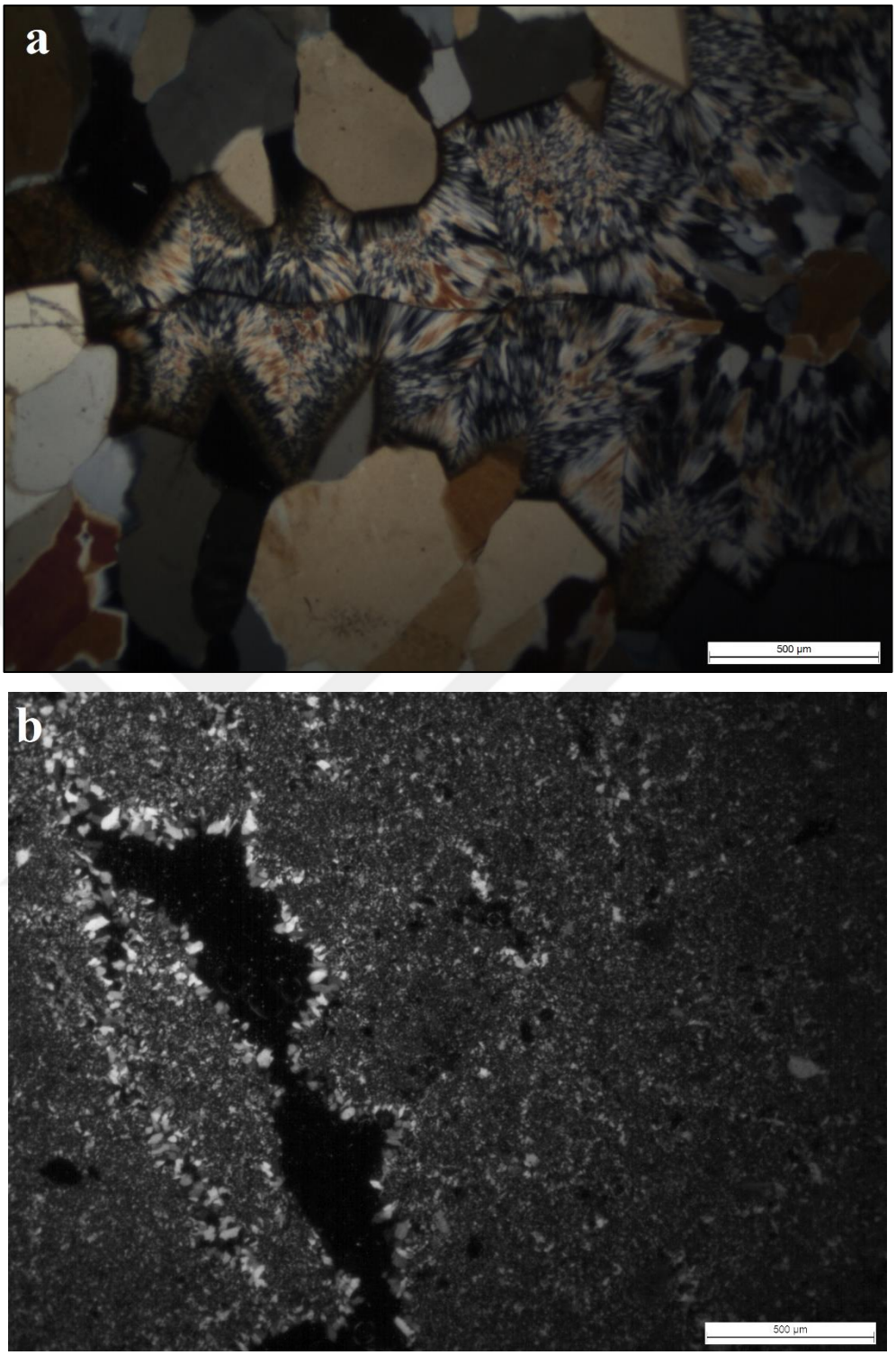

Figure 4.9. The photomicrograph illustrating (a) comb textured coarse-grained quartz matrix and colloidal textured quartz (b) fine-grained matrix and comb texture

During petrographic studies on jasperoids, 3 different phases of quartz minerals are observed (Figure 4.9). The first phase is pre-syn-ore stage quartz. This type of quartz

is responsible for decarbonatization and the silicification of the limestones (Figure 4.14). Decarbonization of the limestone increases the permeability of the rock. Second phase quartz minerals observed as generally medium to fine-grained and comb textured crystals. Stibnite minerals generally observed together with second type quartz minerals. Sulfur minerals (pyrite-arsenopyrite and stibnite) observed on medium to fine-grained and cob (boxwork) textured quartz minerals. The last phase is generally low temperature (chalcedonic quartz or relatively low temperature) quartz crystals. This type of quartz minerals observed as filling quartz.

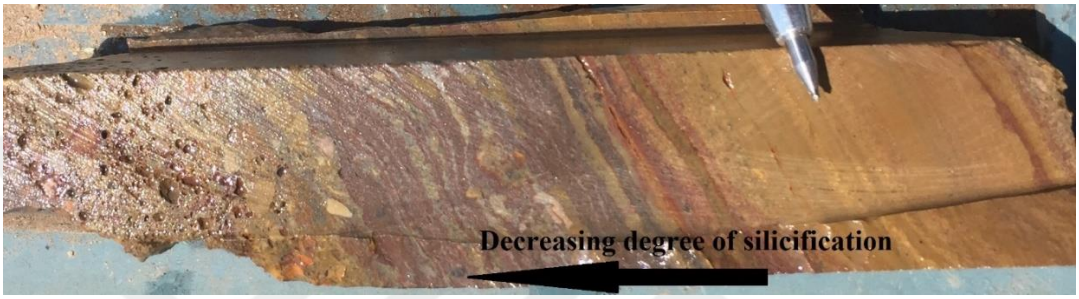

Figure 4.10. Change of silicification in jasperoids

4.2. Mineralization and Orebodies

Fieldworks show that the main gold mineralization occurs at four main orebodies, Keşkek Hill, Güngörmez Hill, Kaleüstü Hill, and Demirci Hill West in the study area (Figure 1.2). Northwest directed normal faults are related to the mineralization in the orebodies. In these orebodies, jasperoidal rocks are the most common rock type that refers to pervasive dissolution and silicification of carbonate rocks. The field works and analytical results on the samples indicate that the ore body at the Güngörmez Hill is characterized by the most sulfide-rich one in the study area. Stibnite (Sb_2S_3), fine-grained pyrite (FeS_2), and arsenopyrite (FeAsS) are observed in jasperoidal rocks, matrix-supported breccia rocks and quartz veinlets (Figures 4.12; 4.13). The discovery of gold at the prospect was done on the Keşkek Hill orebody with a sample that returned 2.81 ppm of gold (Figure 4.4). All orebodies have similar alteration characteristics and mineralization.

The field works supplemented by analytical works show that jasperoidal rocks at Keşkek Hill, Demirci Hill, Kaleüstü Hill, and Demirci Hill West are aligned to certain

directions conformable to or parallel to the direction of some faults in the area (Figure 1.2)

Most of the jasperoids contain stibnite and oxidized equivalent of stibnite, valentinite (Sb_2O_3) (Figures 4.11; 4.12, and 4.16). The gold content of the jasperoidal rocks ranges between 0.1 ppm and 10 ppm. The gold grade increases with stibnite at the samples collected at shallower depths or close to surface, whereas, at the deeper levels, the gold content increases with arsenic content (As) represented by arsenopyrite (Figures 4.15; 4.13) (Table 6.2). The core samples from deeper levels of the drill holes have a higher correlation coefficient (0,53) (Table 6.2).

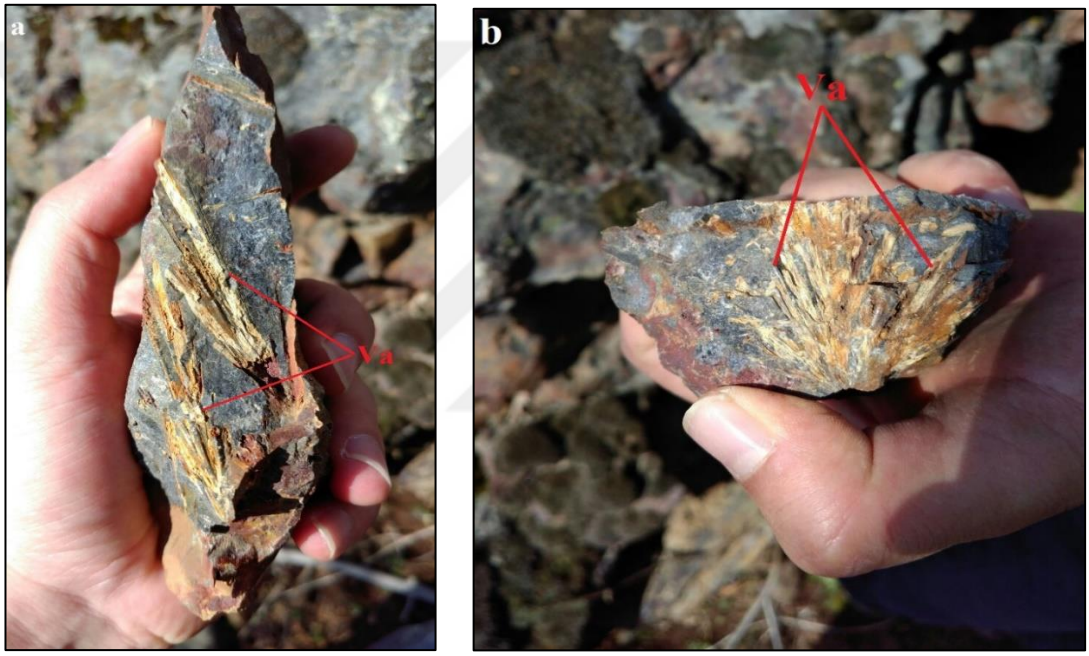

Figure 4.11. Samples with valentinite (Va) in jasperoidal rocks

Figure 4.12. Sample with stibnite (st) and jasperoid (Jd) clasts in late (second phase) quartz

Figure 4.13. Arsenopyrite in pervasively silicified and strongly oxidized jasperoid

4.2.1. The Keşkek Hill orebody

The Keşkek Hill orebody is characterized by isolated ore bodies that form two discrete clusters in NE direction (Figure 1.2). The jasperoidal bodies are hosted by BLL. The

jasperoids are nearly 300m from south to north along N-S trending high-angle fault and 200m from west to east. The maximum thickness of jasperoids is 73m. The jasperoids trending in NW-SE direction are hosted by BLL on the hanging-wall block of the high-angle fault. Whereas the RXL is located on the footwall and is cut by calcite veinlets only. The jasperoids at the Keşkek Hill orebody contain the highest gold-bearing bodies in the study area. The fine-grained stibnite and very fine-grained pyrite are identified as the main sulfides within the ore bodies. Deeper core sample results show that arsenic mineralization is increasing from surface to deeper part of the orebody. Orebody mainly observed as pervasively oxidized and silicified.

4.2.2. Kaleüstü Hill orebody

The Kaleüstü orebody has characteristics similar to those of Keşkek Hill. It is situated to the NE extension of the same high-angle normal fault that also controlled the silicified outcrops at the Keşkek hill. Therefore, it is likely that these two ore bodies may be considered to be two edges of a larger blind (not exposed to the surface) ore bodies. Six rock samples were collected from this body and one sample returned 0.5 ppm of gold content as the highest one. On the samples and outcrops, fine-grained pyrite mineralization was observed during field works.

4.2.3. Güngörmez Hill orebody

Güngörmez ore body is the longest and largest orebody observed in the study area (Figure 4.4). It has 1200 by 300-meter dimensions. Based on the relief difference between the exposures at the highest and lowest elevations, the orebody is measured to be 100m in thickness. Oxidation level and sulfide mineral content of the Güngörmez Hill orebody has similar paragenesis with Keşkek Hill. Comb textured quartz veinlets, which includes stibnite minerals, are observable and more than Keşkek Hill.

4.2.4. Demirci Hill West orebody

Demirci Hill West orebody (Figure 1.2) is slightly different from other orebodies in the study area. Gold mineralization is generally observed in strongly clay altered shear zone. Shear zone belongs to low angle thrust fault trending in N5 with a dip of 10 degrees to the northwest (Figure 5.1). The hanging wall of this fault is pervasively

oxidized and silicified. Both the hanging and footwall blocks include gold grades ranging from 0.1 ppm to 0.8 ppm (Table 6.1). The jasperoids on the hanging wall block include disseminated pyrite. It is noteworthy that the rocks at the footwall block contain nickel mineralization of 4000 ppm.

4.3. Petrography of Alterations

The petrographic studies show how decarbonatization (dissolution) and silicification take place on calcite (Figure 4.14) in the BLL. The petrographic studies also revealed the variable size distribution of the quartz that cemented the matrix of breccia. Colloidal and comb textures are the main textures in thin sections (Figures 4.9a and 4.9b). The quartz crystal tends to be coarser from central to marginal parts of the jasperoids. Quartz is nearly the only mineral observed in thin sections, but in some sections, residual calcite is also observed (Figure 4.14).

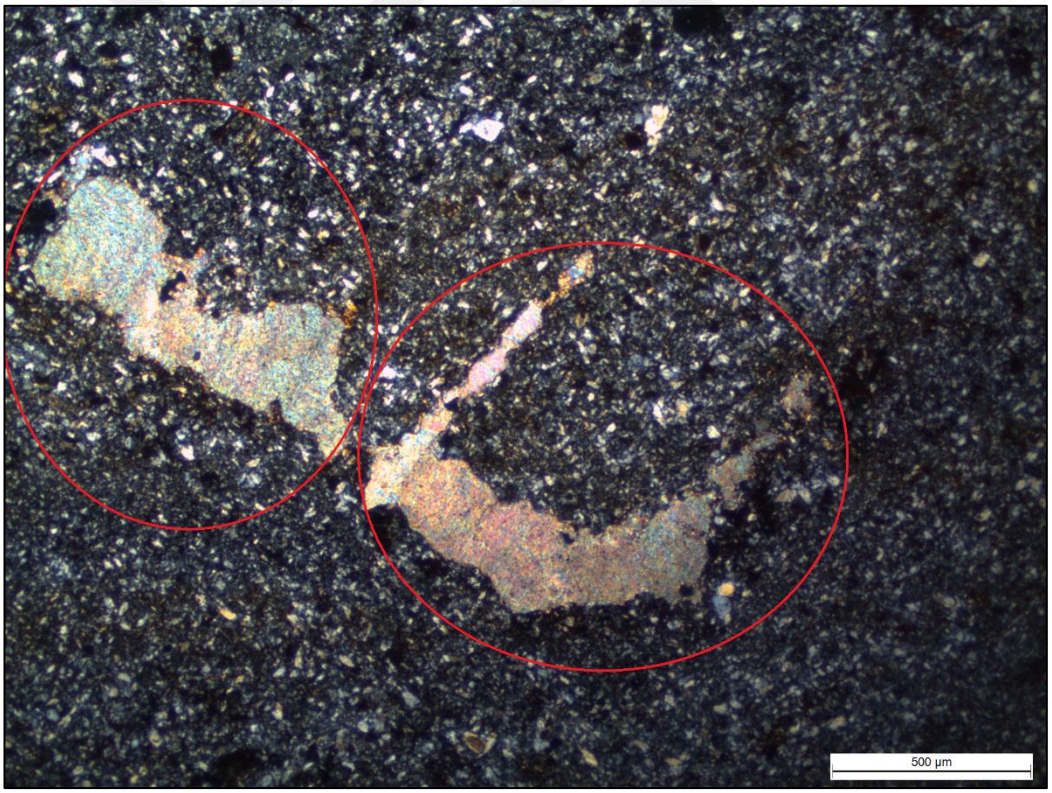

Figure 4.14. The photomicrograph showing the unreplaced islands of calcite (red circles) within the fine-grained quartz matrix.

Petrographical studies on polished sections show that the main sulfide minerals are pyrite and arsenopyrite (Figures 4.5; 4.13 and 4.15) in the jasperoidal rocks. The pyrites generally were observed as fine-grained and patchy textured, disseminated crystals at the outcrops. Most of the pyrite on jasperoidal rocks are oxidized to form iron oxides and iron hydroxides at the surface, and the drill cores. Pyrite from deeper core samples is unoxidized and fine-grained in nature. Pyrite is also a common sulfide hosted by jasperoidal rocks formed by the silicification of matrix-supported breccia (Figures 4.15 and 4.1). Arsenopyrite is another patchy sulfide hosted by jasperoids. Field and core logging observations on pyrite and arsenopyrite show that both of the minerals occurred as syngenetic in a deeper part of the mineralization (Figure 4.5). Patchy arsenopyrite minerals observed together with the fine-grained unoxidized pyrites (Figure 4.13). Jasperoids outcrops on the Demirci Hill West orebody unoxidized arsenopyrite minerals observed together with oxidized pyrite minerals (Figure 4.13). The stibnite is one of the most abundant minerals of the jasperoidal rocks. Stibnite predominates at veins or siliceous rocks close to the surface and samples collected from the shallower intersections of core samples (Figure 1.5). The stibnite is partly altered to valentinite (Figure 4.16) by oxidation at the shallower core and grab-channel samples (Figure 4.11).

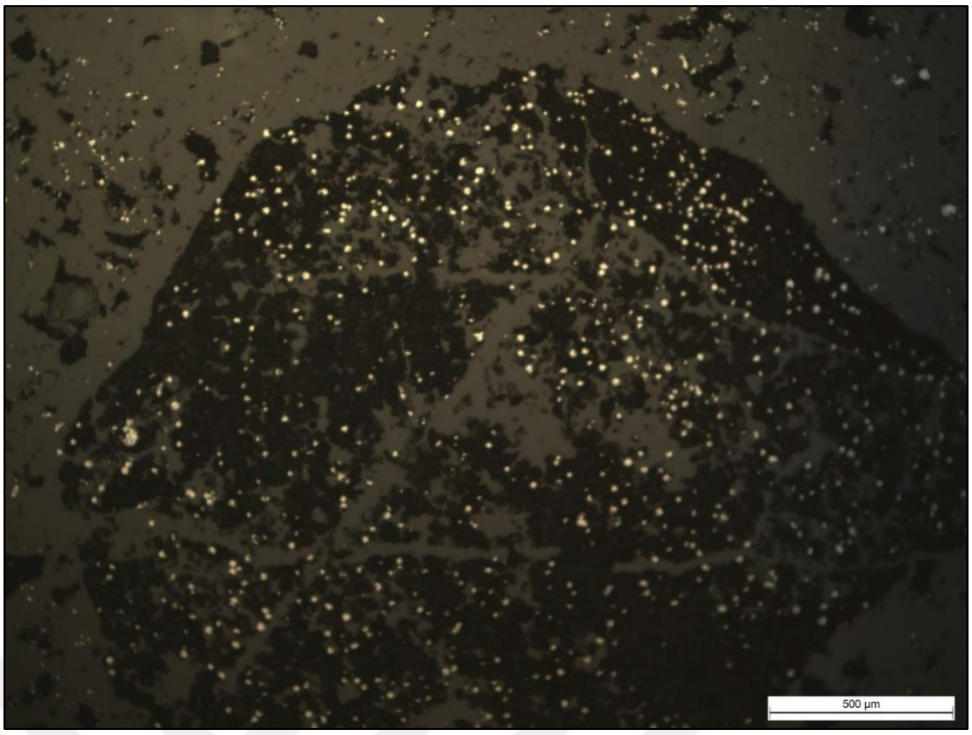

Figure 4.15. Photomicrograph showing fine-grained, disseminated pyrite crystals on a clast and matrix.

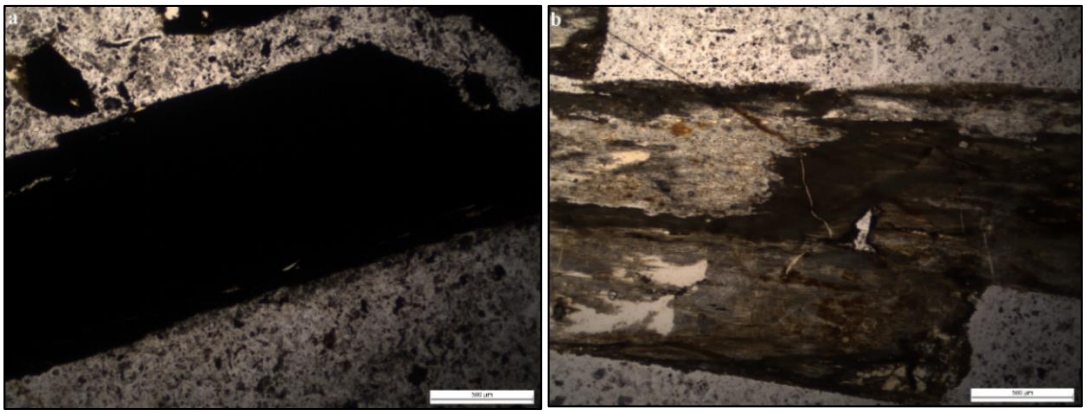

Figure 4.16. The photomicrograph showing (a) stibnite; b) valentinite crystals

The fluids responsible for decarbonization and silicification of dirty limestone (BLL) are termed as pre-syn-ore stage fluids. These fluids resulted in pre-syn ore stage silicification (Figure 4.20). During this stage, the calcites have been partly dissolved

leaving mainly behind the dolomite crystal. The quartz also partly replaced calcite or infilled the cavities formed decarbonatization. This process and brittle deformation (normal faults) on the BLL increase the permeability. The pervasive silicification is referred to be syn-ore stage silicification that brings the gold, pyrite, stibnite, and arsenopyrite in the system. The pervasively silicified, jasperoidal rocks are traversed by comb textured quartz veinlets. The dissolution (decarbonatization) is evidenced by the boxwork texture (Figure 4.8). The ore stage silicification is observed in thin-section studies and field studies (Figures 4.12 and 4.15). During thin section studies and field works stibnite observed within the comb textured quartz veinlets (Figure 4.18). Two phases of silicification also observed during field works as a brecciated rock including quartz clasts in the quartz matrix (Figure 4.17). Third and last silicification (Figure 4.20) observed only on a thin section study (Figure 4.9) as filling the empty spaces (interstitial) between the comb quartz crystals. This type of silicification e is characterized by colloidal quartz (Figure 4.9) and is termed as post-ore stage silicification (Figure 4.20).

During thin section and ore microscopy studies, pyrite and rare arsenopyrite minerals observed together on the fine-grained quartz crystals and these samples selected from gold grade include samples (Figure 4.5).

Field observations and petrographic studies show that gold is associated with pyrite, arsenopyrite, and stibnite. A small amount of silver should be mineralized during gold mineralization. Oxidization of the jasperoids due to meteoric water is pervasive. The oxidization stage could be started from the syn-ore stage and continue to post ore stage (Figure 4.20). Oxidization generally observed as hematitization, but in some locations, goethite and limonitic rocks are also observed on jasperoids (Figure 4.19).

Tectonism has the most important role in the mineralization of the Keşkek Hill Project area. Pre-ore stage tectonism is thrusting of the ophiolitic suit on Menderes Massive metamorphic units. The mechanism turns the compressional system to extensional tectonism with the effect of Western Anatolia extension. This thrust faults in the area act like a detachment fault in the area and normal faults occurred on this thrust with very high angle dips. Brecciation could be started during this time because while field and core logging works breccia clasts and matrix belongs to fault zone are also

observed as silicified, and also pyrite minerals observed on clasts as same as matrix and jasperoids (Figure 4.15). The mineralization in the study area observed on this normal fault. Mineralization should be syngenetic with the normal faulting. After mineralization extensional tectonism continuing the activity in the regime. During fieldwork, mineralized jasperoids observed as cut by normal faults, and these faults must be post-ore stage. Drilling and field works show that mineralization is cut by strike-slip faults in the area. These faults are also post-ore stage faults in the study area.

Figure 4.17. Quartz clasts in quartz matrix and small of amount of jig-saw puzzle texture

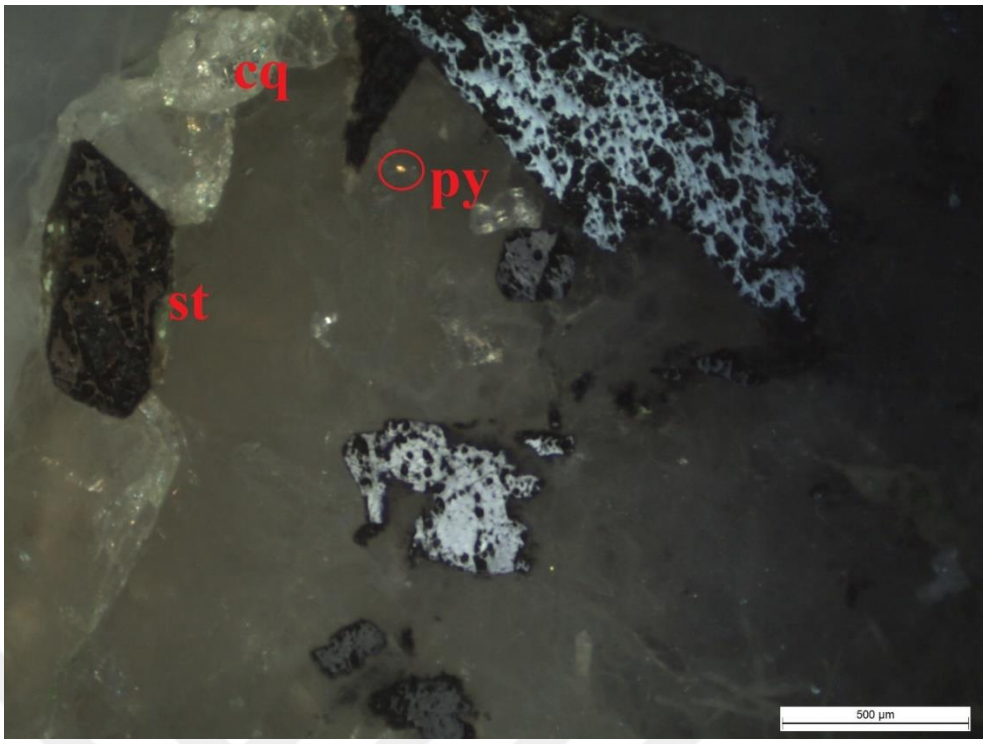

Figure 4.18. Ore microscopy image shows that stibnite (st) and pyrite (py) mineralization on comb textured (cq) quartz veinlet

Figure 4.19. Strongly silicified and pervasively oxidized jasperoid includes valentinite (Va) which is oxidized mineral of stibnite (post-ore stage).

.

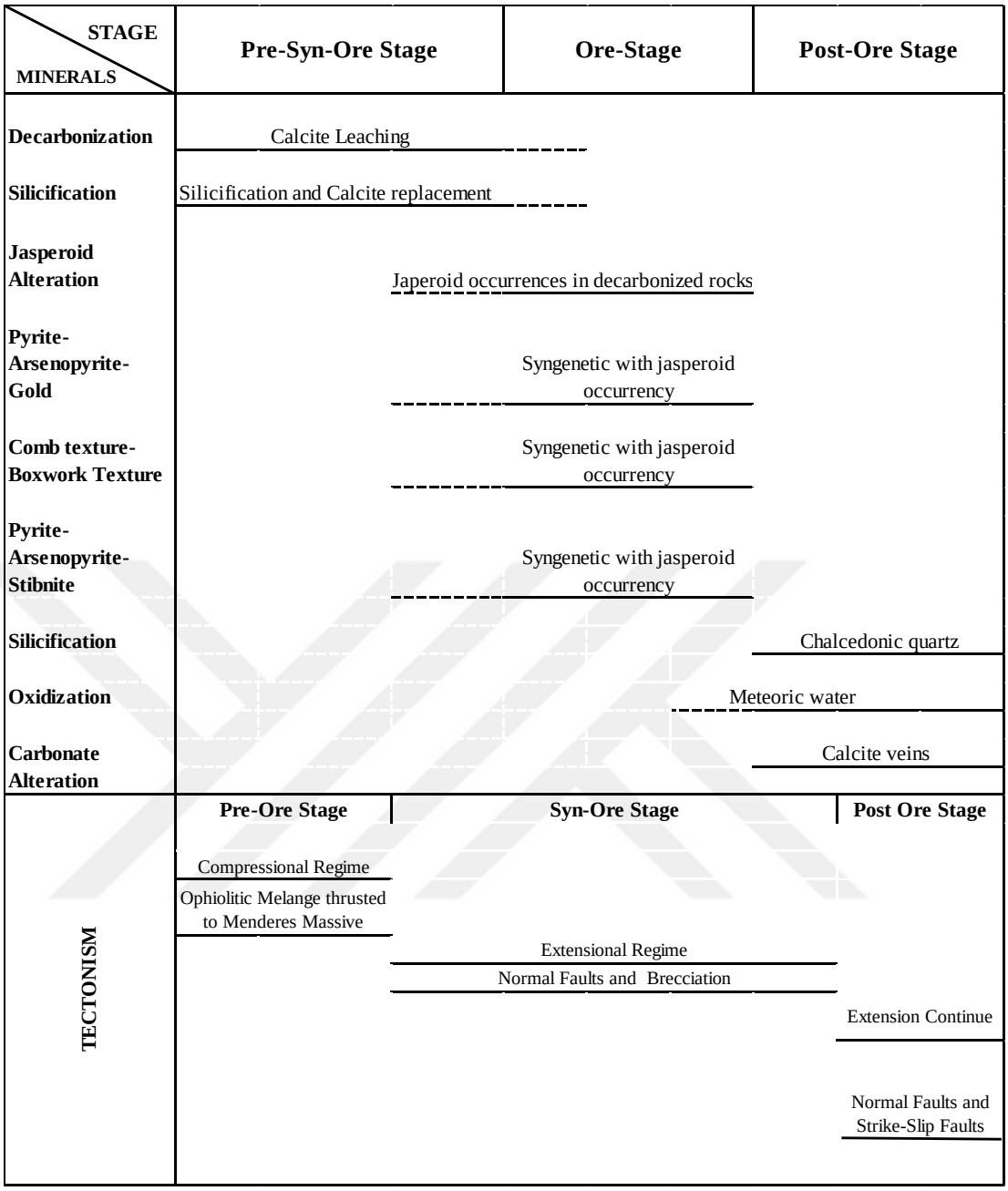

Figure 4.20. Paragenesis of the Keşkek Hill Project.

4.4. Carbonate Alteration

Calcite veins traversing both the BLL and jasperoids are termed as carbonate alteration. The calcite veins are mostly irregular along strike and dip. The calcite veins exhibit pitch-swell structure and have stockworking nature (Figures 3.12 and 3.14). These veins tend to localize at the vicinities of the jasperoidal rocks and silicified

breccias. The thickness of the veins does not exceed 3-5 cm. These veins can also be mapped at distances quite away from the jasperoidal rocks.

5. STRUCTURAL GEOLOGY

The study area was affected by three deformation periods (Rojay, 2004). Both compressional and extensional tectonism are reported in the study area (Rojay, 2004). The tectonic evolution of the study area began with the NNE-SSW trending compressional deformation from Late Cretaceous to Eocene followed by the E-W trending extensional deformation system in the Miocene period (Rojay, 2004). The tectonic evolution of the study area ended with the NW-SE directed transtensional period in the Post-Miocene period (Rojay, 2004). The compressional period observed as thrust faults between Menderes Massif metamorphic basement and Bornova Flysch Zone ophiolitic mélange. While the extensional period this thrust faults acting like a detachment fault in the study area. Normal faults that occurred in the study area are vertically dipping to this detachment fault.

5.1. Thrust Faults

In the study area, the thrust faults are observed as NNE-SSW directed low angle faults. The footwall rocks are highly deformed and sheared. The deformed and sheared rocks on the fault plane are characterized by pervasive oxidization, brecciation, and clay alteration (Figure 5.1).

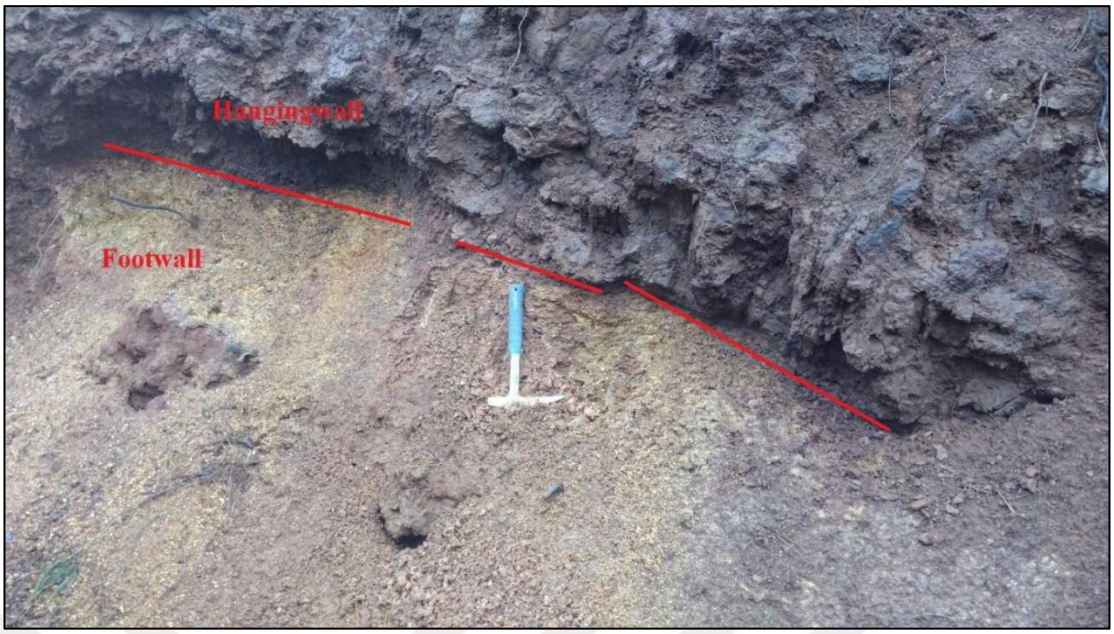

Figure 5.1. The thrust fault displacing ophiolitic mélange; footwall rock is highly altered ultramafic rock, hanging wall rock is highly sheared and brecciated

5.2. Normal Faults

The normal faults are observed in limestones as silicified rocks. 6 different measurements taken from these rocks. Measurements of the fault zones show that NW-SE and nearly E-W trending faults were active during and after the mineralization period. Post-mineral normal faults are formed after the formation of silicification and are observed on jasperoids in a NE-SW direction and they cut the mineralization (Figure 5.2)

Figure 5.2. Jasperoidal rock cut by post mineralization normal fault.

5.3. Strike-Slip Faults

The northern part of the Gıcırlar river is formed along a strike-slip fault at N8E/90. At the end of the fault, slicken lines, and striations on the fault plane are identified during the field works (Figure 5.3). During drilling, this fault was intersected at shallower and deeper levels (KTS-6, KTS-7, and KTS-12). When this drill holes modeled in a 3D program, fault observed as a normal fault with the N8E/85NW direction. However, both of the components of this fault cut the mineralized rocks, the normal fault component could be mineralized too.

Figure 5.3. Fault plane with slice lines indicating a strike-slip movement on jasperoidal rock

5.4. Structural Analyses and Structural Controls

The structural analyses include the determination of the predominant trend and trends of the major faults in the study area. Directions of the normal faults and strike-slip

faults were measured (Table 5.1). The faults were classified as faults and post-mineral faults, and their strike and dips were measured (Table 5.1). The attitudes of these faults identified during field works were used for structural analysis. Thrust faults (NNE-SSW directed) were measured from ultramafic-clay altered zone contacts and silicified ultramafic-limestone contacts (Figure 5.1). Normal faults (NE-SW and E-W directed) were measured from limestone and jasperoidal rocks (Figure 5.2) Strike-slip faults (NNE-SSW directed) were measured from the outcrops at the northern part of Gıcırlar River (Figure 5.3). Using the measured strike of the faults for the rose diagram was prepared (Figure 5.4).

Table 5.1. Fault and Jasperoidal rock measurements

Azimuth/dip			Fault Type
Azimuth	Dip	Dip Direction	
N40W	90	50	Jasperoid
N20W	42	140	Jasperoid
N40W	73	45	Jasperoid
N50W	77	50	Jasperoid
N40W	75	45	Jasperoid
N8E	62	90	Strike-Slip Fault
N20E	57	90	Post Mineral Fault
N40W	90	50	Normal Fault
N85W	90	355	Normal Fault
N5E	10	90	Thrust Fault
N30E	84	315	Post Mineral Fault
N8E	86	315	Normal Fault

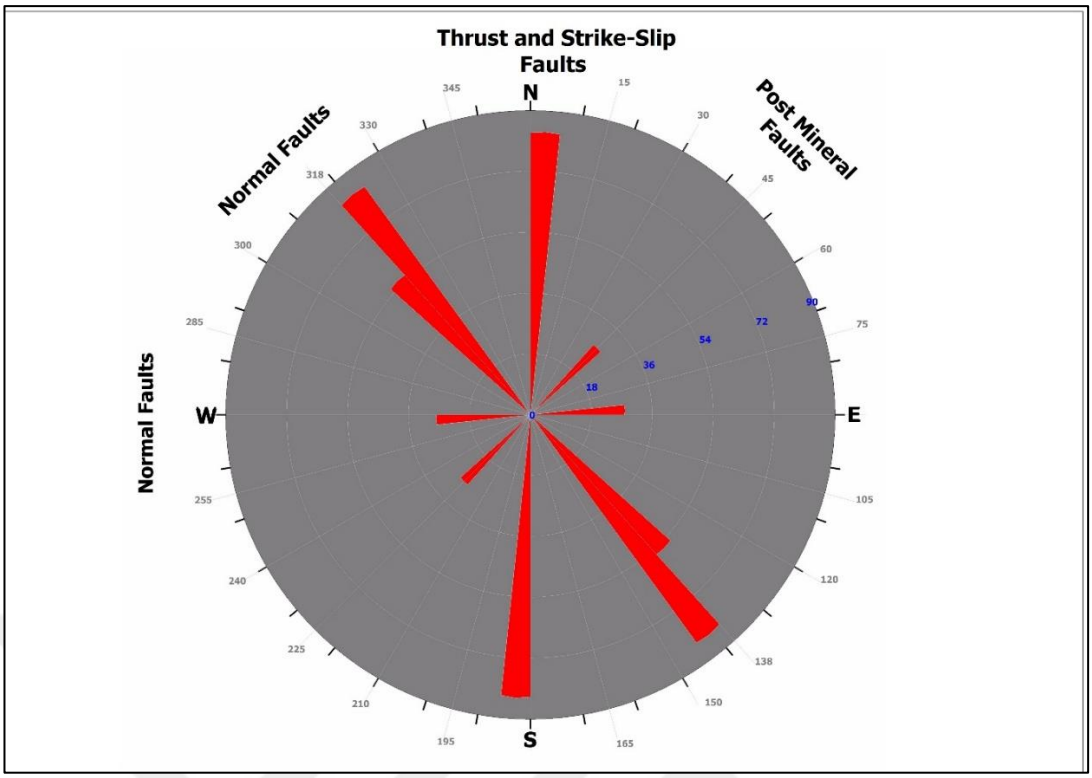

Figure 5.4. The rose diagram shows that the predominant directions for the normal, strike-slip, and thrust faults in the study area

Jasperoidal rock measurements were done during field works. The rose diagram prepared for the jasperoids (Figure 5.5) showed that the predominant direction for the jasperoids is in the NW-SE direction (N35-45W). Measurements and rose diagrams show that mineralization is related to the normal faults in the study area. During field studies, jasperoidal rocks are observed at the places where normal faults are located in beige laminated limestones. Gold mineralized fluids could be used the normal faults as a path. Also, normal faults could have been prepared for the area for the mineralization.

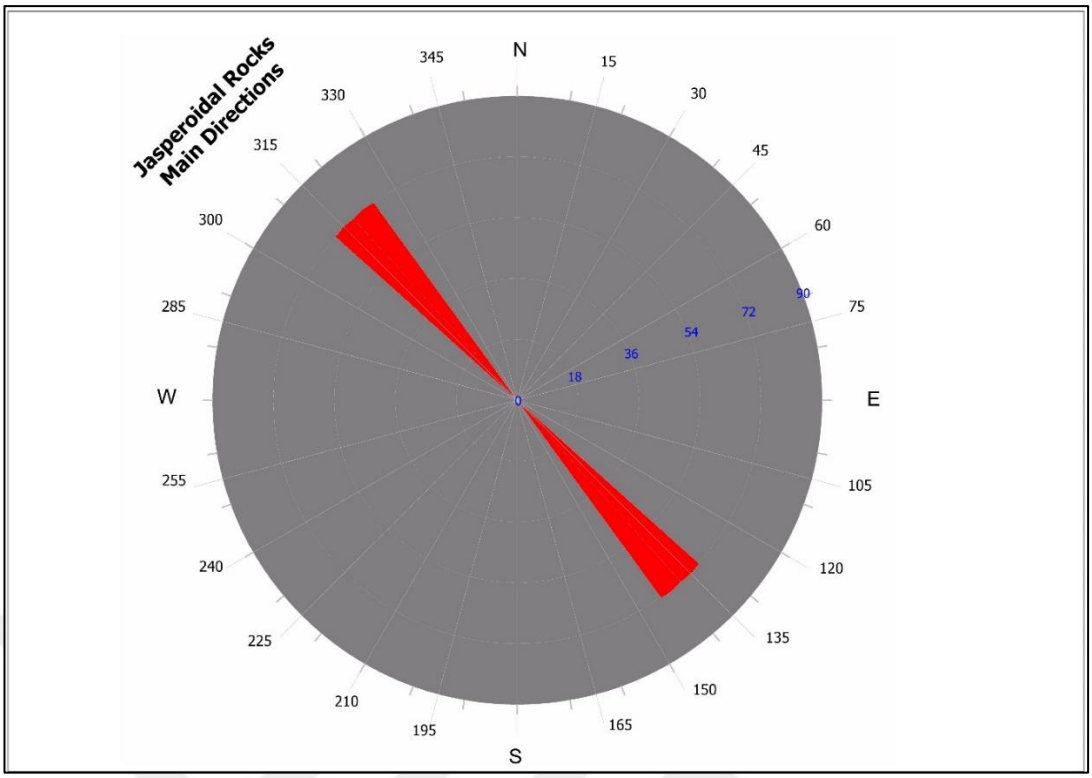

Figure 5.5. The rose diagram shows that the predominant directions for jasperoidal rocks in the study area

6. MINERALOGY AND CHEMISTRY OF THE ORE BODIES

The ore bodies in the study are characterized by oxide close to the surface (upper) and sulfide below the surface (lower) zones. The oxidized and sulfide zones are both strongly silicified and contain predominantly of quartz. The quartz grain size at each zone differs in that the oxidized zone has coarser quartz crystals.

The samples from the oxidized zone consist primarily of fine to coarse-grained quartz associated with iron oxides (mostly hematite and goethite) and gold. The petrographical works showed that nearly 99 percent of the original calcite was removed and replaced by quartz and other minerals above. In that sense, they exhibit more pervasive silicification and oxidation compared to the sulfide zone. Besides, the fracture analyses revealed higher permeability and porosity characteristics in this zone. As the name also impels, common sulfides such as pyrite arsenopyrite and stibnite are not present in this zone. Antimony minerals observed as valentinite in this zone (Figure 4.19).

The sulfide zone is defined as a silicified zone containing abundant stibnite and arsenopyrite along with occasional pyrite. The predominant sulfide in this zone is stibnite that occurs as radiating to rosette-like fibrous crystals. It occurs as disseminations or as patches throughout the silicified rocks. The stibnite is also observed as relict crystals within valentinite (Sb_2O_3) close to the oxide zone. The pyrite is not as common as other sulfides in this ore body and occasionally occur at surface samples from Keşkek Hill as fine-grained and disseminated crystals in jasperoidal rock and within matrix and clasts of matrix-supported breccias.

Both zones have been sampled by grab rock and channel rock sampling methods. Table 6.1 tabulates the abundance of Au, As and Sb of the grab and channel samples collected from the orebodies. The analytical results show that antimony and arsenic are negatively correlated to each other at Güngörmez Hill.

Table 6.1. Abundance of gold, arsenic, and antimony in the grab and channel samples at the ore bodies in the prospect

Grab-Channel Samples					
Orebody_Area	**Sample_ID**	**Description**	**Au (ppm)**	**As (ppm)**	**Sb (ppm)**
Keşkek Hill	**1000**	**Jasperoid**	0.100	678	156.440
Keşkek Hill	**1001**	**Jasperoid**	0.470	560	5073.186
Keşkek Hill	**1002**	**Jasperoid**	0.130	422	577.019
Keşkek Hill	**1003**	**Jasperoid**	0.670	569	208.010
Keşkek Hill	**1004**	**Jasperoid**	0.670	308	4082.461
Keşkek Hill	**1005**	**Matrix supported breccia**	1.270	496	431.668
Keşkek Hill	**1006**	**Jasperoid**	1.030	614	1041.660
Keşkek Hill	**1007**	**Jasperoid including quartz veinlets and stibnite**	1.133	262	13481.027
Keşkek Hill	**1008**	**Jasperoid including quartz veinlets and stibnite**	0.433	169	92044.409
Keşkek Hill	**1009**	**Jasperoid**	0.533	533	1251.059
Demirci Hill West	**1010**	**Jasperoid**	0.200	157	2852.092
Demirci Hill West	**1011**	**Jasperoid**	0.367	1359	910.956
Demirci Hill West	**1012**	**Jasperoid**	0.867	1537	627.187
Demirci Hill West	**1013**	**Jasperoid**	0.200	2620	532.478
Demirci Hill West	**1014**	**Jasperoid**	0.700	2046	136.581
Kaleüstü Hill	**1015**	**Matrix supported breccia**	0.133	279	798.772
Kaleüstü Hill	**1016**	**Matrix supported breccia**	0.133	476	282.528
Kaleüstü Hill	**1017**	**Matrix supported breccia**	0.467	404	2964.257
Güngörmez Hill	**1018**	**Jasperoid including quartz veinlets and stibnite**	0.700	964	545.418
Güngörmez Hill	**1019**	**Jasperoid including quartz veinlets and stibnite**	1.033	243	24220.380
Güngörmez Hill	**1020**	**Jasperoid**	0.133	211	643.747
Güngörmez Hill	**1021**	**Jasperoid including quartz veinlets and stibnite**	0.367	327	137176.642
Güngörmez Hill	**1022**	**Jasperoid**	0.833	1330	1701.336
Güngörmez Hill	**1023**	**Jasperoid**	0.366	530	195.050
Güngörmez Hill	**1024**	**Jasperoid**	0.867	541	1347.752
Güngörmez Hill	**1025**	**Jasperoid**	0.116	371	321.667
Güngörmez Hill	**1026**	**Jasperoid**	0.379	414	831.730
Güngörmez Hill	**1027**	**Jasperoid**	0.341	276	2139.650
Güngörmez Hill	**1028**	**Jasperoid**	0.390	501	336.730
Güngörmez Hill	**1029**	**Jasperoid**	0.402	2434	636.154
Güngörmez Hill	**1030**	**Matrix supported breccia**	0.117	4250	75.293
Güngörmez Hill	**1031**	**Matrix supported breccia**	0.130	5321	83.171
Güngörmez Hill	**1032**	**Jasperoid**	0.255	1749	297.275
Güngörmez Hill	**1033**	**Jasperoid**	0.119	289	148.854

Table 6.1. Continued

Grab-Channel Samples					
Orebody_Area	**Sample_ID**	**Description**	**Au (ppm)**	**As (ppm)**	**Sb 121 (ppm)**
Keşkek Hill	**1034**	**Jasperoid**	0.323	789	428.890
Keşkek Hill	**1035**	**Jasperoid**	0.223	5	2.574
Keşkek Hill	**1036**	**Jasperoid**	0.104	144	110.127
Demirci Hill	**1037**	**Jasperoid**	0.474	32	26.691
Güngörmez Hill	**1038**	**Jasperoid**	0.127	91	195.677
Güngörmez Hill	**1039**	**Jasperoid**	0.145	257	184.963
Güngörmez Hill	**1040**	**Jasperoid**	0.356	442	466.067
Güngörmez Hill	**1041**	**Jasperoid**	0.123	233	221.447
Güngörmez Hill	**1042**	**Jasperoid including quartz veinlets and stibnite**	0.113	338	58627.123
Demirci Hill West	**1043**	**Jasperoid**	0.220	17	1.101
Demirci Hill West	**1044**	**Jasperoid**	0.428	215	35.604
Demirci Hill West	**1045**	**Jasperoid**	0.164	119	374.396
Demirci Hill West	**1046**	**Jasperoid**	0.170	75	3.599
Demirci Hill West	**1047**	**Jasperoid**	0.126	103	180.699
Demirci Hill West	**1048**	**Jasperoid**	0.101	149	191.576
Kaleüstü Hill	**1049**	**Jasperoid**	0.230	161	138.274
Kaleüstü Hill	**1050**	**Jasperoid**	0.244	5	55.627
Kaleüstü Hill	**1051**	**Jasperoid**	0.158	131	222.529
Kaleüstü Hill	**1052**	**Jasperoid**	0.112	8	75.096
Kaleüstü Hill	**1053**	**Jasperoid**	0.109	142	81.486
Kaleüstü Hill	**1054**	**Jasperoid**	0.119	5	49.311
Kaleüstü Hill	**1055**	**Jasperoid**	0.184	1096	146.002
Kaleüstü Hill	**1056**	**Jasperoid**	0.220	170	283.461
Kaleüstü Hill	**1057**	**Jasperoid**	0.310	126	239.315
Kaleüstü Hill	**1058**	**Jasperoid**	0.250	151	858.039
Güngörmez Hill	**1059**	**Jasperoid**	0.703	307	159.066
Güngörmez Hill	**1060**	**Jasperoid**	0.438	275	572.512
Güngörmez Hill	**1061**	**Jasperoid**	0.297	888	574.606
Güngörmez Hill	**1062**	**Jasperoid**	0.252	200	244.005
Güngörmez Hill	**1063**	**Jasperoid**	0.228	354	272.914
Güngörmez Hill	**1064**	**Jasperoid**	0.282	349	1410.167
Güngörmez Hill	**1065**	**Jasperoid**	0.399	181	5775.559
Güngörmez Hill	**1066**	**Jasperoid**	0.535	111	202.292
Güngörmez Hill	**1067**	**Jasperoid**	0.429	253	669.832
Güngörmez Hill	**1068**	**Jasperoid**	0.188	294	474.784
Güngörmez Hill	**1069**	**Jasperoid**	0.804	165	959.622
Güngörmez Hill	**1070**	**Jasperoid**	0.282	1078	250.910

6.1. Geochemical Characteristics of Elements in the Ore Bodies

Geochemical analyses are used to understand the association of gold with the other elements. Correlation tables prepared on excel spreadsheets to observe which elements have a positive correlation with gold (Table 6.2 and 6.3).

The correlation table of core samples shows that gold has a good correlation with arsenic and silver. Grab and channel sample correlation table does not give a correlation between gold and other elements as geochemical data. But during field studies stibnite and valentinite used as a pathfinder mineral to find gold mineralized areas. Fine-grained pyrite is generally observed as oxidized to hematite. In the areas such as deep valleys and new road cuts helped to map the unoxidized pyrite, stibnite, and rare arsenopyrite in jasperoids and breccia clasts in brecciated jasperoids (matrix-supported breccia) (Table 6.1).

Table 6.2. Correlation table for core samples

	Au (ppm)	*Ag (ppm)*	*Al (ppm)*	*As (ppm)*	*Sb (ppm)*	*Ca (ppm)*	*Cd (ppm)*	*Co (ppm)*	*Cr (ppm)*	*Cu (ppm)*	*Fe (ppm)*	*Mg (ppm)*	*Mn (ppm)*	*Na (ppm)*	*Ni (ppm)*	*Pb (ppm)*	*Sc (ppm)*	*Zn (ppm)*	*K (ppm)*	*Ti (ppm)*	*Hg (ppm)*	*% S*
Au (ppm)	1.00																					
Ag (ppm)	0.70	1.00																				
Al (ppm)	0.16	0.04	1.00																			
As (ppm)	0.53	0.56	0.30	1.00																		
Sb(ppm)	0.12	0.02	0.08	0.06	1.00																	
Ca(ppm)	-0.33	-0.05	-0.67	-0.33	-0.17	1.00																
Cd (ppm)	0.03	0.03	0.10	0.04	-0.04	-0.01	1.00															
Co (ppm)	0.00	0.00	0.23	0.43	0.01	-0.27	0.03	1.00														
Cr(ppm)	0.03	0.01	0.18	0.49	0.01	-0.27	0.03	0.92	1.00													
Cu(ppm)	0.00	0.00	0.12	0.06	0.06	-0.11	0.01	0.07	-0.02	1.00												
Fe (ppm)	0.07	0.03	0.53	0.52	0.02	-0.49	0.06	0.89	0.86	-0.02	1.00											
Mg (ppm)	-0.14	-0.03	-0.29	-0.09	-0.06	0.14	-0.20	-0.03	-0.04	-0.04	-0.14	1.00										
Mn (ppm)	-0.04	-0.02	0.55	0.28	0.01	-0.46	0.05	0.73	0.63	0.06	0.80	-0.07	1.00									
Na (ppm)	0.02	-0.01	0.25	0.05	0.11	-0.23	0.03	0.04	0.06	0.00	0.14	0.04	0.17	1.00								
Ni (ppm)	0.00	0.00	0.13	0.41	0.01	-0.20	0.02	0.95	0.91	-0.02	0.87	-0.01	0.66	0.03	1.00							
Pb (ppm)	-0.01	0.00	0.12	0.08	-0.07	-0.07	0.06	0.07	-0.01	0.92	-0.01	-0.04	0.05	0.02	-0.01	1.00						
Sc (ppm)	0.04	0.05	0.36	0.26	0.06	-0.27	0.06	0.49	0.38	0.46	0.47	0.01	0.51	0.05	0.43	0.39	1.00					
Zn (ppm)	0.02	0.00	0.15	0.07	0.12	-0.14	0.01	0.08	0.00	0.95	0.00	-0.05	0.09	0.00	0.00	0.81	0.48	1.00				
K (ppm)	0.22	0.10	0.87	0.30	0.09	-0.62	0.08	0.11	0.05	0.08	0.37	-0.24	0.34	0.23	0.01	0.07	0.23	0.10	1.00			
Ti (ppm)	0.03	0.02	0.54	0.13	0.00	-0.23	0.07	0.11	0.08	0.06	0.29	-0.20	0.34	0.02	0.06	0.07	0.23	0.07	0.20	1.00		
Hg(ppm)	-0.02	-0.01	0.00	-0.02	0.09	0.02	-0.13	-0.02	-0.02	0.02	-0.03	0.02	-0.03	-0.03	-0.02	-0.02	0.00	0.03	0.00	0.04	1.00	
%S	0.03	0.00	0.01	0.01	0.01	-0.03	0.02	0.00	-0.02	-0.01	0.00	-0.05	0.03	0.02	-0.01	0.00	-0.01	-0.01	0.02	-0.02	-0.02	1.00

Table 6.3. Correlation table for grab and channel samples

	Au (ppm)	*Ag (ppm)*	*Al (ppm)*	*As (ppm)*	*Sb (ppm)*	*Ca (ppm)*	*Cd (ppm)*	*Co (ppm)*	*Cr (ppm)*	*Cu (ppm)*	*Fe (ppm)*	*Mg (ppm)*	*Mn (ppm)*	*Na (ppm)*	*Ni (ppm)*	*Pb (ppm)*	*Sc (ppm)*	*Zn (ppm)*	*K (ppm)*	*Ti (ppm)*	*Hg (ppm)*	*% S*
Au (ppm)	1.00																					
Ag (ppm)	0.23	1.00																				
Al (ppm)	-0.01	0.20	1.00																			
As (ppm)	0.01	-0.12	-0.06	1.00																		
Sb(ppm)	0.05	0.26	-0.01	-0.10	1.00																	
Ca(ppm)	-0.11	0.05	0.23	-0.02	0.00	1.00																
Cd (ppm)	0.13	0.85	0.26	-0.09	0.05	0.08	1.00															
Co (ppm)	0.02	0.09	0.11	0.67	-0.07	0.09	0.16	1.00														
Cr(ppm)	-0.18	0.08	-0.24	0.41	-0.10	-0.12	0.14	0.46	1.00													
Cu(ppm)	0.03	0.19	0.15	-0.01	-0.10	-0.07	0.25	0.20	0.18	1.00												
Fe (ppm)	0.03	0.13	0.25	0.52	-0.11	0.01	0.20	0.65	0.37	0.45	1.00											
Mg (ppm)	-0.12	0.06	0.28	0.02	-0.04	0.98	0.10	0.12	-0.10	-0.09	0.04	1.00										
Mn (ppm)	-0.07	0.12	0.53	0.08	-0.08	0.43	0.18	0.35	0.03	0.20	0.39	0.41	1.00									
Na (ppm)	-0.07	0.04	0.45	-0.07	0.06	0.28	0.08	0.09	-0.07	-0.02	0.12	0.22	0.41	1.00								
Ni (ppm)	-0.01	0.05	-0.06	0.66	-0.07	0.00	0.09	0.83	0.55	0.13	0.70	0.03	0.20	-0.03	1.00							
Pb (ppm)	-0.08	0.07	0.09	-0.08	-0.05	-0.02	0.10	-0.05	-0.10	0.12	0.11	-0.02	0.22	-0.05	-0.02	1.00						
Sc (ppm)	0.00	0.22	0.68	0.30	-0.05	0.28	0.25	0.42	0.16	0.12	0.47	0.30	0.65	0.43	0.32	0.04	1.00					
Zn (ppm)	0.09	0.19	0.11	0.22	0.04	0.09	0.26	0.37	0.34	0.24	0.52	0.09	0.47	0.14	0.52	0.16	0.37	1.00				
K (ppm)	0.08	0.16	0.80	-0.03	0.02	0.06	0.23	0.04	-0.25	0.26	0.25	0.13	0.30	0.07	-0.07	0.22	0.43	0.07	1.00			
Ti (ppm)	-0.22	0.13	0.35	-0.21	-0.09	0.06	0.17	-0.02	0.14	0.09	-0.01	0.08	0.22	0.17	-0.11	-0.08	0.34	-0.02	0.00	1.00		
Hg(ppm)	-0.27	0.11	0.40	-0.10	-0.05	0.20	0.25	0.05	0.04	0.15	0.11	0.17	0.26	0.04	-0.02	-0.12	0.28	-0.03	0.21	0.33	1.00	
%S	0.31	0.04	0.14	0.06	0.28	-0.04	0.07	0.07	-0.09	-0.08	-0.02	-0.02	-0.05	-0.01	-0.01	-0.06	0.05	-0.02	0.20	-0.05	0.00	1.00

To constrain the vertical extension and mineralization potential at depth, six drill holes have been relogged, and cores have been sampled. The logging is in the form of a quick-log showing only the main lithologies and hosts rocks along with structural, alteration, and mineralogical data identified during logging. The quick-logs show that the deeper levels (intersections) at ore bodies at the Keşkek Hill and Güngörmez Hill share similarities in terms of Au abundance, alteration, and mineralogy (Figure 6.1). In these intersections, fine-grained pyrite-arsenopyrite have been identified within the clasts of matrix-supported breccia, and stibnite was observed in the jasperoidal rocks (Table 6.4).

Table 6.4. The quick-logs showing the abundance, lithology, and alterations intersected by the drill holes at the prospect

Hole ID	From	To	Description	Au (ppm)	As (ppm)	%S	Sb (ppm)
KTS-6	33.00	34.80	Jasperoid	0.125	5	0.012	217.388
KTS-6	36.00	38.10	Jasperoid	0.261	299	0.016	351.647
KTS-6	72.60	73.50	Jasperoid including pyrite-arsenopyrite	0.114	138	0.124	5.000
KTS-7	65.35	66.20	Moderatly silicified and strongly oxidized jasperoid (fault zone)	0.189	151	0.000	159.772
KTS-7	66.20	67.00	Matrix supported breccia including pyrite-arsenopyrite	2.656	324	0.875	411.111
KTS-7	67.00	67.55	Matrix supported breccia including pyrite-arsenopyrite	3.175	536	0.008	578.042
KTS-7	67.55	68.25	Jasperoid	0.632	559	0.021	1184.587
KTS-7	68.25	69.20	Jasperoid	0.474	269	0.012	410.176
KTS-7	69.90	70.70	Jasperoid	0.170	38	0.101	101.305
KTS-7A	27.00	28.40	Jasperoid including arsenopyrite	0.526	1711	-	982.123
KTS-7A	28.40	29.25	Jasperoid including arsenopyrite and stibnite	0.637	1873	-	10744.427
KTS-7A	29.25	30.60	Jasperoid	0.542	750	-	601.012
KTS-7A	30.60	31.20	Jasperoid	0.164	673	-	483.740
KTS-7A	32.00	33.00	Jasperoid	0.160	1105	-	794.354
KTS-7A	33.00	34.00	Jasperoid	0.410	914	-	525.988
KTS-7A	34.00	35.05	Matrix supported breccia	1.524	623	-	2048.660
KTS-8	6.80	7.80	Matrix supported breccia including stibnite-arsenopyrite	1.365	1725	-	1203.889
KTS-8	7.80	8.40	Matrix supported breccia including pyrite-arsenopyrite	1.116	1148	0.077	336.485
KTS-8	8.40	9.00	Matrix supported breccia including pyrite-arsenopyrite	0.778	1160	-	400.765
KTS-8	9.00	10.20	Matrix supported breccia including pyrite-arsenopyrite	1.896	1628	-	671.797
KTS-8	10.20	10.90	Matrix supported breccia including pyrite-arsenopyrite	10.072	12209	-	2770.226
KTS-8	10.90	11.60	Matrix supported breccia including pyrite-arsenopyrite	5.289	18662	-	560.748
KTS-8	11.60	12.30	Matrix supported breccia including pyrite-arsenopyrite	2.066	9135	-	1215.891
KTS-8	12.30	13.30	Jasperoid including stibnite	0.295	610	-	6489.174
KTS-8	13.30	14.30	Jasperoid including stibnite	0.569	998	-	4628.224
KTS-8	14.30	15.25	Jasperoid including stibnite	2.580	846	-	1451.558
KTS-8	18.50	19.00	Jasperoid including stibnite	0.655	516	-	3684.501
KTS-8	19.00	19.50	Jasperoid including stibnite	0.388	411	-	7648.413
KTS-9	17.70	18.15	Jasperoid including stibnite	0.168	157	-	54525.779
KTS-9	18.15	19.00	Jasperoid including stibnite	1.257	1298	-	2204.718
KTS-9	19.00	19.90	Jasperoid including stibnite	0.778	3743	-	1667.385
KTS-9	19.90	20.60	Jasperoid	0.192	3286	-	378.937
KTS-9	20.60	21.40	Jasperoid	0.163	6177	-	251.105
KTS-9	21.40	22.00	Jasperoid	0.196	5333	-	169.050
KTS-9	22.00	22.50	Jasperoid	0.871	5565	-	234.497
KTS-9	22.50	23.20	Jasperoid	0.341	1383	-	53.237
KTS-9	23.20	23.90	Jasperoid	0.960	1407	-	138.297
KTS-9	23.90	24.55	Jasperoid	0.712	2284	-	449.947
KTS-9	24.55	25.40	Jasperoid	0.686	1742	-	175.220
KTS-9	25.40	25.80	Jasperoid	0.519	3480	-	461.523
KTS-9	26.50	27.20	Jasperoid	0.127	168	-	19.186
KTS-9	28.40	28.75	Jasperoid including stibnite	0.583	731	-	39537.774
KTS-12	16.00	16.85	Jasperoid including stibnite	0.461	216	-	49353.511
KTS-12	16.85	17.70	Jasperoid including stibnite	0.209	570	-	386.298
KTS-12	20.40	21.40	Jasperoid including stibnite	0.317	381	-	9037.339
KTS-12	21.40	22.50	Jasperoid including stibnite	0.130	919	-	426.828
KTS-12	24.20	25.00	Jasperoid including stibnite-arsenopyrite	0.142	2372	-	370.675

7. FLUID INCLUSION/MICROTHERMOMETRIC ANALYSES

Fluid inclusion analysis is an important tool to find out the Physico-chemical conditions of the hydrothermal fluids which are responsible for the alteration and mineralization processes. The aim of the fluid inclusion analyses in this thesis is to identify the Physico-chemical characteristics of the trapped fluids and changes in these through time at the Keşkek Hill Project area.

7.1. Petrography and Inclusion Types

Quartz crystals and quartz veinlets contain numerous fluid inclusion assemblages. Fluid inclusion studies have been carried out on the first (pre-syn-ore stage) and second phase quartz crystals (syn-ore stage). The third phase colloidal textured chalcedonic quartz crystals were too small to measure inclusion. Two samples were examined for proper fluid inclusion types (Figure 7.1a and 7.1b). The petrographic study of fluid inclusion identifies the overall paragenesis and type of fluid inclusion assemblage. One of the samples was taken from jasperoidal rock with syn-ore stage quartz, sample Q-1 and the other one is from a pre-syn ore stage quartz and syn-ore comb textured quartz-stibnite bearing sample (QSB-1). While measuring the QSB sample pre-syn ore stage and syn-ore stage-related inclusions were found and measured. The homogenization temperatures of Q-1 and stibnite bearing comb textured quartz are similar to each other. But pre-syn-ore stage quartz inclusions' homogenization temperatures are much higher than the syn-ore-stage quartz minerals. Both of the samples have proper homogenized primary fluid inclusion (Q-1 and QSB-1) (Figure 7a1a and 7b1b).

Fluid inclusion measurements completed on primary inclusions classified as type 2 based on the scheme proposed by Shepherd at al., (1985) and Nash (1976). Type 2 inclusions are defined as two-phase (liquid-vapor; L-V) fluid inclusions. The vapor percentage is variable but mostly comprise 10% of the inclusion. Only a few inclusions contain a vapor phase comprising about 20 (Figure 7.1a and 7.1b)). The dimensions of the inclusions range from 4.4 to 19.3 μm mostly (~ 9μm), and are irregular in shape (Table 7.1).

Table 7-1. Fluid inclusion types, and microthermometric analyses on the inclusions

Sample ID	Host Mineral	Type	Shape	Phases Room T	Vapor %	Size (μm)	Te app (°C)	Tm ice (°C)	Th L-V (°C)	Th total(°C)	NaCl %
Q_1	Quartz	Primary	Irregular	L-V	10	9.7			175.1	175.1	0.0
Q_2	Quartz	Primary	Irregular	L-V	10	11.7	-42.1	-2.2	179	179	3.7
Q_3	Quartz	Primary	Irregular	L-V	10	12.1	-46.8	-2.6	173.5	173.5	4.3
Q_4	Quartz	Primary	Irregular	L-V	10	11.7	-39.1	11.9	136	136	15.9
Q_5	Quartz	Primary	Irregular	L-V	10	14.4	-45.3	0.4	160	160	0.7
Q_6	Quartz	Primary	Irregular	L-V	20	15	-47.8	-2.4	182	182	4.0
Q_7	Quartz	Primary	Irregular	L-V	10	7	-48.9	-2.8	156	156	4.6
Q_8	Quartz	Primary	Irregular	L-V	10	9.6	-47.4	-1.9	176.6	176.6	3.2
Q_9	Quartz	Primary	Irregular	L-V	10	8.6	-47.2	8.1	168.9	168.9	11.8
Q_10	Quartz	Primary	Irregular	L-V	10	4.4	-48.1	6.3	172.5	172.5	9.6
Q_11	Quartz	Primary	Irregular	L-V	10	8.8	-41.3	5	176.1	176.1	7.9
Q_12	Quartz	Primary	Irregular	L-V	10	5.1	-48.7	-3.5	182.7	182.7	5.7
Q_13	Quartz	Primary	Irregular	L-V	10	7.6	-52.3	-1.7	168	168	2.9
Q_14	Quartz	Primary	Irregular	L-V	10	6.9	-42.5	4.2	164	164	6.7
Q_15	Quartz	Primary	Irregular	L-V	10	5.3	-47.6	0.6	169.5	169.5	1.1
QSB_1	Quartz	Primary	Irregular	L-V	10	4.7	-51.8	-3.5	288.7	288.7	5.7
QSB_2	Quartz	Primary	Irregular	L-V	10	12.3	-57.8	-4.8	313	313	7.6
QSB_3	Quartz	Primary	Irregular	L-V	10	12.1	-47.6	4.8	172.8	172.8	7.6
QSB_4	Quartz	Primary	Irregular	L-V	10	6.1	-49.2	7.8	170.2	170.2	11.5
QSB_5	Quartz	Primary	Irregular	L-V	10	4.4	-48.7	6.2	164.1	164.1	9.5
QSB_6	Quartz	Primary	Irregular	L-V	10	9.6	-59.2	-3.9	291.6	291.6	6.3
QSB_7	Quartz	Primary	Irregular	L-V	10	19.3	-63.5	-3.9	290	290	6.3

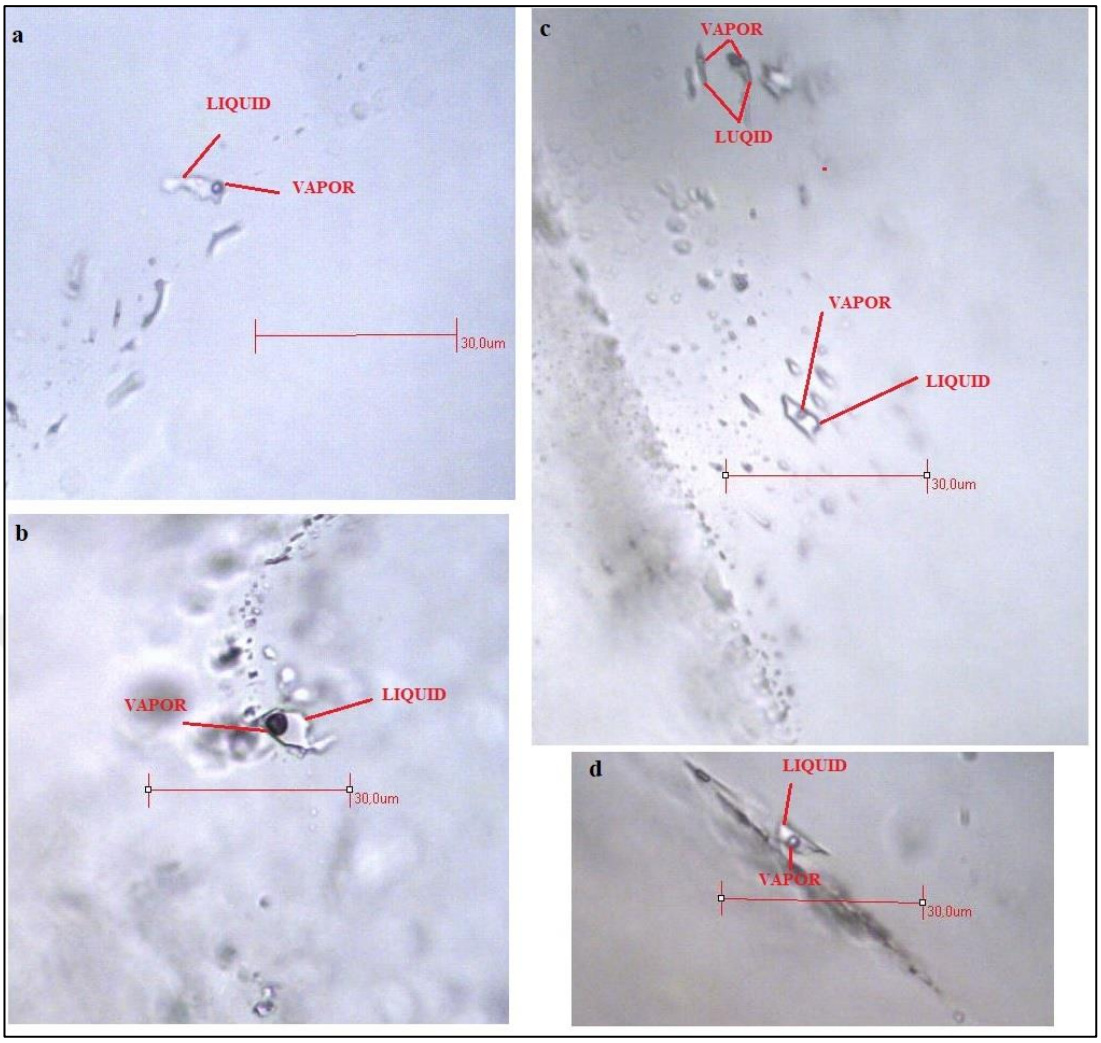

Figure 7.1. Two phases (L-V) inclusions; a, c and d showing inclusions with 10% vapor b) inclusion with 20% vapor

7.2. Microthermometric Analysis

The homogenization temperatures (T_h °C) were measured from Type 2 two-phase inclusions (Table 7.1). The melting temperature (Tm °C) and salinity (NaCl%) are estimated based on Bodnar (1993) equations.

7.2.1. Microthermometric analyses on samples from pre-syn-ore stage and syn-ore stage quartz minerals in jasperoid

The fluid inclusion analyses from pre-syn-ore and syn-ore stage quartz refer to type 2 inclusions at sample QSB-1. QSB-1 sample thin section studies show that there are three phases in this sample. The first phase is observed as amorph quartz crystals, the

second one is observed as comb texture with stibnite and the last phase is colloidal textured quartz minerals (Figure 4.9). The microthermometric analyses on type 2 inclusions show that the homogenization temperature (T_h °C) of the first phase quartz minerals ranges from 288.7 °C to 313 °C (Figure 7.2). The ice melting temperature (Tm_{ice}) changing from -4.8°C to -3.5 °C and the salinity ranges from 5.71 to 7.59 wt. % NaCl eq (Figure 7.3), and was estimated using the formula of Bodnar (1993). The microthermometric analyses on type 2 inclusions show that the homogenization temperature (T_h °C) of the second phase quartz minerals ranges from 164.1 °C to 172.8 °C (Figure 7.2). The ice melting temperature (Tm_{ice}) changing from 4.8°C to 7.8 °C and the salinity ranges from 7.6 to 11.5 wt. % NaCl eq (Figure 7.3), and was estimated using the formula of Bodnar (1993).

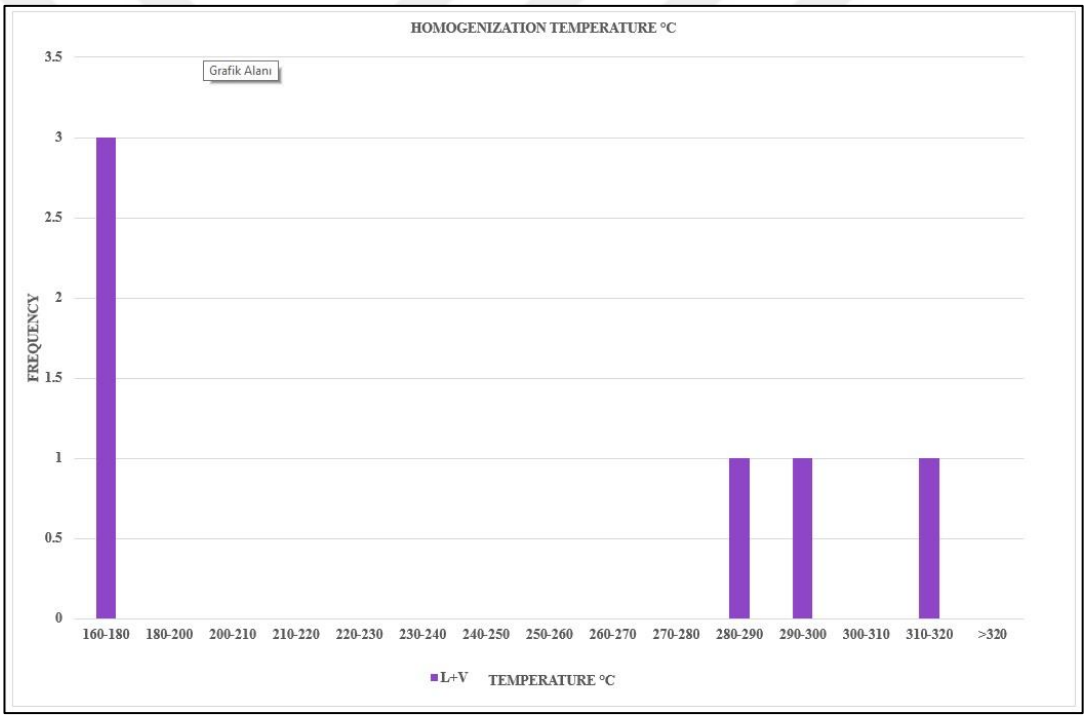

Figure 7.2. The frequency graph illustrating homogenization temperature of type 2 inclusions from QSB-1

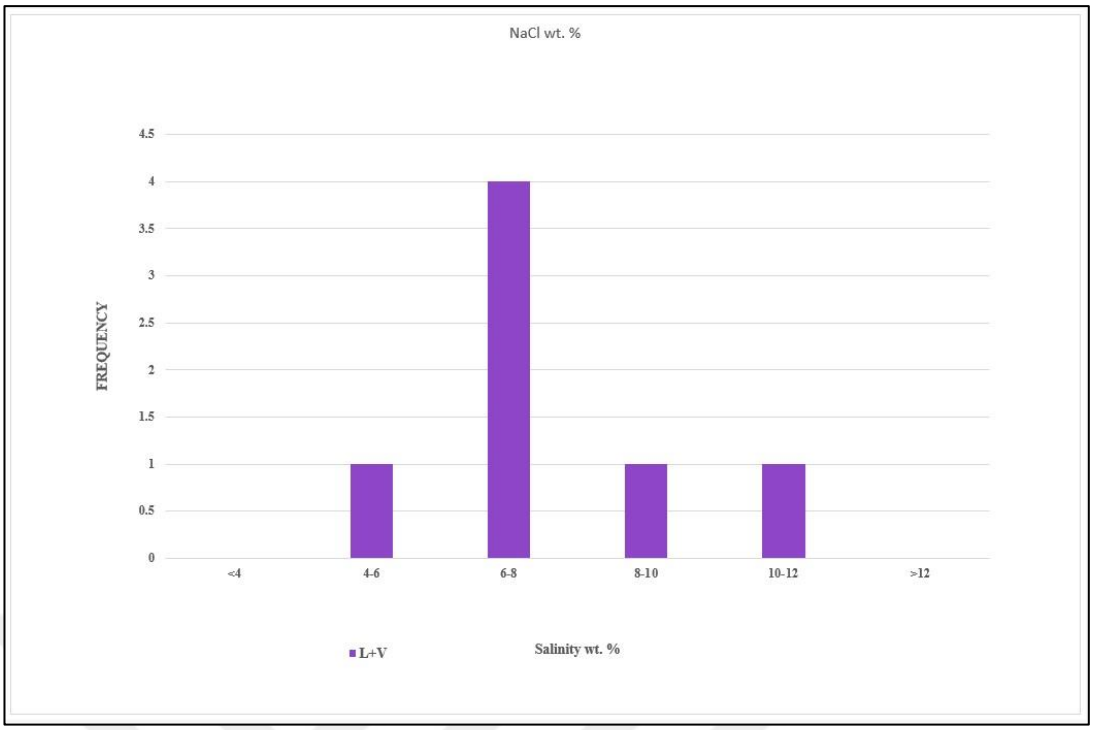

Figure 7.3. The frequency graph illustrating salinity (NaCl wt. % equivalent) of type 2 inclusions from QSB-1 Microthermometric analysis on samples from pre-syn-ore and syn-ore stage quartz in jasperoid

Q-1 sample petrographic studies include thin sections and field works. Thin section studies show that the Q-1 sample includes quartz minerals, which are changing texture from fine-grained to coarse-grained, could be the syn-ore stage quartz. This sample also includes micron-sized comb textures (Figure 4.9). Q-1 sample quartz minerals selected for oxygen stable isotope analyses and jasperoid including these quartz minerals also selected for hydrogen stable isotope analyses. Q-1 sample contains syn-ore stage quartz crystals. These samples' homogenization temperature (T_h °C) of type 2 inclusions ranges from 136 °C to 182.7 °C (Figure 7.5). The ice melting temperature (Tm_{ice}) changing from -3.5 °C to 11.9 °C. The salinity ranges from 0.70 to 15.86 wt. % NaCl eq. (Figure 7.6) which was calculated by using the formula of Bodnar (1993).

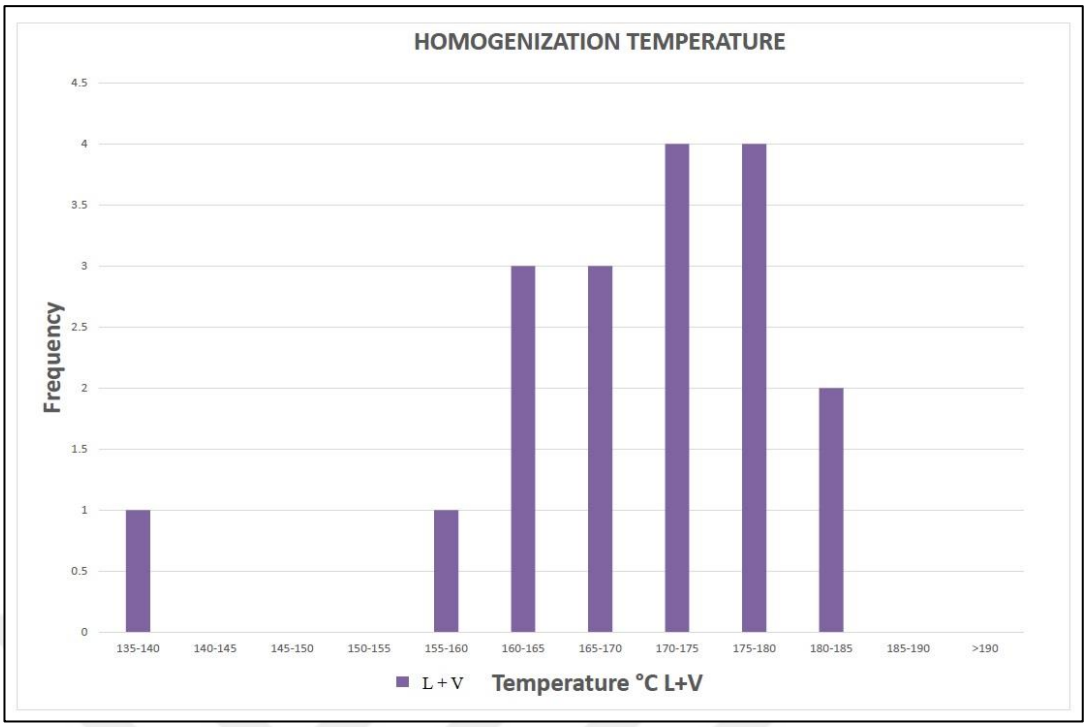

Figure 7.4. The frequency graph illustrating homogenization temperature of syn-ore stage quartz in Q-1

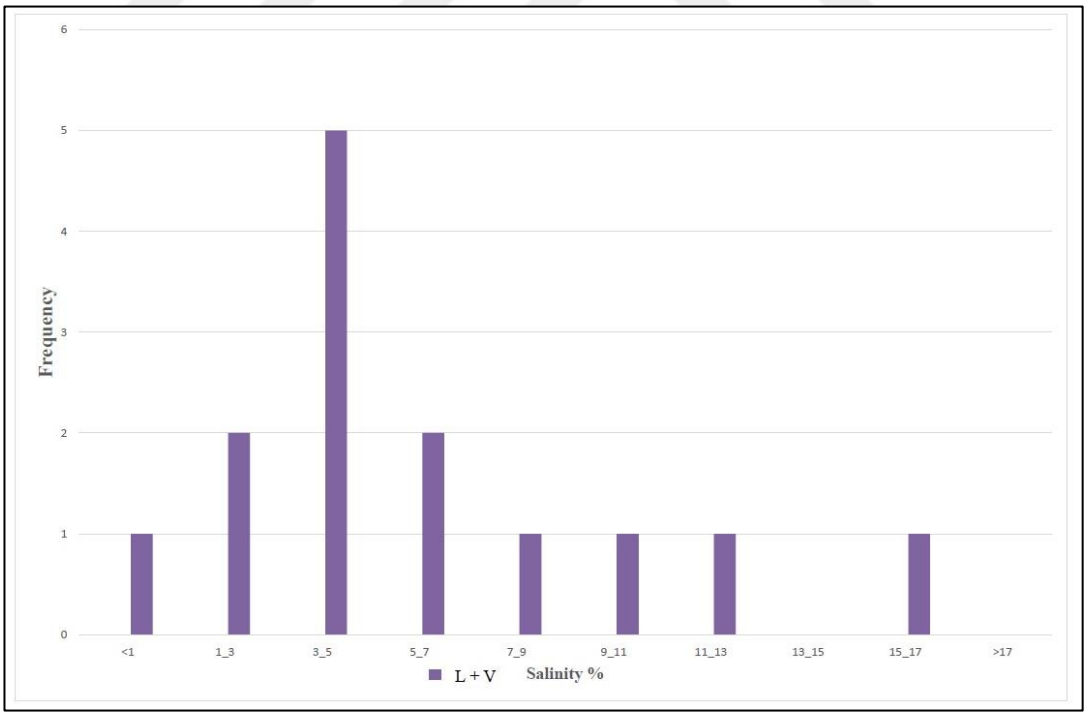

Figure 7.5. The frequency graph illustrating salinity (NaCl wt.% equivalent) of syn-ore stage quartz in Q-1

8. STABLE ISOTOPE GEOCHEMISTRY

To better understand the source and evolution of the hydrothermal fluids and mineralization in the study area, the oxygen and hydrogen isotopes analyses have been conducted (Cline and Hofstra, 2000). During this study, two samples on which the fluid inclusion analyses were also conducted were selected for stable isotope geochemistry.

8.1. Oxygen – Hydrogen Isotopes

The isotopic compositions of oxygen ($^{18}O/^{16}O$; $\delta^{18}O$) and hydrogen (deuterium, δD) from quartz and whole-rock separates are shown in Table 8.1. Oxygen isotope analyses show that the $\delta^{18}O_{(quartz)}$ values for sample syn-ore stage quartz, Q-1 is 11.1‰. $\delta D_{(quartz)}$ value of the whole rock sample is -89‰. Since these values refer to $\delta^{18}O$ and δD isotope compositions of mineral separates (quartz in jasperoid and jasperoid), the isotopic composition of fluid in equilibrium with quartz should be calculated by using isotope fractionation equation (Table 8.2).

The $\delta^{18}O$ and δD values for fluid ($\delta^{18}O_{(fluid)}$ and $\delta D_{(fluid)}$) in equilibrium with the quartz crystals in jasperoid and jasperoid whole-rock were calculated using the quartz-H_2O fractionation equation and the average homogenization temperature (169 °C) of inclusions at Q-1 (Table 8.2).

The calculated $\delta^{18}O$ and δD values given in Table 8-1. Results are plotted in the $\delta^{18}O_{fluid}$ vs δD_{fluid} diagram (Figure 8.1).

Table 8.1. Stable isotope analytical results for minerals

Sample ID	Th °C	Kelvin	Kelvin Temperature	Calculation	$\delta^{18}O$(Quartz) ‰	$\delta^{18}O$(fluid) ‰	δD (jasperoid)	δD (fluid)‰
Q-1	175.1	273.15	448.25	13.42	11.1	-2.32	-89	-102.42
Q-2	179	273.15	452.15	13.13	11.1	-2.03	-89	-102.13
Q-3	173.5	273.15	446.65	13.54	11.1	-2.44	-89	-102.54
Q-4	136	273.15	409.15	16.79	11.1	-5.69	-89	-105.79
Q-5	160	273.15	433.15	14.62	11.1	-3.52	-89	-103.62
Q-6	182	273.15	455.15	12.92	11.1	-1.82	-89	-101.92
Q-7	156	273.15	429.15	14.95	11.1	-3.85	-89	-103.95
Q-8	176.6	273.15	449.75	13.31	11.1	-2.21	-89	-102.31
Q-9	168.9	273.15	442.05	13.90	11.1	-2.80	-89	-102.90
Q-10	172.5	273.15	445.65	13.62	11.1	-2.52	-89	-102.62
Q-11	176.1	273.15	449.25	13.35	11.1	-2.25	-89	-102.35
Q-12	182.7	273.15	455.85	12.87	11.1	-1.77	-89	-101.87
Q-13	168	273.15	441.15	13.97	11.1	-2.87	-89	-102.97
Q-14	164	273.15	437.15	14.29	11.1	-3.19	-89	-103.29
Q-15	169.5	273.15	442.65	13.85	11.1	-2.75	-89	-102.85
Hisaralan-1	Aksoy et al. (2009)					-8.05		-63.10
Hisaralan-3						-7.94		-48.00
Hisaralan-7						-8.98		-61.40
Hisaralan-8						-8.95		-61.30
Hisaralan-10						-9.04		-61.80
Hisaralan-12						-8.67		-59.00
Hisaralan-14						-8.55		-57.30
Hisaralan-16						-8.05		-63.10
Hisaralan-8A						-7.94		-48.00
Horzum/Sazdere Hot Spring	Bülbül (2009)					-3.17		-53.90
Alaşehir Hot Spring						-7.55		-48.97
Alaşehir Hot Spring						-8.88		-50.23
Alaşehir Geothermal Drill 1						-4.69		-62.82
Acıdere Hot Spring						-6.95		-43.67
Alaşehir Geothermal Drill 2						-1.96		-40.67
Alaşehir-Kula Donations Tap						-7.28		-39.85
Şendurak-Kasaplar Drill Hole						-5.62		-51.92
Sarıkız Mineral Water Spring						-8.5		-46.11
Sarıkız Mineral Water Spring						-9.66		-51.89
Snow Sample Around Dededağ-Ayıdağı						-8.11		-37.07
Drill Hole Close to Tariş-Tat INC.						-10.26		-59.39

Table 8.2. Isotope fractionation equations

Isotope fractionation equations	Temperature ranges (°C)	Reference
Oxygen		
$1000\ln\alpha_{(quartz)}\text{-}H_2O = 3.38 \times 10^6 \times T^{-2} - 3.4$	0-500	Clayton et al., 1972
Hydrogen		
$1000\ln\alpha_{(quartz)}\text{-}H_2O = 3.38 \times 10^6 \times T^{-2} - 3.4$	0-500	Clayton et al., 1972
$1000\ln\alpha \approx \delta^{18}O(mineral) - \delta^{18}O(fluid)$		Beaudoin and Therrien, 2004

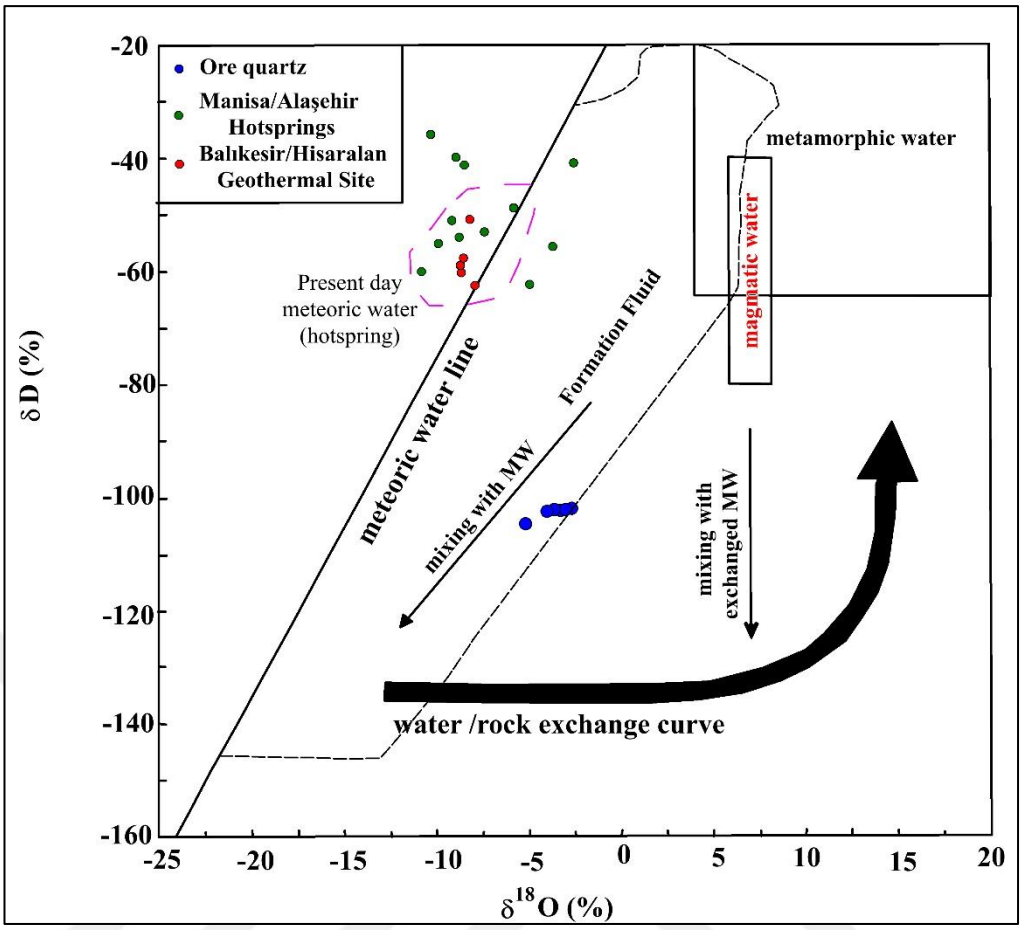

Figure 8.1. Calculated δ18O (fluid) and δD (fluid) values for hydrothermal fluids in equilibrium with quartz in jasperoid and jasperoid in Keşkek Hill prospect (modified from Cline and Hofstra, 2000). The formation water area is taken from Taylor and Sheppard (1986). MW means meteoric water.

The $\delta^{18}O_{(fluid)}$ vs $\delta D_{(fluid)}$ data collected as modern meteoric water isotopic composition from areas, which are Hisaralan and Alaşehir hot springs. Hisaralan/Sındırgı/Balıkesir hot springs are approximately 57.2 km away with the highway from the study area and Alaşehir/Manisa hot springs are approximately 114 km away with the highway from the study area. Collected data also plotted on the same diagram to observe the effect or potential mixing by local meteoric water. The modern /present-day meteoric water isotopic composition is environed as a purple dashed circle (Figure 8.1).

The calculated $\delta^{18}O_{(fluid)}$ vs $\delta D_{(fluid)}$ diagram shows that ore stage fluid plot in an array towards meteoric water line, and it also exhibits a pattern similar to mixing trend with meteoric water besides that sample plots lie within the formation water area. This may

suggest that ore-stage fluid is mixed fluid and formed by mixing of fluid gathered from formation water and meteoric water during the mineralization stage (Figure 9.4).

8.2. Sulfur Isotope

The sulfur isotope ($\delta^{34}S_{VCDT}$ ‰) analyses were performed on stibnite (Sb_2S_3) crystals in quartz veinlets (QSB-1) and jasperoids. $\delta^{34}S_{VCDT}$ ‰ isotope value measured as -0.6‰.

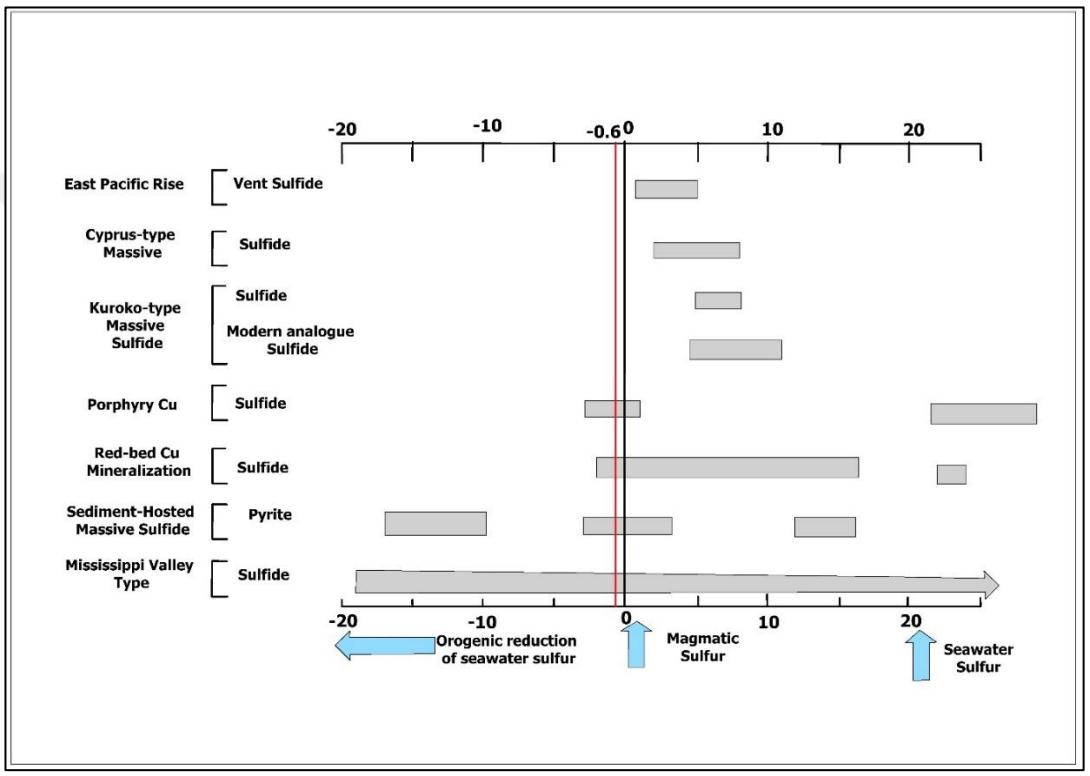

Figure 8.2. Plot of δ34SVCDT ‰ value for stibnite in the study area (red line refers to the value obtained in this study) (Simplified from Rollinson, 1993)

The $\delta^{34}S_{VCDT}$ ‰ value for the stibnite plotted to previous studies on the Carlin deposit sulfur isotope value diagram (Figure 8.3). Keşkek Hill sulfur isotope plot results are similar to previous sulfur isotope studies on the Screamer deposit and Carlin trend in Nevada.

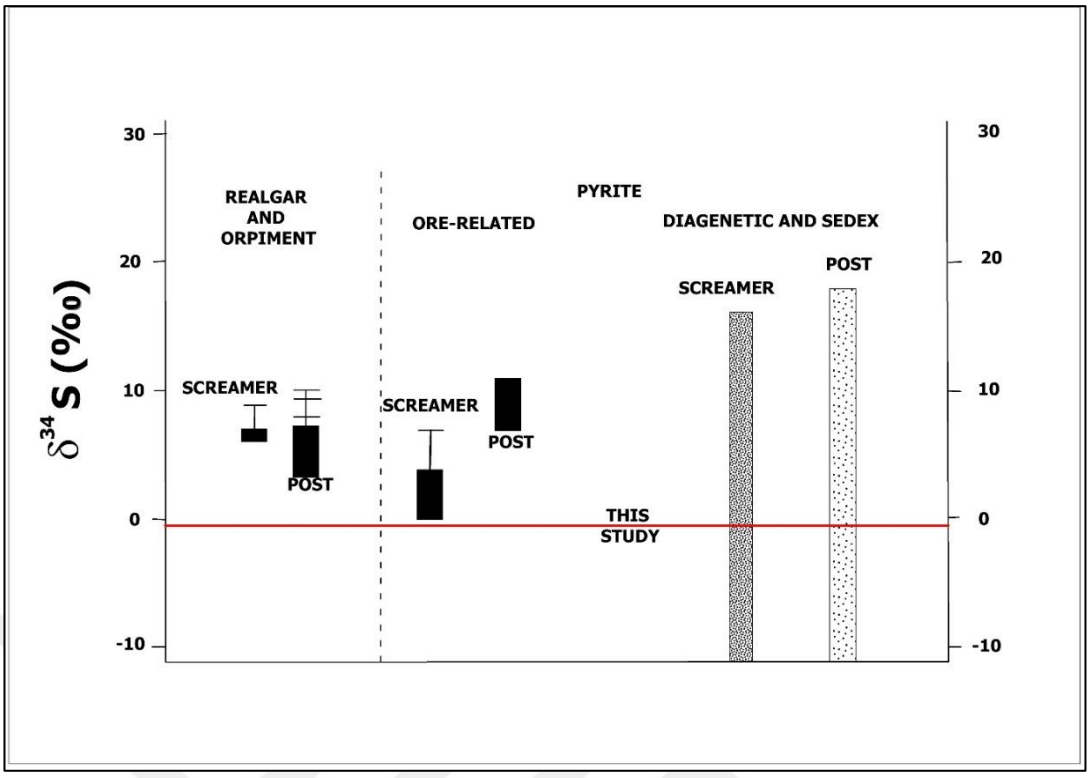

Figure 8.3. Variation in δ34SVCDT ‰ value of stibnite from Keşkek Hill prospect and Carlin trend sulfur isotope values. (Simplified from Kesler et al., 2005).

9. DISCUSSION

9.1. Tectonic Relationship between Ophiolitic Mélange and Jasperoid Occurrences

Keşkek Hill Project area is largely covered by ophiolitic mélange and its products (Figure 3-1). From the northern part to the southern part of the study area, the rocks of the ophiolitic suite observable in the area. The northern part of the study area is mainly composed of limestones and ultramafic rocks (peridotite, harzburgite, and a small amount of pillow basalts) of the ophiolitic suit. Ultramafic rocks are generally serpentinized and blocky in itself. The southern part of the study area covered with sedimentary units (mudstone, low degree metamorphosed sandstone, and limestone blocks) of the ophiolitic unit.

The study area and Gördes Basin are bounded by metamorphic rocks of Menderes Massive to the east and by ophiolitic mélange units of the Bornova flysch zone to western and northern part (Şengör and Yılmaz, 1981, Seyitoğlu and Scott, 1994a, b). The thrust faults in the study area show that ophiolitic mélange is thrusting over the basement rocks with a low angle (Purvis and Robertson, 2005).

The compressional deformation started at Late Cretaceous and ended at the Eocene period. Extensional tectonism in Western Anatolia at Miocene affects the study area (Rojay, 2004). Thrust fault between the ophiolitic mélange and basement metamorphic rocks as a result of extensional tectonism has been changed to detachment fault in the study area. East-West directed faults observed in the study area are perpendicular to this detachment fault plane.

The fluids that resulted in alteration and mineralization, deeply circulated through the normal faults after the extension period. As a result, fluids circulation gave way to decarbonatization, brecciation, and first phase silicification in the area. Continuous extensional tectonism resulted in the exposure of these silicified zones. After this period, the mixing of meteoric water and relatively high-temperature fluids occurred. The mixed fluid was circulated in the brecciated zones and decarbonized-silicified zones. As a result of this circulation jasperoid and mineralization occurred in the area.

9.2. Physico-chemical Evolution of the Alteration and Mineralization

As a result of extensional tectonism lateritization, decarbonatization in dirty limestones (BLL), silicification and meteoric water circulation took place in the study area and surrounding area. Decarbonization in dirty limestone resulted in collapse breccias and cavities in carbonate rocks. Relatively high temperature (at around 300 °C) pre-ore fluids responsible from decarbonization and silicification. After this event relatively low temperature (at around 169 ˚C) meteoric water mixed ore-forming fluids circulate in the decarbonize and silicified cavities and, breccias in the fault zones (Figure 9.1). Meteoric water makes the ore-forming fluid more oxidized and cooler the result of this mixing is Keşkek Hill gold mineralization.

Keşkek Hill gold mineralization is hosted by pervasively silicified and oxidized jasperoidal rocks. Northwest – southeast directed jasperoids are conformable to normal faults. Post mineral faults are generally high angle normal faults.

Dark gray massive recrystallized limestone has dolomite crystals and aged as Jurassic (Canik, 1962). Beige colored laminated limestones in Keşkek Hill area are bounded by faults and these faults also mark the interfaces where RXL and BLL are juxtaposed (Figures 4.2 and 4.3)

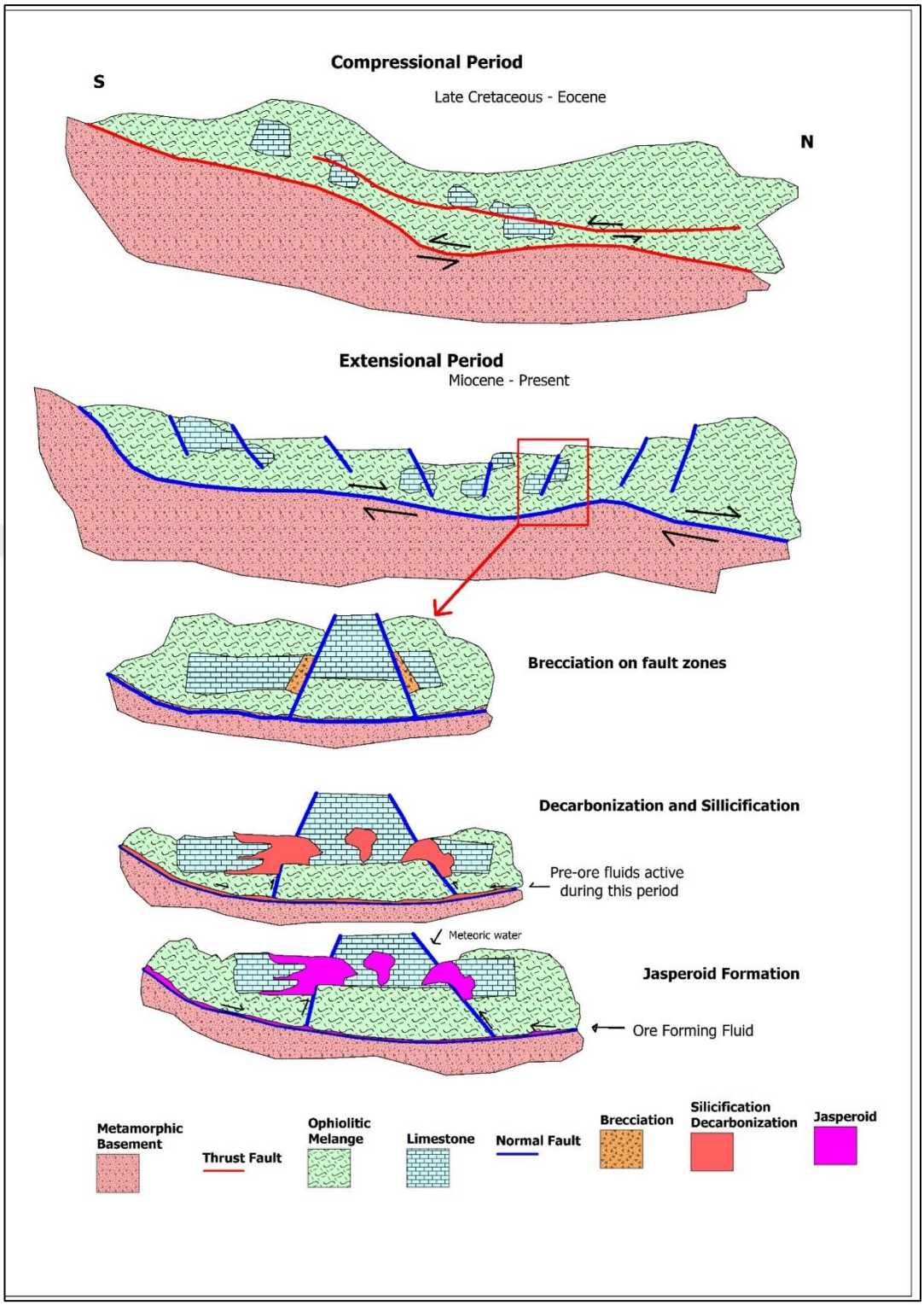

Figure 9.1. Genesis and formation of the Keşkek Hill jasperoids

9.3. Constraints on Styles of Alteration and Mineralization Type in Keşkek Hill Project

Jasperoid was originally described as "a rock type consisting substantially of cryptocrystalline, chalcedonic, or phenocrystalline silica, which formed due to the replacement of other material, especially calcite or dolomite" (Spurr 1898). This definition was not covering all the missing parts describing jasperoid. Due to these missing parts, Lovering (1972) described the jasperoids by using their physical properties and genesis of jasperoid. He also appreciated the jasperoid as a guideline to explore the ore in porphyry copper and carbonate-hosted base-metal replacement areas in the Western United States.

Jasperoid is a rock composed predominantly of silica, which is in the form of aphanitic to fine-grained quartz, and form by replacement of the silty-limestone or dolomite (Lovering, 1972). Decarbonization and silicification in limestone and dolomitic rocks by hydrothermal fluids and metasomatic alteration is named as jasperoid. The estimated alteration product jasperoid, which emplaced quartz replacing limestone, parallel to the replacement and high angle fault planes, is commonly present in Carlin-type deposits (Ilchick and Barton, 1997). Carlin-type Au deposits can be described widely as silicified replacement rock bodies formed by decarbonatization of dirty carbonates (silty-limestone or clay including limestones), (Cline et al., 2005). Romberg (1986) described four adjunct features from previous many studies on Carlin-type deposit: (1) existences of jasperoid; (2) close correlation between pyrite and gold; (3) low amount of base metals; and (4) remarkable dilution of arsenic, antimony, mercury, and thallium in the ores.

Jasperoids in the Keşkek Hill project area are very similar to jasperoids in Carlin trend in terms of petrographic, tectonic setting, mineralogical, microthermic, and isotopic properties. Jasperoidal rocks in the Carlin system generally formed from silty-limestones. In the study area, jasperoid occurrences were observed in beige colored laminated limestones which are highly brittle deformed during or after deposition of ophiolitic mélange. It is broadly accepted that in Carlin-type gold deposits, ore fluids transported vertically along high angle normal faults. Due to low permeability of ophiolitic rocks have fluids cannot migrate laterally, this rock forced fluids to move

upward until reacting with more permeable and porous carbonate rocks (Lubben, 2004).

The geological setting of carlin-type gold mineralization in Nevada nearly has the same geological processes like the Keşkek Hill project area. Tectonic evolution in Carlin setting starting with thrust faulting in the compressional regime, then the tectonic forces changes from compressional to extensional, and also effect of extension tectonism low angle detachment faults occurred in the area. Vertical normal faults occurring on those detachment faults named as Getchell fault system (Cline and Hofstra, 2000). Keşkek Hill tectonic evaluation has similar processes with Carlin-Trend in Nevada. Keşkek Hill project area effected by Northern Anatolian ophiolitic units thrusting on to Menderes Massif. The change of compressional to the extensional regime, the thrust fault between metamorphics and ophiolitic mélange acting like a low angle detachment fault. On this detachment fault, vertical normal faults occurred and as in Carlin deposits, jasperoids were generated in this fault.

Gold grains in Carlin-type deposits are submicron microscopic size. Gold is typically present on arsenic-rich pyrite grains (Theodore and Jones, 2009). For this reason, visible gold does not form and observable in Carlin-type systems (Lubben 2004). Gold in Carlin-type deposits is generally with regard to significant trace elements which include Sb, Hg, Te, Tl, Cu, As, and Ag (Weaver and Cline, 1999; Theodore and Jones, 2009). The correlation tables of Keşkek Hill and field studies state that gold in Keşkek Hill has a good correlation with Sb, As, and Ag. Silver and sulfur have a very good correlation in grab-channel samples and also antimony is using for pathfinder element on the surface outcrops of jasperoid (Table 4.2).

Jasperoid is the main alteration in the Keşkek Hill prospect. Decarbonatization of limestones resulted in silicification and jasperoid occurrences in the area. Calcification is the last stage of the alteration. Calcite minerals and veinlets occurred in post mineralization stage fractures in jasperoids and limestones.

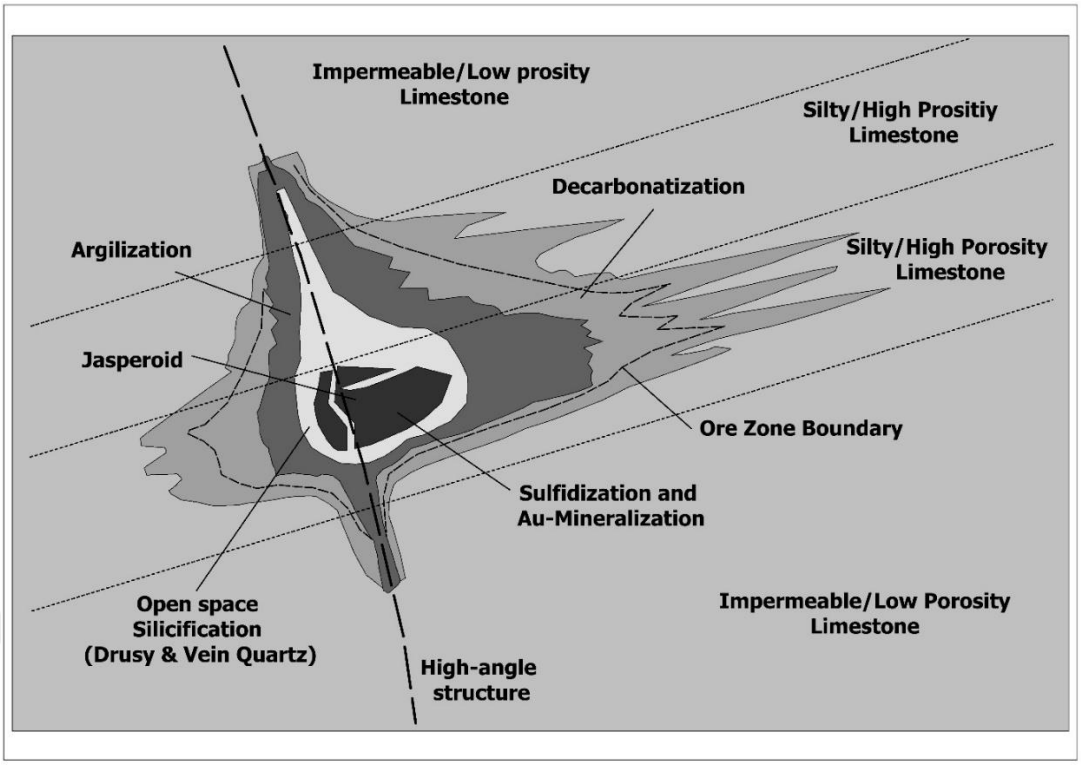

Figure 9.2. Schematic cross-section through a Carlin-type deposit ore zone showing the main alteration and mineralization zones connected to a fluid channel (modified from Arehart, 1996).

Instead of the argillic zone, the other alteration zones and mineralization zones observed in Keşkek Hill prospect. The argillic alteration zone could be eroded due to high tectonism and weathering conditions.

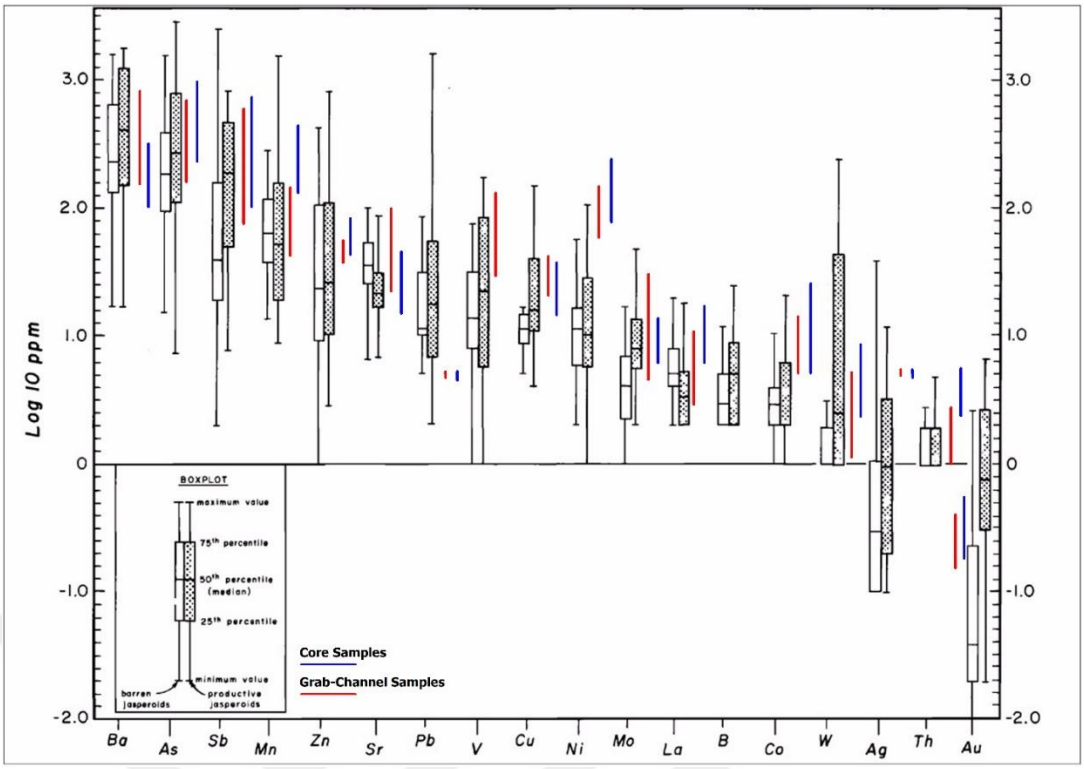

Figure 9.3. Multiple boxes and capilliform plot of trace element geochemical data (Holland et al., 1988), appendix. Jones and Leveille (1989) plotted in order of decreasing median concentration, from left to right. Dot included boxes showing the distribution of values of the given element in 32 samples of gold-bearing jasperoids, open boxes represent the distribution of 33 samples taken from gold-barren jasperoids. Blue and red lines represent the gold-bearing jasperoid samples in Keşkek Hill prospect. Instead of Au, all red and blue lines represent the element on their left.

Trace element diagram shows that most of the samples of Keşkek Hill prospect have similar values with the Carlin-type system (Figure 9.3). Nickel values are higher than the Carlin-type system because there is a nickel laterite mineralization around the mineralized area. Weathering and eroded materials of nickel laterite deposit could be contaminating the samples and give high nickel values.

9.4. Physicochemical Characteristic of Hydrothermal Fluids and Their Evolution

Previous studies on the Carlin-type gold deposits state that the paragenesis of gold mineralization is particularly associated with jasperoid mineralization (Arehart, 1996; Hofstra and Cline, 2000). Fluid inclusion studies on ore-quartz of jasperoid signified that ore fluid temperatures changing from 180°C to 240 °C (Figure 9.4; Cline and Hofstra, 2000). Cline and Hofstra (2000) observed that pre-ore stage quartz inclusions ore fluid temperatures ranging from 270 to 290 °C.

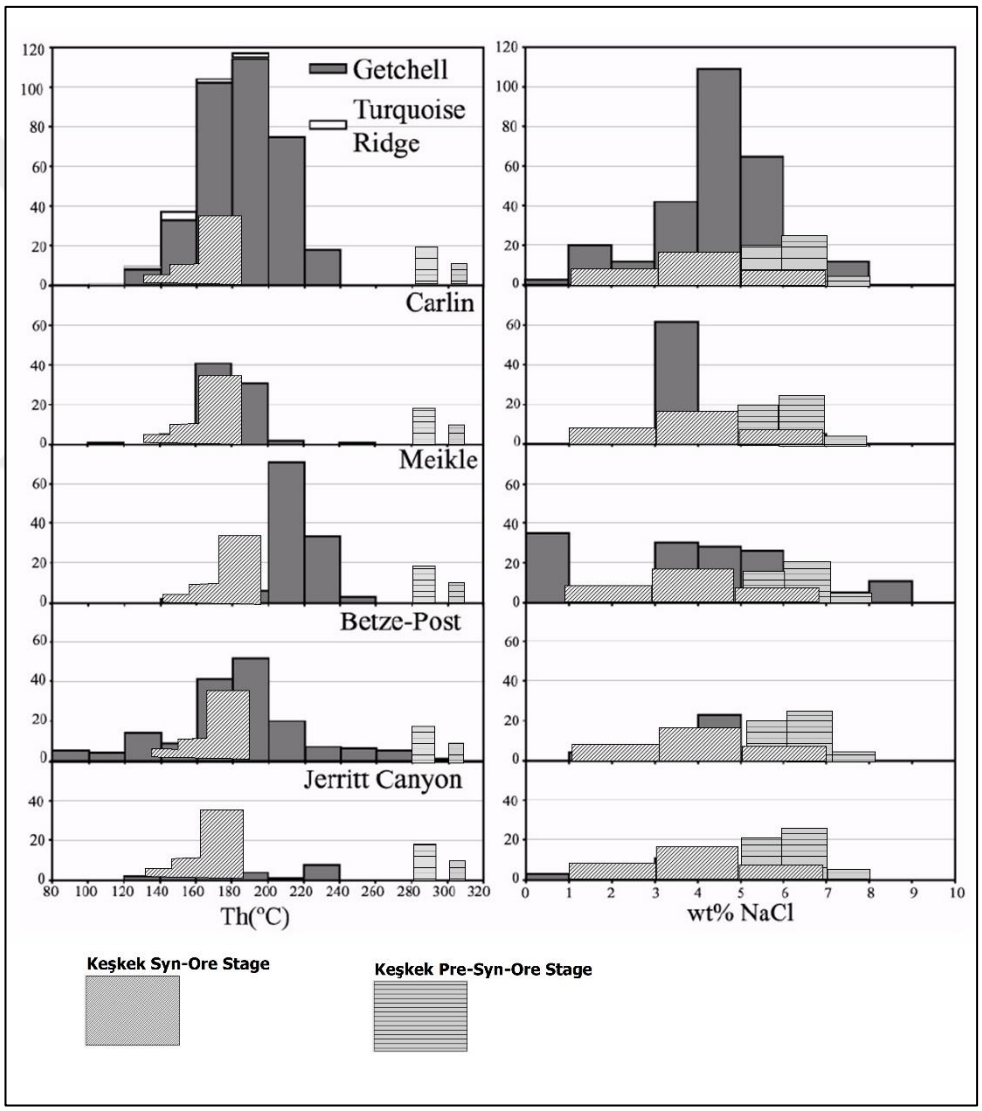

Figure 9.4. Microthermometric data for fluid inclusions in Carlin-type gold deposits and comparing with Keşkek Hill data. Data collected from Hofstra, 1994 (Jerrit Canyon), Lumb,

1995 (Meike), Kuehn, 1989 (Carlin), Cline and Hofstra, 2000 (Getchell), and Shigehiro, 1999 (Turquoise Ridge).

Keşkek Hill fluid inclusion studies have been performed on the pre-syn-ore stage and syn-ore stage quartz. The homogenization temperature ranges of syn-ore stage quartz range from 136 °C to 182.7 °C. Salinity values of this stage quartz are from 0.70 to 15.86 wt. % NaCl. The average value of the salinity calculated as 6.7 wt. % NaCl and this value is nearly the same as previous studies in Carlin-type systems. The calculated average value of homogenization temperature obtained from measurements of syn-ore stage quartz is 169 °C and, this value also nearly the same with previous studies in Carlin-type systems.

The homogenization temperature ranges of pre-syn-ore stage quartz minerals range from 288.7 °C to 313 °C. The salinity values of this stage quartz are between 5.7 and 7.6 wt. % NaCl. The calculated average value of salinity is 6.5 wt. % NaCl. The average value of the homogenization temperature calculated as 295.83 °C. Keşkek Hill homogenization temperature and salinity values gathered from quartz minerals are nearly as same as to data measured Getchell deposit (Cline and Hofstra, 2000) and Carlin (Kuehn, 1989).

Isotope analyses have been carried out on quartz (O isotope) and whole-rock (jasperoid) (H isotope) from which fluid inclusion measurements have also been done. Jasperoid generally includes hydrogen in several sources which are including fluid inclusion H_2O, gases like CH_4 and H_2S, OH^- regions in quartz, or inclusions of hydrogen including organic materials (Faure, 2003). The $\delta^{18}O$ and δD values in the fluid phase are calculated by using the isotope fractionation equation from Clayton et al. (1972). Calculation results plotted on the $\delta D_{(fluid)}$ vs $\delta^{18}O_{(fluid)}$ diagram, which is modified from Cline and Hofstra (2000), to find out the origin of the fluid which is active during the syn-ore stage.

The data on the $\delta D_{(fluid)}$ vs $\delta^{18}O_{(fluid)}$ diagram plot in the formation water area close to the meteoric mixing area (Figure 9.5). The fluid-related with the syn-ore stage could be generated from formation water during or after thrusting of ophiolite mélange onto the metamorphic basement. By extensional tectonism and high angle normal faulting

this relatively deep circulating water migrates the upper zones of mélange and by the time due to extension and brittle deformation in limestones, meteoric water can reach deeper areas from the surface. These two waters could be mixed in somewhere of limestones and they started to mineralization of gold in decarbonized rocks. Mixing of formation and meteoric water is responsible for gold mineralization in the Keşkek Hill area.

The plot of data for Keşkek Hill compared with data in Carlin-type deposits in Nevada (Figure 9.5). Samples of Keşkek Hill prospect have a very good correlation with the Carlin-type deposits isotope ratios.

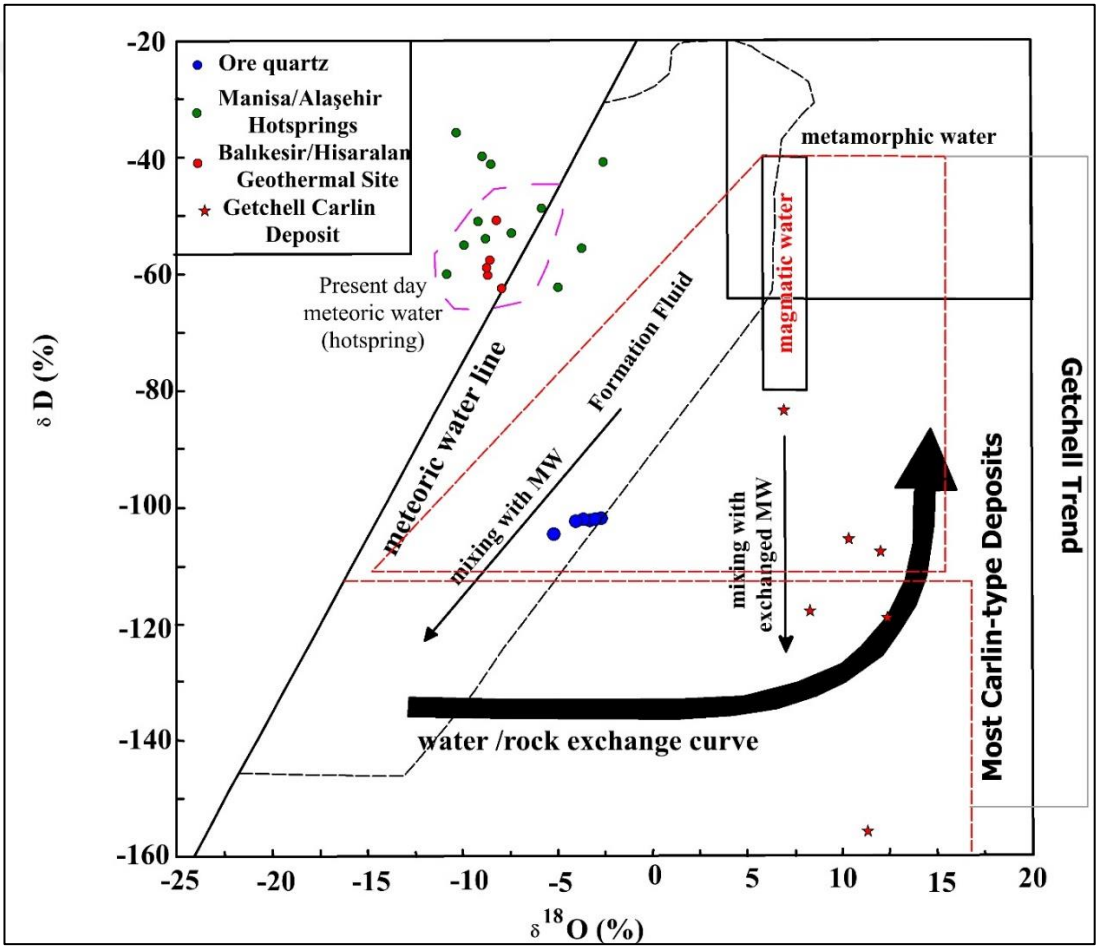

Figure 9.5. Hydrogen and oxygen isotope plot, which belongs to Keşkek Hill jasperoid quartz and modern water isotope analyses, values determined for inclusion fluids in the syn-ore stage. Most Carlin-type deposits lines (red lines) and Getchell trend lines are taken from Lubben (2004) (modified from Cline and Hofstra, 2000). Red lines show the area where Carlin-type deposits isotope values observed. Blue dots represent data from this study.

Sulfur isotope analyses were done on stibnite associated comb textured quartz veinlets within jasperoids. $\delta^{34}S_{VCDT}$ ‰ values were plotted on the sulfur diagram modified from Rollinson (1993) (Figure 8.2). Plotted data are observed close to the magmatic sulfur line. Fluid inclusion and oxygen-hydrogen stable isotope analysis show that fluids in the study area plot within the formation water area close to the meteoric water line, even if sulfur isotope value plots close to magmatic sulfur. The reason why sulfur isotopes are more likely to be magmatic is may be due to the deep circulation of the fluids within the ultramafic rocks that cover large areas. Even if the ultramafic rocks serpentinized, the rocks have a magmatic origin. The ore fluid could be generated from these formations and this could be the reason to why the sulfur isotope plot observed close to magmatic sulfur (Figure 9.6 and 9.7)

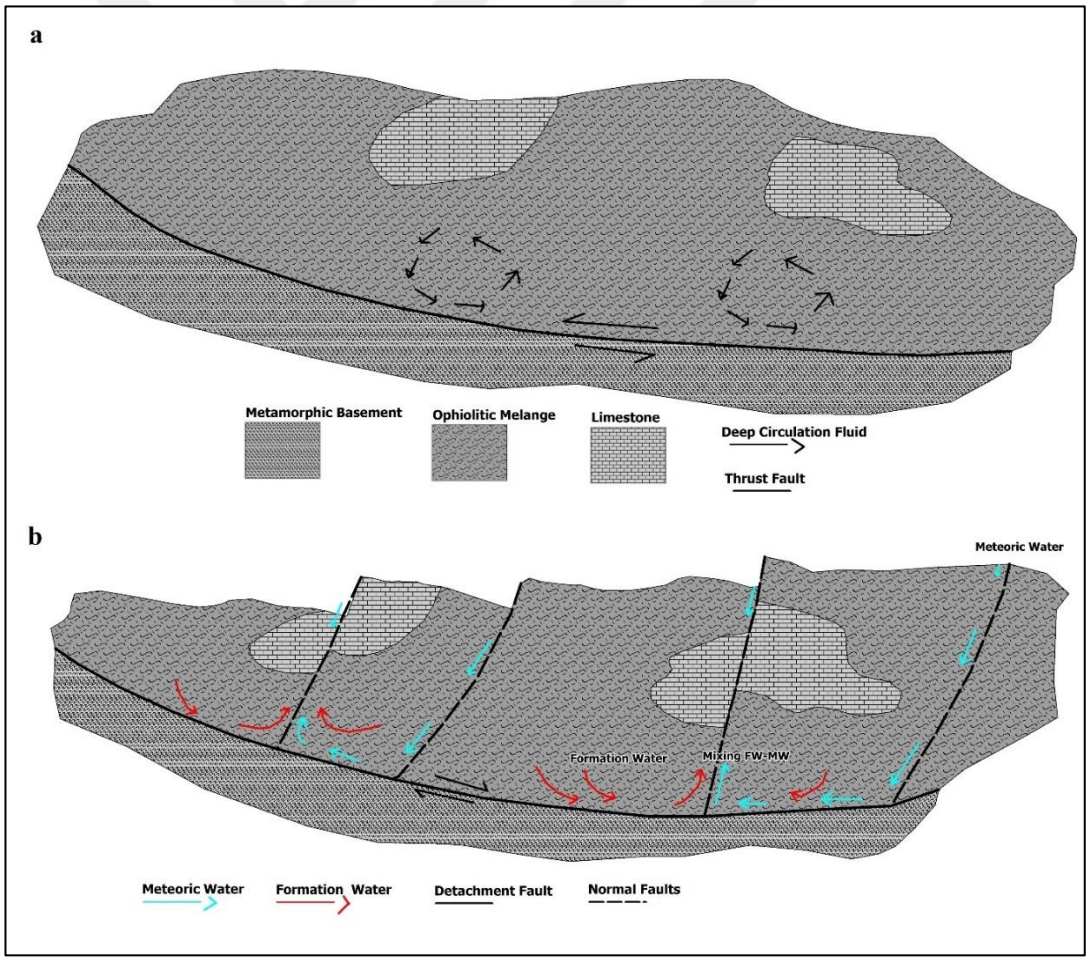

Figure 9.6. Continued

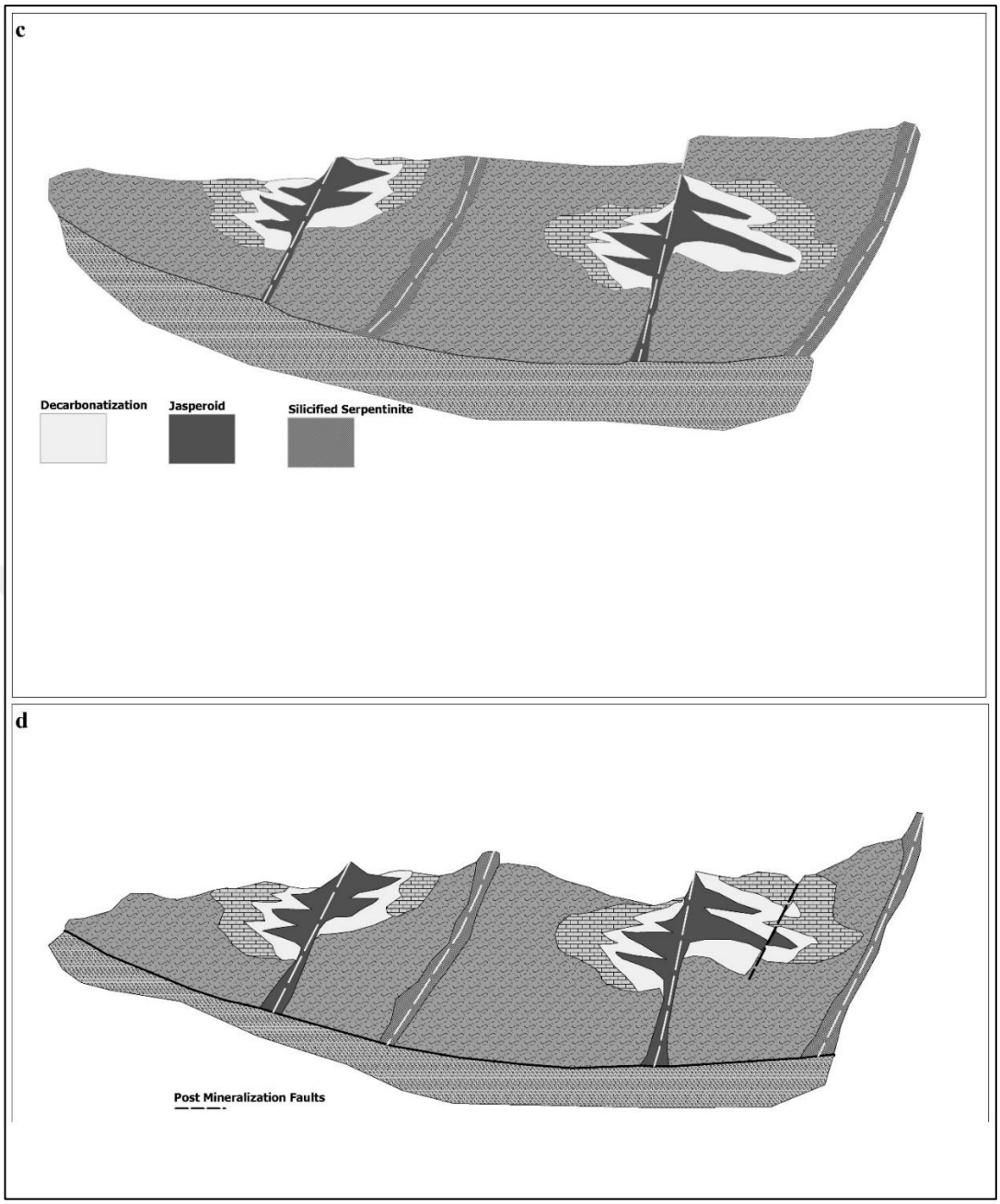

Figure 9.7. Genetic model and evaluation of Keşkek Hill gold prospect in terms of alteration and mineralization.

10. CONCLUSIONS

The main conclusions obtained from this thesis are given below:

- Ten different units; namely ultramafic rocks, dark gray recrystallized limestone, epi-ophiolitic sequences, light gray laminated limestone, beige laminated limestone, matrix-supported breccia, quartzite, ankerite, and laterite have been mapped and described in the study area.
- Silicification, decarbonization, jasperoids, and calcification are the main alterations in the study area. Silicification and decarbonization identified from thin section studies. Relict calcite in a thin section supports the decarbonization process involved within the system in the area. Jasperoid occurrence in the study area resulted from decarbonization and silicification alterations. Jasperoids are the main alteration units in Carlin-type systems. The main characteristics of jasperoids observed in the study area are their strongly silicified and oxidized nature. The host rock of this type alteration observed as BLL in the study area. Quartz is the main alteration mineral in jasperoids. Comb texture, boxwork texture, and liese-gang texture are the main textures observed on jasperoids. Matrix supported breccia also evaluated as a part of jasperoid alteration. Calcification and intense oxidization are the post mineralization alterations observed on all units identified in the study area. This alteration type identified during thin section studies and field works. Calcite occurrences observed as open space-filling and as veins. Primary calcite veins, fractures in jasperoids are cut by calcite veins.
- Gold mineralization in the study area was only observed in jasperoids. In some core and grab-channel samples very low grade of gold mineralization observed in BLL. Pyrite, antimony, and arsenopyrite are the main pathfinder minerals. Paragenetic sequins of these elements are syngenetic with gold mineralization. Most of the pyrite and antimony (stibnite) minerals are observed as oxidized (valentinite) during field studies. Unoxidized pyrite and antimony minerals are mostly observed in core samples or protected deep valleys. Jasperoids have low abundances of base metal, instead of gold.
- The main structures in the study area are high angle normal faults. The direction of these faults is measured mostly NW-SE with a dip angle between 73° and 90°. The direction of mineralized jasperoids observed as same as direction with these faults. Post mineral faults are a high angle normal in a NE-SW direction. The other faults in the study area are thrust faults and strike-slip

faults. Thrust faults trend in NNE to SSW with a low angle dip. Observations on these thrust faults show that they act like a detachment fault during mineralization. NNE-SSW directed strike-slip fault observed in the northeastern part of the study area. This strike-slip fault observed along the Gıcırlar River.

- Jasperoid alteration used as a pathfinder to find different gold mineralization occurrences in the study area. Upon this work, 4 different orebodies have been discovered by the meaning of collected grab-channel samples.
- Syn-ore stage quartz is a result of moderately low temperature and low salinity formation water mixed with meteoric water (T_h 169°C within 1.1 to15.9 wt. % NaCl eq salinity). The homogenization temperature and salinity of pre-syn ore stage quartz are measured as 295.83°C and 5.7 to 7.6 wt. % NaCl eq salinity. The $\delta D_{(fluid)}$ vs $\delta^{18}O_{(fluid)}$ plotted data stated that ore-forming fluids are formation water which mixed with meteoric water.
- Presence of jasperoid, petrographic, microthermometry studies, a close association between pyrite and gold, low abundances of base metal and remarkable concentrations of arsenic and antimony in the ore, and also microthermometry and isotope geochemistry studies stated that Keşkek Hill gold mineralization could be a Carlin-type deposit. However, more data should be collected for accurate results.

REFERENCES

Aksoy, N., Demirkıran, Z., ve Şimşek, C. (2009) Sındırgı-Hisaralan (Balıkesir) Jeotermal Sahasının Jeokimyasal Özelliklerinin Değerlendirilmesi. *IX. Ulusal Tesisat Mühendisliği Kongresi. TMMOB, İzmir,* 61-72.

Arpat, E. and Norman, T. (1961) Akhisar 70/4 Paftasının Batı Yarısının Kapsadığı Sahalarda Jeolojik İnceleme. *MTA Derleme No: 3458* Unpublished.

Arehart, G. B. (1996) Characteristics and origin of sediment-hosted disseminated gold deposits: A review. *Ore Geology Reviews, v. 11,* 383-403.

Beadoin, G. and Therrien, B. (2004) The web Stable Isotope Fractionation Calculator. *Handbook of stable isotope analytical techniques,* 1:1045-1047.

Bodnar, R. (1993) Revised equation and table for determining the freezing point depression of H2O-NaCl solutions. *Geochimica et Cosmochimica Acta,* 57: 683-684.

Bülbül, A. (2009) *Alaşehir (Manisa) sıcak ve soğuk su sistemlerinin Hidrojeolojik ve Hidrojeokimyasal açıdan incelenmesi.* Dokuz Eylül Üni., Doktora tezi.

Canik B, 1962, 1/100.000 Ölçekli Akhisar 70/1 Paftasının Doğu Kısmı İle Akhisar 70/2 Paftaları Jeoloji Raporu. *MTA Derleme No: 3465* Unpublished.

Clayton, N. R., O'Neil, R. J. and Mayeda, K. T. (1972) Oxygen Isotope Exchange between Quartz and Water. *Journal Geophysical Research,* 77: 3057- 3066.

Cline, S. J. and Hofstra, H. A. (2000) Ore-fluid evolution at the Getchell Carlin-type gold deposit, Nevada, USA. *Europan Journal of Mineralogy,* 12: 195-212.

Cline, S. J., Hofstra, H. A., Muntean, L. J., Tosdal, M. R., and Hickey, A. K. (2005) Carlin-Type Gold deposits in Nevada: Critical Geologic Characteristics and Viable Model. *Society of Economic Geologists, Inc,* Economic Geology 100th Anniversary Volume: 451-484.

Dubertret L. and Kalafatçıoğlu A., 1973, 1/500.000 ölçekli Türkiye Jeoloji haritası izahnamesi. *MTA,* 115.

Engin, T. and Özkan, Y. Z. (2008) General Geological Report of the Kocakağan (Akhisar)- Kınık (Sındırgı)- Çiçekli (Gördes) Ni-Co Concession Areas. *Dama Engineering report to Meta Nikel Kobalt Madencilik A.Ş.*, A-154.

Erkül, F., Erkül, T. S., Manap, S. H. and Çolak, C. (2017) An extensional and transtensional origin of elongated magmatic domes and localized transfer faults in the northern Menderes Metamorphic core complex, western Turkey. *Geodynamic Acta,* 29,1:139-159.

Ersoy, Y. E. (2011) *Stratigraphy, tectonic evolution and petrogenesis of the volcanic rocks in the Gördes, Demirci and Emet Basins, Western Anatolia*. Dokuz Eylül Üniversitesi, Doktora tezi.

Faure, K. (2003) δD values of fluid inclusion water in quartz and calcite ejecta from active geothermal systems; do values reflect those of original hydrothermal water? *Economic Geology,* 98:657-660.

Goldfarb, R. J. (2016) Orogenic Gold Deposits, *MNG Gold lecture and presentation*.

Helvacı, C. (2015) Geological Features of Neogene Basins Hosting Borate Deposits: An Overview of Deposits and Future Forecast, Turkey. *Bulletin of the Mineral Research and Exploration,* 151: 169-215.

Hofstra, A. H. and Cline, J. S. (2000) Characteristics and models for Carlin-type gold deposits. *Society of Economic Geology Reviews,* 13: 163-220.

Hofstra, A. H. (1994) *Geology and genesis of the Carlin-Type gold deposits in the Jerrit Canyon district, Nevada*. Unpublished Ph.D. Dissertation, Boulder, University of Colorado, 719.

Holland, P. T., Beaty, D. W. and Snow, G. G. (1988) Comparative elemental and oxygen isotope geochemistry of jasperoid in the northern Great Basin: Evidence for distinctive fluid evolution in gold-producing hydrothermal systems. *Economic Geology*, 83:1401-1423.

http://www.mta.gov.tr/v2.0/birimler/laboratuvarlar/index.php?id=SiviKapanim

https://www.queensu.ca/geol/qfir

http://yebim.ankara.edu.tr/

Ilchick, R. P. and Barton, M.D. (1997) An amagmatic origin of Carlin-type gold deposits. Economic Geology, 92: 269-288.

Jones, K. B., and Leveillle, A. R. (1989) Comparative elemental and oxygen isotope geochemistry of jasperoid in the northern Great Basin: Evidence for distinctive fluid evolution in gold-producing hydrothermal systems – A Discussion. *Economic Geology*, 94: 1705-1712.

Kesler, E. K., Riciputi, C. L. and Ye, Z. (2005) Evidence for a magmatic origin for Carlin-type gold deposits: isotopic composition of sulfur in the Betze-Post-Screamer Deposit, Nevada, USA. *Mineralium Deposita*, 40: 127-136.

Konak, N, Akdeniz, N. and Armağan. F, 1980, Akhisar Gölmarmara Gördes Sındırgı Dolaylarının Jeolojisi. *MTA Derleme,* 6916 Unpublished.

Kuehn, C.A. (1989) *Studies of disseminated gold deposits near Carlin, Nevada, Evidence for a deep geologic setting of ore formation*. State College, Pennsylvania, The Pennsylvania State University, Ph.D., dissertation, 395.

Kuşcu, İ., Tosdal, R. M., Gencalioğlu - Kuşçu, G., Friedman, R., and Ullrich, T. D. (2013) Late Cretaceous to Middle Eocene Magmatism and Metallogeny of a Portion of the Southeastern Anatolian Orogenic Belt, East-Central Turkey. *Economic Geology*, 108: 641‑666.

Kuşcu, İ. (2018) Gördes (Manisa) Sahasındaki Silisleşmiş Breşlere Bağlı Altın Cevherleşmelerine Yönelik Arazi Gözlem-Sondaj Değerlendirmeleri ve Jeofizik Etüt Önerileriyle İlgili Rapor. *Meta nikel Kobalt Madencilik A.Ş.* danışmanlık raporu.

Lubben, D. J. (2004) Silicification across the Betze-Post Carlin-type Au Deposit: Clues to ore fluid properties and sources, Northern Carlin Trend, Nevada. *The University of Nevada, Las Vegas,* M.Sc. thesis.

Lumb, J. B. (1995) *A petrographic and fluid inclusion study of the purple vein and Post-Betze orebodies, Carlin, Nevada, Unpublished M.S. thesis.* Las Vegas, University of Nevada, 126.

Lovering, T. G. (1972) Jasperoid in the United States – Its characteristics, origin, and economic significance. *U.S. Geological Survey Professional Paper,* 710: 164.

Michaud, D. (2015) https://www.911metallurgist.com/blog/carlin-type-gold-deposit

MTA (2002) Geological Map of Turkey, 1:500,000, *Maden Tektik ve Arama Genel Müdürlüğü, (General Directorate of Mineral Research and Exploration*), Ankara.

Nash, J. T. (1976) Fluid Inclusions Petrology – Data from Porphyry Copper Deposits and Applications to Exploration. *Geological Survey Professional Paper,* 907 – D.

Nebert, K. (1961a) Linyit İhtiva Eden Çıtak (Akhisar, Manisa) Neojen Sahasının Jeolojik yapısı ve maden Jeolojisi. *Maden Tektik ve Arama Genel Müdürlüğü Raporu,* 2928.

Nebert, K. (1961b) Gördes (Batı Anadolu) Bölgesindeki Neojen Volkanizması Hakkında Bazı Bilgiler. *Maden Tektik ve Arama Genel Müdürlüğü Raporu.*

Okay, I. A. and Siyako, M. (1993) The New Position of the İzmir-Ankara Neo-Tethyan Suture Between İzmir and Balıkesir. *Tectonics and Hydrocarbon potential of*

Anatolia and Surrounding Regions. Proceedings of the Ozan Sungurlu Symposium, Ankara, 333-355.

Okay, A.I. & Göncüoğlu, M. C. (2004) Karakaya Complex: a review of data and concepts. *Turkish Journal of Earth Sciences*, 13, 77-95.

Okay, I. A., İşintek, İ., Altıner, D., Altıner, Ö. S. and Okay, N. (2012) An Olistrostrome-melange belt formed along a suture: Bonova Flysch Zone. *Tectonophysics*, 568-569: 282-295.

Purvis, M., and Robertson, A. H. F. (2004) A pulsed extension model for the Miocene NE-SW-trending Selendi and Gördes Basins and the Neogene-Recent E-W trending Alaşehir (Gediz) Graben, W Turkey. *Tectonophysics*, 391: 171-201.

Purvis, M., and Robertson, A. H. F. (2005) Miocene sedimentary evolution of the NE-SW-trending Selendi and Gördes Basins, W Turkey: implications for extensional processes. *Sedimentary Geology*, 174: 31-62.

Robertson, A. H. F., Parlak, O., and Ustaömer, T. (2009) Mélange genesis and ophiolite emplacement related to subduction of the northern margin of the Tauride-Anatolide continent, central and western Turkey. *Geological Society, London, Special Publications*, 311: 9-66.

Roedder, E., Ingram, B., and Hall, W. E. (1963) Studies of fluid inclusions III: extraction and quantitative analysis of inclusions in the milligram range. *Economic Geology*, 58: 353-374.

Rojay, B. F. (2004) Gördes Area Structural Geology Report, *Arcasoy Consulting and Engineering Inc.,* Meta Nikel Kobalt Madencilik A.Ş. Structural Geology Report.

Rojay, B. F. (2014) Post-Paleogene (post-Eocene-pre-Miocene) Deformation in central Anatolia, (Turkey). *Egu General Assembly, Vienna,16.*

Rollinson, H. R. (1993) Using Geochemical Data: Evaluation, *Presentation, Interpretation*. Edinburg: Pearson Education Limited.

Romberg, S. B. (1986) Ore deposits #9.-Disseminated gold deposits. *Geoscience Canada*, 13-1: 23-31.

Seyitoğlu, G. and Işık, V. (2015) Late Cenozoic extensional tectonics in western Anatolia: Exhumation of the Menderes core complex and formation of related basins. *Bulletin of the Mineral Research and Exploration*, 151: 49-109.

Seyitoğlu, G., and Scott, B. C. (1994a). Late Cenozoic basin development in western Turkey. Gördes basin: tectonics and sedimentation. *Geological Magazine*, 13: 631-637.

Seyitoğlu, G. Benda, L., and Scott, B. C. (1994b). Neogene palynological and isotopic age data from Gördes basin, West Turkey. *Newsletter Stratigraphy* 31: 133-142.

Shepherd, T., Rankin, A. H., and Alderton, D. H. (1985) *A practical guide to fluid inclusion studies.* Glasgow: Blackie.

Shigehiro, M. (1999) *Mineral paragenesis, and ore fluids at the Turquoise Ridge gold deposit, Nevada.* Unpublished M. Sc. Thesis, Las Vegas, University of Nevada, 152.

Spurr, J. E. (1898) Geology of the Aspen mining district, Colorado, with atlas. *U. S. Geological Survey Monograph*, 31: 260, and atlas of 30 sheets folio.

Şengör, A. M., and Yılmaz, Y. (1981) Tethyan evolution of Turkey: A plate tectonic approach. *Tectonophysics*, 75, 181-241.

Taylor, H. P., and Sheppard, S. M. F. (1986) Igneous rocks: I. processes of isotopic fractionation and isotope systematics, in Stable İsotopes in high-Temperature Geological Processes. *Washington: Mineralogical Society of America*, 227-271.

Tchihatcheff (1850). Asia Mineure (Description Physigue), *Paris*, 552.

Theodore, G. T., and Jones M. G. (2009) Geochemistry and Geology of Gold in Jasperoid, Elephant Head Area, Lander County, Nevada. U.S. *Geological Survey Bulletin 2009,* 62.

Weaver, K. D. and Cline, J. S. (1999) Geochemistry of ore-stage and non-ore pyrite and marcasite from Getchell Carlin-type gold deposit, Nevada. *Geological Society of America, Program with Abstracts*, 31: A-106.

Yağmurlu, F. (1984) Akhisar Dolayında Kömür İçeren Miyosen Tortullarının Stratigrafisi ve Tektonik Özellikleri. *Türkiye Jeoloji Kurultayı Bülteni,* 5: 3-20.

Yiğit, Ö. (2009) Mineral deposits of Turkey in relation to Tethyan Metallogeny: implications for future mineral exploration. *Econ. Geol.*, 104, 19‑51.

Yiğit, Ö. (2012) A prospective sector in the Tethyan Metallogenic Belt: Geology and geochronology of mineral deposits in the Biga Peninsula, NW Turkey. *Ore Geology Reviews,* 46: 118-148.

CURRICULUM VITAE

PERSONAL INFORMATION

Name:	Abitter GÜNAY
Birth Place:	Ereğli/Konya
Date of Birth:	1.12.1989
Nationality:	T.C.
Driving License:	B
Phone Number:	+90 507 846 71 56
E-mail:	abittergunay@gmail.com

WORK EXPERIENCE

Exploration Geologist/ Meta Nikel Kobalt A.S. (February 2018 -)

GENERAL FIELD
WORKS

-Exploration for gold, copper, nickel and base metals (porphyry, orogenic lodge gold, skarn, nickel laterite, carlin, epithermal)
-Stream sediment sampling, rock sampling, and soil sampling
-District mapping
-Supervising of DC drilling program
-Core logging and core sampling
-Reporting to exploration manager

GENERAL
OFFICE WORKS

-Planning of new targets
-GIS programs

Field Geologist/ Avesoro Resources Inc. /Liberia (Western Africa) (June 2016 - December 2017)

GENERAL

WORKS

-Supervising of Dc and RC drilling program and core logging.

-102000m DC drilling, core logging, and sampling

-21000m RC drilling, logging, and sampling.

-Monthly report to exploration manager

-Ground magnetic survey

-Core yard organization and worker management

-Rig set-up and drill pat organization

-Drilling road opening and drill pat opening

Exploration Geologist/ Tüprag Metal Madencilik San. Tic. A.S. a subsidiary of Eldorado Gold Corporation (July 2015- June 2016)

GENERAL

WORKS

-Dölek Project, Northern Turkey/ Dölek Au Project

-DC drilling and quick logging

-Core logging

-Terraspec and XRF measurements

- Exploration for gold, copper and base metals (porphyry, epithermal, VMS, skarn)

- Stream sediment sampling (regional and local), rock sampling and soil sampling.

- Trimble and magnetic survey.

- District mapping

- Planning for new targets

- GIS programs

Intern Geologist/ Tüprag Metal Madencilik San. Tic. A.S. a subsidiary of Eldorado Gold Corporation (July 2014- September 2014)

GENERAL
WORKS

- Stream sediment sampling (regional and local), rock sampling, and soil sampling.
- Trimble and magnetic survey.
-Reconnaissance stage work involves initial and courses activities in the favorable districts at around Northern and Western Turkey

Intern Geologist/ Tüprag Metal Madencilik San. Tic. A.S. a subsidiary of Eldorado Gold Corporation (June 2013- September 2013)

GENERAL
WORKS

-Dölek Project Porphyry Cu-Au Deposit
-Supervising RC drilling night shift
-RC quick logging
-Konak North Project |VMS Mineralization Type Deposit
-Camping in the project area
- Soil sampling, rock chip sampling, Trimble, and magnetic survey

EDUCATIONAL BACKGROUND

2009-2015

B.Sc. Geological Engineering, Muğla Sıtkı Koçman University
Supervisor: Prof. Dr. Gonca KUŞCU
GPA: 2.97/4.00 **Education Language:** English

Thesis: Characterization of Nisyros Distal Tephra in Hızırşah Village (Datça Peninsula, Turkey)
-As a part of TUBİTAK project

2016-2020	**M.Sc.** Geological Engineering, Muğla Sıtkı Koçman University **Supervisor:** Prof. Dr. İlkay KUŞCU
	GPA: 3.00/4.00 **Education Language:** English **Thesis:** Origin of Gold Mineralization, Source of Ore Fluid and Structural Controls of Keşkek Hill Gold Mineralization (Gördes, Manisa)

EDUCATION

05.2015	Hydrothermal and Porphyry Systems Anaconda Mapping course in Afyon/Sandıklı given by Dr. Richard TOSDAL

COMPUTER SKILLS

ArcGIS Pro and MapInfo Pro
GPS programs (Garmin Basecamp, global mapper, etc.)
Microsoft Office

REFERENCES

Prof. Dr. İlkay KUŞCU	Economic Geology-Geochemistry Muğla Sıtkı Koçman University ikuscu@mu.edu.tr
Metin AVĞAN	Meta Nikel Kobalt A.Ş. Exploration Manager metin.avgan@metanikel.com.tr
Ahmet TUKAÇ	Tüprag Metal Madencilik San. Tic. A.Ş Exploration Manager of Turkey ahmett@tuprag.com